NATIONAL TECHNICAL UNIVERSITY OF ATHENS

SCHOOL OF NAVAL ARCHITECTURE AND MARINE ENGINEERING

SHIPBUILDING TECHNOLOGY LABORATORY

Stiffened Panels subjected to Uniform Pressure Loads:

Theoretical and Numerical Modeling Strategies

by

Efstathios L. Platypodis

Diploma thesis

Thesis Supervisor: Konstantinos N. Anyfantis, Assistant Professor, NTUA

Athens, December 2020

Acknowledgements

I would like to thank my supervisor Assistant Professor Konstantinos Anyfantis for our cooperation. Apart from being an excellent teacher, his gem of wisdom was pivotal for the evolution of this thesis. I feel gratitude for inspiring me and sharing me his love for science and engineering.

I would also like to thank my family and my friends for all the sacrifices that made for me. I feel blessed for the support that I have received all these years.

Περίληψη

Τα ενισχυμένα ελάσματα είναι βασικά κατασκευαστικά στοιχεία, τα οποία χρησιμοποιούνται στην γάστρα του πλοίου και ειδικότερα στην περιοχή του διπύθμενου, στα πλευρικά ελάσματα και στο άνω κατάστρωμα. Η μελέτη αντοχής των ενισχυμένων ελασμάτων που καταπονούνται από ομοιόμορφα φορτία πίεσης επιτυγχάνεται μέσω της ανάλυσης των δευτερευουσών τάσεων-αυτών που προκύπτουν από τα ενισχυτικά μαζί με το συνεργαζόμενο έλασμα ως μια δοκό που κάμπτεται, και των τριτευουσών, δηλαδή των τάσεων που προκύπτουν από την κάμψη του ελάσματος μεταξύ των ενισχυτικών.

Η παρούσα διπλωματική εργασία εστιάζεται στις δευτερεύουσες τάσεις υπό ομοιόμορφα φορτία πίεσης. Η θεωρία κάμψης δοκού των Euler-Bernoulli δίνει μικρότερες τιμές για το τασικό πεδίο λόγω του φαινομένου υστέρησης σε διάτμηση. Εξετάζονται γι' αυτόν το λόγο τόσο θεωρητικά όσο και αριθμητικά μοντέλα, με την μέθοδο των πεπερασμένων στοιχείων, με σκοπό την τεκμηρίωση και τη διατύπωση της πιο ασφαλούς στρατηγικής για την μοντελοποίηση του εξεταζόμενου φαινομένου.

Επιπλέον, μελετάται η επίδραση των εγκάρσιων ενισχυτικών στις δευτερεύουσες τάσεις των διαμήκων ενισχυτικών σε ενισχυμένα ελάσματα και στις δύο κατευθύνσεις. Για διαστάσεις ενισχυμένων ελασμάτων που χρησιμοποιούνται στη ναυπηγική βιομηχανία, καθορίζονται οι οριακές συνθήκες που επιβάλλουν τα εγκάρσια ενισχυτικά στα διαμήκη. Το αποτέλεσμα της παρούσης ερευνητικής εργασίας είναι η δημιουργία ενός πίνακα που συσχετίζει το είδος στήριξης που επιβάλλουν τα εγκάρσια ενισχυτικά σε σχέση με άλλες παραμέτρους των ενισχυμένων ελασμάτων.

Stiffened Panels subjected to Uniform Pressure Loads:

Theoretical and Numerical Modeling Strategies

by

Efstathios L. Platypodis

Abstract

Stiffened panels are main structural components that are used in hulls of ships and in particular in double bottom, side shell and upper deck. The strength analysis of stiffened panels that are subjected to uniform pressure loads is accomplished examining both the secondary stresses, that are induced considering the stiffener with the attached plate as a beam, and the tertiary stresses, that are induced considering the bending of the plate between the stiffeners.

The present thesis focuses on the study of the secondary stresses under uniform pressure loads. The Euler-Bernoulli beam theory underestimates the stress field due to the shear lag phenomenon. Both theoretical and numerical models, with finite element analysis, are examined in order to deduce about the safest strategy to examine this phenomenon.

Moreover, the effect of the transverse stiffeners to the secondary stresses of longitudinal stiffeners at cross-stiffened panels is examined. For real ship scantlings, the boundary conditions, which the transverse stiffeners create, are determined. For this reason, a table is provided which relates the type of support, that the transverse stiffeners can be modeled, with other variables of a stiffened panel.

Table of contents

1. Introduction and objectives

1.1 Stiffened panels in ship structures

A ship is subjected to longitudinal, transverse and local strength loads. The longitudinal strength loads concern the overall strength of the hull of the ship. These loads are the bending moment, the shear force and the torsional moment acting on the hull girder. Because of the slender shape of the ship, from the point view of global deformation, we can consider that it behaves like a beam.

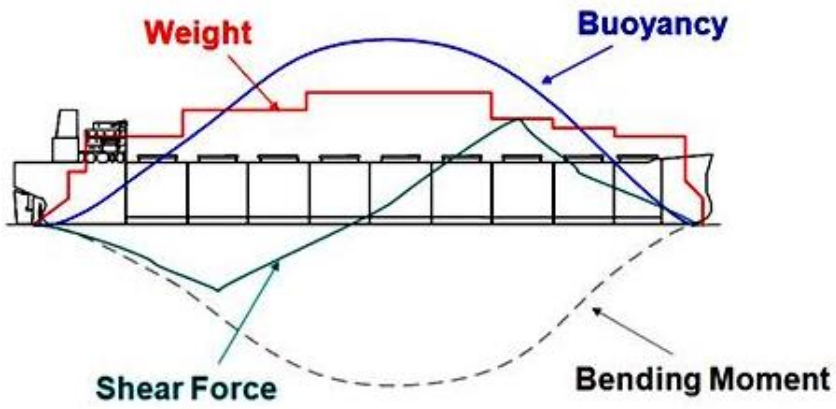

Figure 1.1: Longitudinal strength loads

The transverse strength loads act on transverse members and cause structural distortion of a cross section. These loads include the hydrostatic pressure on the outer shell, the weight of cargo load working on the bottom structure and the water ballast pressure. These loads are not always equal to each other at every point. As a result, the transverse members are distorted. It is considered that the distortion due to longitudinal loads does not affect the deformation of the transverse section.

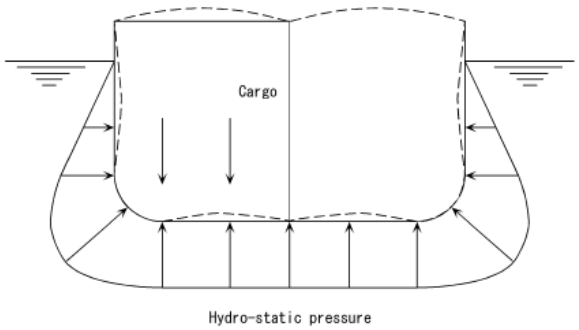

Figure 1.2: Transverse strength loads

The local strength loads affect the local strength members such as shell panels, stiffeners and connecting constructions between stiffeners.

The procedure of structural strength evaluation includes 3 significant modes for the structural designers: yielding, buckling and fatigue. Yielding is the failure mode that once the load exceeds a certain critical value, the elongation increases rapidly. Buckling is the failure mode that in case of a structure under compression load, the structure may be deflected when the load reaches a critical value. Fatigue is the failure mode that the structure may be fractured by small loads when the loads are provided repeatedly to the structure. In this diploma thesis, the problems that are examined, evaluate the yielding failure mode.

In order to construct a ship, panels are welded. Plates are slender construction elements and have small resistance to bending moment due to the small thickness in comparison with the other two dimensions. Specifically, the ratio between the width and the thickness of the plate is the following: $b/t > 25$. In order to increase the bending stiffness of the plates, stiffeners are welded parallel to one or two dimensions of the panel. This procedure results to the formation of panels with smaller dimensions (from $L_G \times 3l$ to $s \times l$) as shown in the Figure 1.3 .

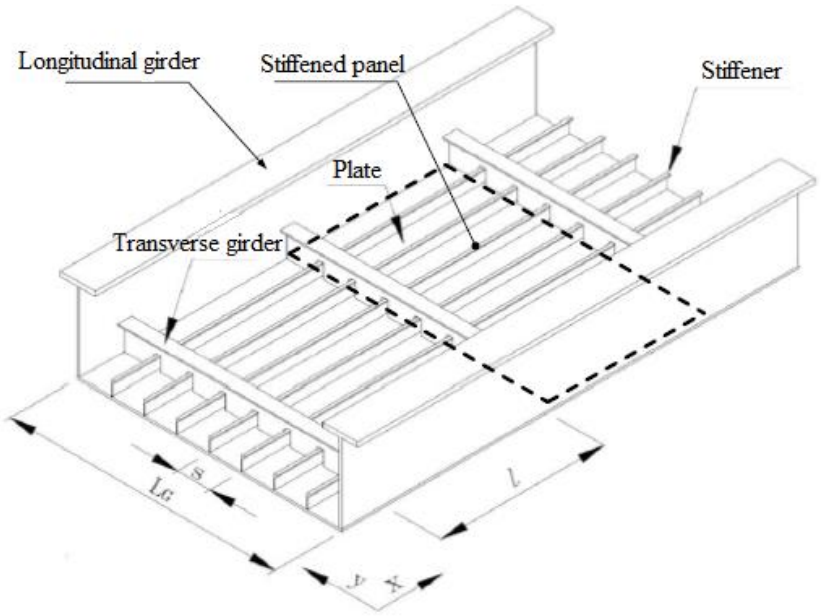

Figure 1.3: From $\mathbf{L_G \times 3l}$ to $\mathbf{s \times l}$

As a result, the requirements of the regulations of the classification, for the bending of the plates, are satisfied. The optimized solution, regarding the weight of the panel, requires the use of longitudinal and transverse girders with large cross sections and long distances L_G or l . The construction elements between two longitudinal and two transverse girders and are supported by stiffeners of small cross section are called stiffened panels. The diploma thesis deals with topics of stiffened panels under uniform pressure loads studying the bending of stiffeners along with the attached plate.

The hull structure consists of stiffened panels; bottom construction, side shell construction and upper deck construction for a variety of types of ships, such as tankers and bulk carriers. Typical cross sections of stiffeners in shipbuilding industry are depicted in Figure 1.4.

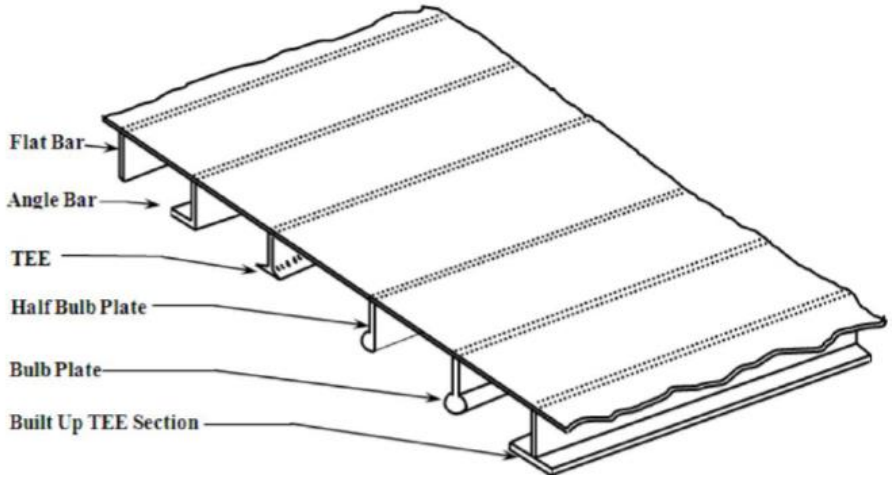

Figure 1.4: Typical cross sections of stiffeners

The double bottom consists of grillage beams of I profile between of them, stiffened panels are found, as shown in Figure 1.5. The girders, which extend along the longitudinal axis of the ship, constitute the web and the flanges are the attached plates which are found in inner and outer bottom. The inner bottom (upper flange) is subjected to the weight of the transferred cargoes and the outer bottom (bottom flange) to hydrostatic and hydrodynamic pressure. The difference of these pressure loads is transferred to the girders as shear forces. As a result, curvature is appeared to the double bottom.

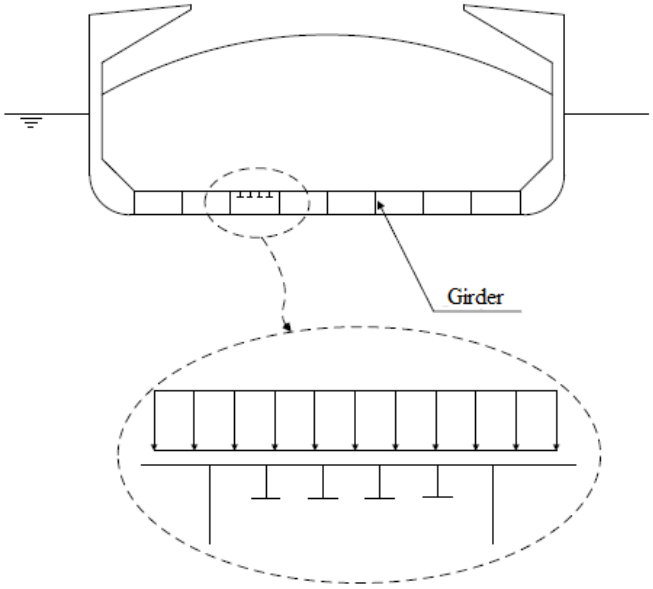

Figure 1.5: Uniform pressure subjected to the stiffened panels of inner bottom

The floors, which extend across the width of the ship, reinforce the double bottom to the transverse direction. The stiffened panels, between girders and floors, are subjected to vertical pressure loads. In order to evaluate the strength of the stiffened panels, the stresses are categorized to secondary and tertiary. The secondary stresses are calculated considering the stiffeners along with the attached plate as a beam. Applying the theory of bending of beams, we can take a good estimation. The tertiary stresses are calculated considering the bending of the plate between the stiffeners.

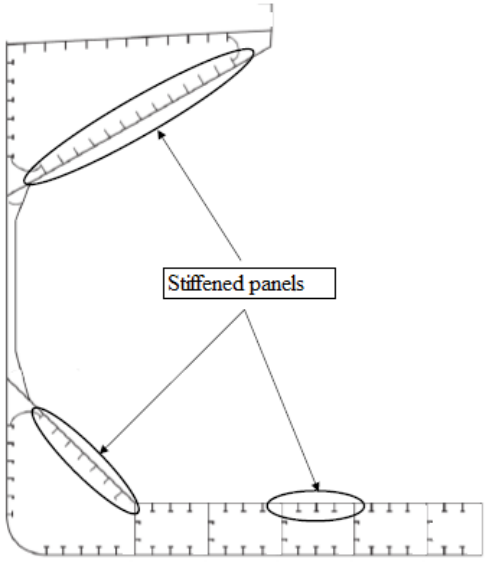

Figure 1.6: Stiffened panels for a bulk carrier

1.2 Aims and scope of work

This diploma thesis deals with topics concerning the secondary stresses of stiffened panels under uniform pressure loads and has two main objectives. The first is to assess bending of one-way stiffened panels due to uniform pressure by theoretical and numerical methods. For stiffened panels, due to the shear lag phenomenon which is described in the following chapters, the theory of bending underestimates the stresses. The scope is to be examined both theoretical and numerical modeling strategies to evaluate the stresses of the stiffeners with the attached plate of each method. The theoretical modeling strategies consider the shear lag phenomenon and at the end the most safe and conservative method is suggested. For numerical modeling strategies, the commercial software of Finite Element Analysis, Abaqus, is used, in order to examine the appropriate element for analysis of secondary stresses. The second objective is to simplify bending of cross-stiffened panels by downsizing the problem to bending in one direction and hence using Euler's bending theory. The scope is to study the secondary stresses of the longitudinal stiffeners between of the transverse stiffeners with aim to find a relation for the boundary conditions across the transverse stiffeners that are applied to longitudinal stiffeners. Calculating the stresses and the boundary conditions in each case, it is feasible to assess the design variables, namely the thickness of the plate and the dimensions of the stiffeners.

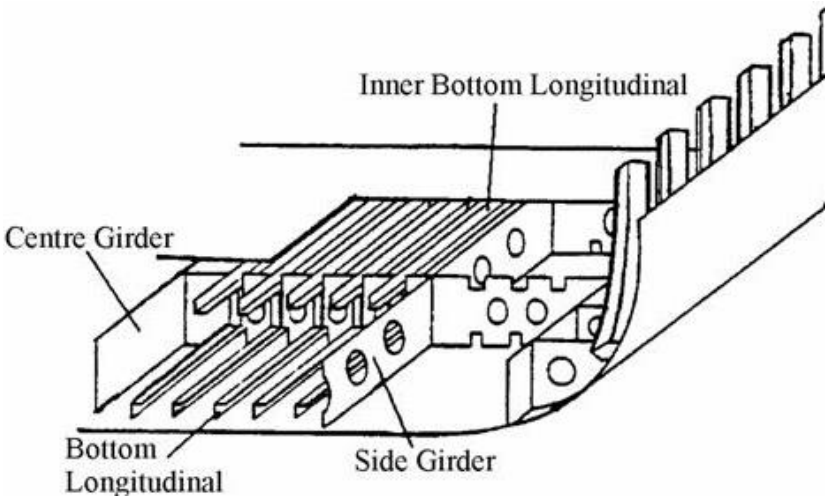

Figure 1.7: One-way stiffened panel in double bottom

2. Theoretical background

2.1 Theory of stiffened panels – 1D stiffening

This subchapter discusses topics of strength of stiffened panels that are subjected to vertical loads examining the bending of stiffeners along with the attached width of the plate. Considering the periodicity of the geometry and the stress field, the stiffened panel can be examined to a beam of equivalent cross section (see Figure 2.1) to apply the theory of the bending of beams. The distribution of axial stresses, according to the bending theory, can be calculated according to the formula:

$$\sigma_x(z) = -\frac{M_y}{I_y} z \tag{2.1}$$

This relation, from Euler-Bernoulli theory of the bending of beams, ignores the warping of cross section due to the shear stresses. The warping has as a result the increase of the real distribution of axial stresses. This mechanical behavior is the basis for shear lag phenomenon. Numerical simulations and experimental measurements conclude that the real distribution of axial stresses is non linear along the width of attached plate due to shear lag effect.

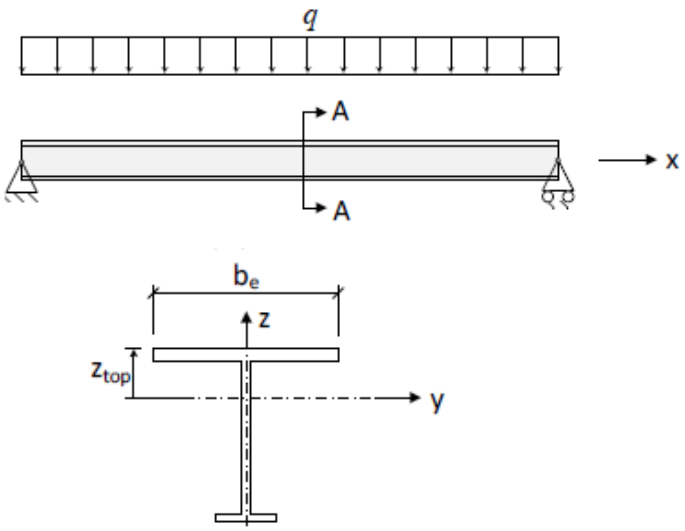

Figure 2.1: Reduction from stiffened panels to a beam of equivalent cross section.

2.1.1 Beam theory

When analyzing beams, it is necessary to distinguish between pure bending and non uniform bending. Pure bending is defined a flexure of a beam under a constant bending moment that occurs under the presence of force couple. Therefore, pure bending occurs only in regions of a beam where the shear force is zero. On the other hand, non uniform bending that occurs due to presence of concentrated or distributed loads is defined as the flexure in the presence of shear forces, which means that the bending moment is not constant as we move along the axis of the beam.

In pure bending, the resulting strains and stresses in the beam are directly related to the curvature of the deflection curve, with radius of curve ρ (see Figure 2.2) and vary linearly with distance from the neutral surface regardless of the shape of the stress-strain curve of material. The neutral axis passes through the centroid of the cross sectional area when the material follows Hooke's law and there is no axial force acting on the cross section. The axial stresses remain constant along the x-axis and vary only with the height of cross section. The maximum tensile and compressive bending stresses acting at any given cross section occur at points located farthest from the neutral axis.

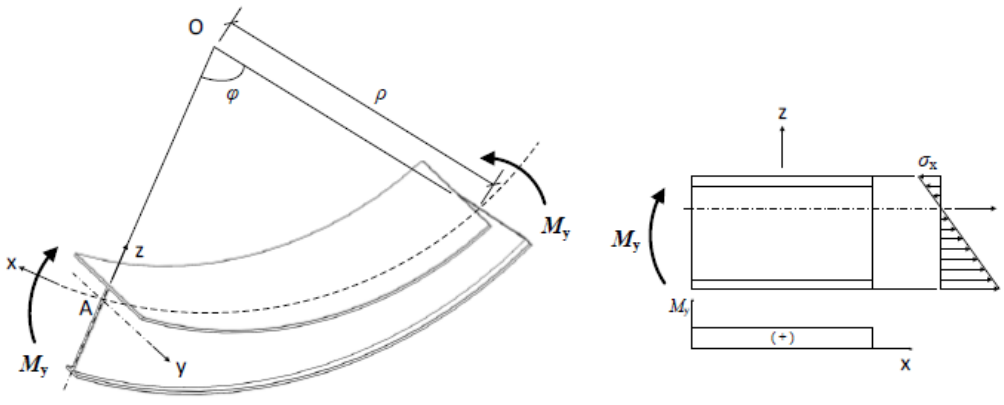

Figure 2.2: Pure bending of a beam

In non uniform bending, under the presence of vertical loads, the beams (the stiffeners along with the attached width of plate) are used to receive these vertical loads (see Figure 2.3). Examining the static equilibrium of a section Δx of the beam ($\Sigma F_z = 0$), the relation that results between the shear force V and the distribution of the vertical load w, is:

$$\frac{dV}{dx} = -w \tag{2.2}$$

Integrating the equation (2.2) between A and B, it results that:

$$V_B - V_A = -\int_{x_A}^{x_B} w\, dx \tag{2.3}$$

Examining the equilibrium of moment ($\Sigma M = 0$), the relation that results between the bending moment M and the shear force V, is:

$$\frac{dM}{dx} = V \tag{2.4}$$

Integrating the equation (2.4) between A and B, it results that:

$$M_B - M_A = -\int_{x_A}^{x_B} V\, dx \tag{2.5}$$

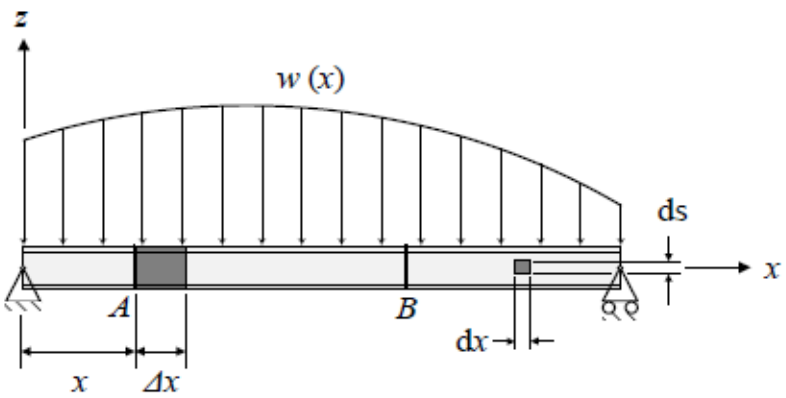

Figure 2.3: Beam under the presence of vertical loads

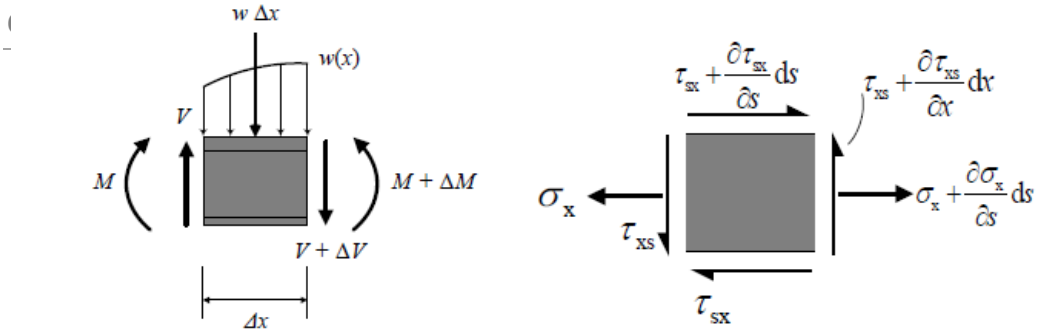

Figure 2.4: Stress field due to shear force and bending moment

Examining an infinitesimal element with dimensions dxds (see Figure 2.4), we conclude that the static equilibrium of forces ($\Sigma F = 0$) prerequisites the presence of shear stress field τ_{sx}. The equation of equilibrium of stresses is:

$$\frac{\partial \sigma_x}{\partial x} + \frac{\partial \tau_{sx}}{\partial s} = 0 \tag{2.6}$$

The equilibrium of moments ($\Sigma M = 0$) prerequisites the presence of shear stresses τ_{xs} that are equal with τ_{sx} and tangent to vertical side ds. It results that:

$$t\frac{\partial \sigma_x}{\partial x} + \frac{\partial q}{\partial s} = 0 \tag{2.7}$$

where $q = \tau_{sx}\, t$ and is called shear flow. It is considered that the distribution of shear stresses along the thickness of the element remain constant. Substituting the axial stress σ_x with the formula that is given by the theory of pure bending, it results that:

$$-t\frac{\partial M_y}{\partial x}\frac{z}{I_y} + \frac{\partial q}{\partial s} = 0 \tag{2.8}$$

Applying the equation (2.4) to (2.8), it results that:

$$\frac{\partial q}{\partial s} = \frac{V}{I_y}\, t\, z \tag{2.9}$$

Integrating the equation (2.9), it results that:

$$q_s - q_o = \frac{V}{I_y}\int_0^s t\bar{z}ds \tag{2.10}$$

Alternatively:

$$\Delta q = \frac{VQ}{I_y} \tag{2.11}$$

where $Q = \int_0^s t\bar{z}ds$ is the first moment of inertia of the cross section. With the equation (2.11), we can calculate the distribution of shear stress to the cross section because of the zeroing of the shear stress at free edges of the cross section. In Figure 2.5, it is observed that the location of maximum shear flow is along the web q_w , that ascertains that the web is the structural element of a cross section which receive the vertical loads. The attached width of the plate and the flange develop shear flow q_p and q_f. However, the web has the biggest contribution to receive the shear stresses.

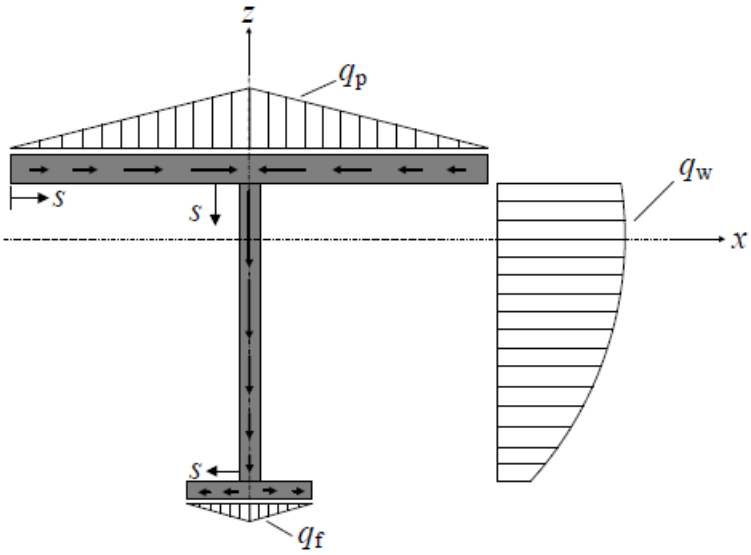

Figure 2.5: Distribution of shear flow along the cross section

2.1.2 Shear lag

According to the analysis that was described, it can be concluded that the beams that are subjected to vertical loads develop both bending moment and shear stresses. Examining discrete structures, where the width of flange is small, the effect of shear stresses can be neglected. However, in case that we examine the strength of stiffened panels, considering equivalent with prismatic beam, the effect of shear stresses cannot

be neglected as the shear lag phenomenon can result to material failure. The increase of the equidistant *s* between the stiffeners, can result to an equivalent cross section with big attached width of plate. As a result, the flange has more contribution to the receipt of shear stresses τ_{xy} . The non uniform shear stress field results to the warping of the attached plate (see Figure 2.6). The shear stresses τ lead to the development of shear strains γ. This results to the change of the angle of an infinitesimal element and to the elongation *e* of the fibers of flanges. The prerequisite for the elongation of the fibers, due to planar shear, is that $\frac{\partial \tau}{\partial x} \neq 0$. The non uniform elongation *e* is added to the uniform elongation *u*, due to pure bending.

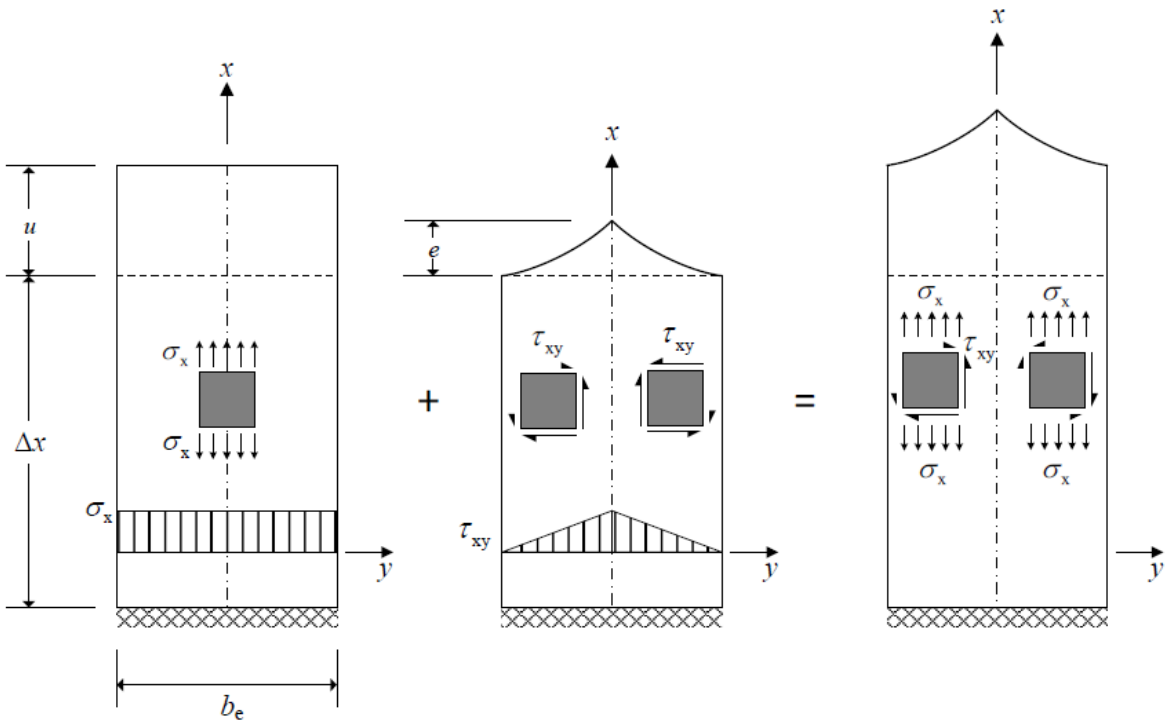

Figure 2.6: Depiction of the stress field that is developed to the attached plate

As a result, the real distribution of the stresses in the flange is non linear (see Figure 2.7). The shear lag phenomenon occurs to thin-walled cross sections that receive both shear stresses and axial stresses due to the bending. The shear lag phenomenon occurs

even to the cross section of the ship (see Figure 2.8), but it can be neglected for most of the ships where L/B > 5 (where L the length and B the width of the ship).

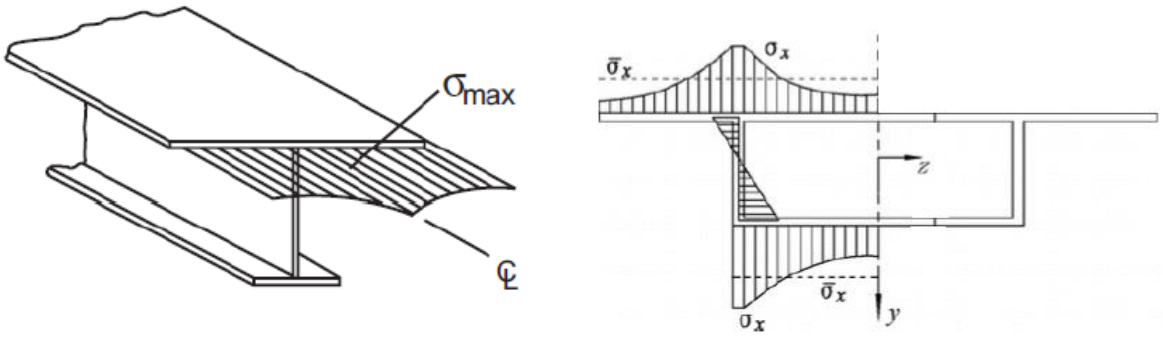

Figure 2.7: Real distribution of axial stresses to thin-walled cross sections

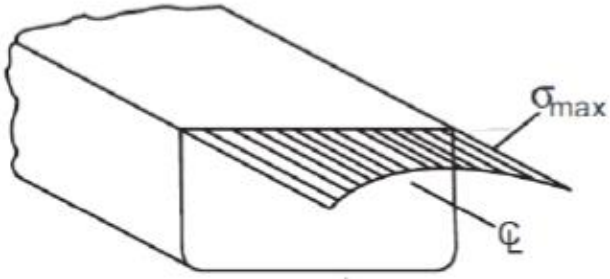

Figure 2.8: Real distribution of axial stresses to the bottom of a ship

The plate effectiveness, regardless of the reason of the non uniform distribution, is characterized by a parameter b_e which is a width over which the maximum membrane stress at the intersection of the flange and web is considered to occur uniformly. Thus the total stress carried in effective width being the same as that applied by the actual non uniform distribution across the flange. The effective width b_e can be evaluated by:

$$\mathrm{b_e} = \frac{\int_{-\mathrm{b}/2}^{\mathrm{b}/2} \sigma_x \mathrm{dy}}{\sigma_{x\,max}} = \mathrm{b}\frac{\sigma_{xav}}{\sigma_{x\,max}} \qquad (2.12)$$

where σ_x = non uniform membrane stress, σ_{xav} = average stress, $\sigma_{x\,max}$ = maximum membrane stress at plate/web junctions.

2.1.3 Analytical solution of Paik

An analytical formulation of the effective width for a plate-beam combination under shear lag is now derived. To compute the stress distribution, the classical theory of elasticity can be applied. For two dimensional problems, the relation between strains and displacements is given by:

$$\varepsilon_x = \frac{\partial u}{\partial x}, \qquad \varepsilon_y = \frac{\partial v}{\partial x}, \qquad \gamma_{xy} = \frac{\partial u}{\partial y} + \frac{\partial v}{\partial x} \tag{2.13}$$

where ε_x , ε_y is the normal strain in the *x* and *y* direction, γ_{xy} the shear strain and *u*, *v* the displacements in the x and y direction.

The relationship between stresses and strains for two dimensional problems is given by:

$$\varepsilon_x = \frac{1}{E}(\sigma_x - \nu\sigma_y), \qquad \varepsilon_y = \frac{1}{E}(\sigma_y - \nu\sigma_x), \qquad \gamma_{xy} = \frac{2(1+\nu)}{E}\tau_{xy} \tag{2.14}$$

where τ_{xy} the shear stress and *v* the Poisson's ratio.

The stress distribution of two dimensional problems can be obtained by solving the following compatibility equation:

$$\frac{\partial^4 F}{\partial x^4} + 2\frac{\partial^4 F}{\partial x^2 \partial y^2} + \frac{\partial^4 F}{\partial y^4} = 0 \tag{2.15}$$

where F is Airy's stress function which satisfies that:

$$\sigma_x = \frac{\partial^2 F}{\partial y^2}, \qquad \sigma_y = \frac{\partial^2 F}{\partial x^2}, \qquad \tau_{xy} = -\frac{\partial^2 F}{\partial x \partial y} \tag{2.16}$$

In order to calculate the non uniform stress in the attached plating, it is assumed that the plate lateral deflection is proportional to $\sin(\frac{2\pi x}{\omega})$ where ω is the deflection wave length depending on the rigidities of the stiffener and the type of load application. For stiffeners that are used in marine structures, we take $\omega = L$. In this case, the

longitudinal axial displacement u along the plate/web intersection, namely for $y = \pm b/2$ (see Figure 2.9), can be calculated as follows:

$$u = u_0 \cos\frac{2\pi x}{\omega} \tag{2.17}$$

where u_0 is the amplitude of axial displacement function.

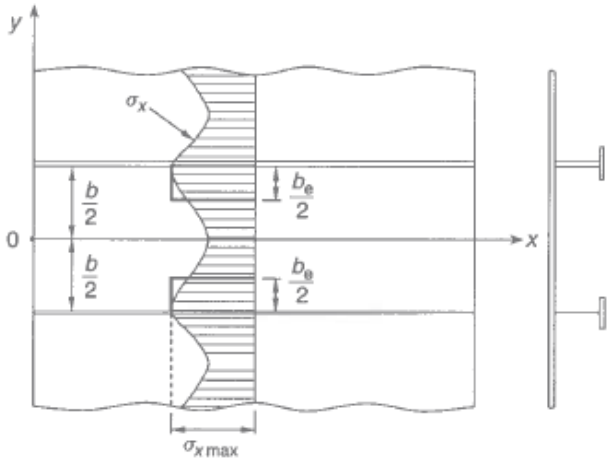

Figure 2.9: Effective width of the attached plating in a stiffened panel

The axial strain ε_x at $y = \pm b/2$ can be calculated as follows:

$$\varepsilon_x|_{y=\pm b/2} = \frac{\partial u}{\partial x}\Big|_{y=\pm b/2} = \varepsilon_0 \sin\frac{2\pi x}{\omega} \quad where\ \varepsilon_0 = u_0(\frac{2\pi}{\omega}) \tag{2.18}$$

The stress function F, to satisfy the equation (2.15) can be expressed as follows:

$$F = f(y) \sin\frac{2\pi x}{\omega} \tag{2.19}$$

where

$$f(y) = C_1 \frac{2\pi y}{\omega} \sinh\frac{2\pi y}{\omega} + C_2 \cosh\frac{2\pi y}{\omega} \tag{2.20}$$

with C_1, C_2 to be constants which are determined by the boundary conditions.

While equation (2.18) can be one boundary condition, the other one is provided so that the symmetric condition must be attained along the center line of the attached plating between two adjacent stiffeners, which is given by:

$$\left.\frac{\partial \mathrm{v}}{\partial \mathrm{x}}\right|_{y=0} = 0 \tag{2.21}$$

By substituting equation (2.16) into equation (2.14) the axial stress ε_x can be expressed as follows:

$$\varepsilon_x = \frac{1}{E}\left(\frac{\partial^2 \mathrm{F}}{\partial y^2} - \nu\frac{\partial^2 \mathrm{F}}{\partial x^2}\right) \tag{2.22}$$

By substituting equation (2.19) into equation (2.22) and considering equation (2.18), the first boundary condition can be expressed as follows:

$$\frac{\mathrm{d}^2\mathrm{f(y)}}{\mathrm{dy}^2} + \nu\omega^2\mathrm{f(y)} = \mathrm{E}\varepsilon_0 \quad \text{at y} = \pm\frac{\mathrm{b}}{2} \tag{2.23}$$

Using equation (2.13), the second boundary condition can be rewritten as follows:

$$\frac{\partial \gamma_{xy}}{\partial x} = \frac{\partial^2 \mathrm{u}}{\partial x \partial y} + \frac{\partial^2 \mathrm{v}}{\partial x^2} = \frac{\partial^2 \mathrm{u}}{\partial x \partial y} = \frac{\partial \varepsilon_x}{\partial y} \quad \text{at } y = 0 \tag{2.24}$$

Substituting equations (2.13), (2.14), (2.16), (2.19) into equation (2.24), the second boundary condition becomes as follows:

$$\frac{\mathrm{d}^3\mathrm{f(y)}}{\mathrm{dy}^3} - (2+\nu)\omega^2\frac{\mathrm{df(y)}}{\mathrm{dy}} = 0 \quad \text{at y} = 0 \tag{2.25}$$

By substituting f(y), equation (2.19), into equation (2.23) and (2.25), we get that:

$$C_1 = E\varepsilon_0\left(\frac{\omega}{2\pi}\right)^2\left[\left(\frac{3-\nu}{2}\right)\sinh\frac{2\pi b}{\omega} - (1+\nu)\frac{\pi b}{\omega}\right]^{-1}\sinh\frac{\pi b}{\omega}$$

$$C_2 = E\varepsilon_0\left(\frac{\omega}{2\pi}\right)^2\left[\left(\frac{3-\nu}{2}\right)\sinh\frac{2\pi b}{\omega} - (1+\nu)\frac{\pi b}{\omega}\right]^{-1}\left[\left(\frac{1-\nu}{1+\nu}\right)\sinh\frac{\pi b}{\omega} - \frac{\pi b}{\omega}\cosh\frac{\pi b}{\omega}\right]$$

The membrane stress σ_x can now be expressed as follows:

$$\sigma_x = \left(\frac{2\pi}{\omega}\right)^2\left[C_1\frac{2\pi y}{\omega}\sinh\frac{2\pi y}{\omega} + (2C_1 + C_2)\cosh\frac{2\pi y}{\omega}\right]\sin\frac{2\pi x}{\omega} \tag{2.26}$$

By substituting equation (2.26) into equation (2.12), the effective width b_e can be calculated as follows:

$$\mathrm{b_e} = \frac{4\omega\left(\sinh\frac{\pi b}{\omega}\right)^2}{\pi(1+\nu)\left[(3-\nu)\sinh\frac{2\pi b}{\omega} - 2(1+\nu)\frac{\pi b}{\omega}\right]} \tag{2.27}$$

Equation (2.27) can be approximated as follows:

$$\frac{\mathrm{b_e}}{\mathrm{b}} = \begin{cases} 1.0 & \text{for } \mathrm{b}/\omega \le 0.18 \\ 0.18\mathrm{L}/\mathrm{b} & \text{for } \mathrm{b}/\omega \le 0.18 \end{cases} \tag{2.28}$$

The wave length ω may approximately be taken as ω=L for the attached plating between two stiffener transverse frames. In Figure 2.10 is depicted the variation of effective width from equations (2.27) and (2.28) versus the ratio of stiffener spacing to the beam span when ω=L. It is seen that the normalized effective width significantly decreases as the breadth of the attached plating becomes wider or the span length becomes longer.

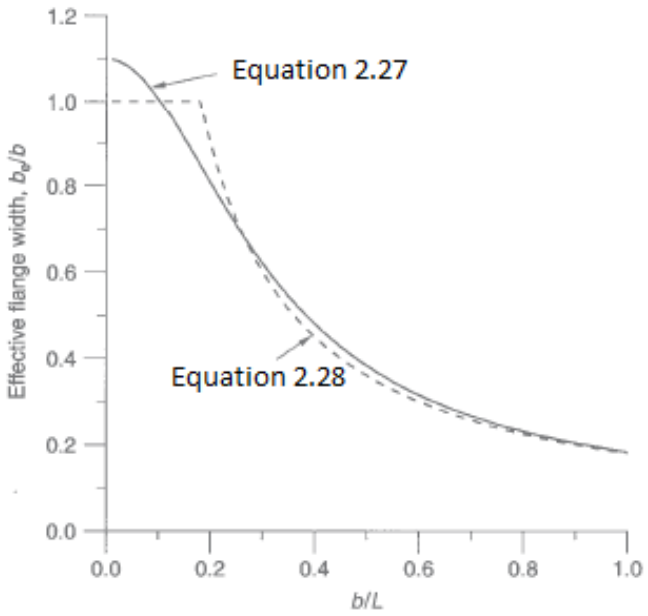

Figure 2.10: Variation of the effective width versus the ratio of stiffener spacing to the beam span when ω=L.

2.1.4 Analytical solution of Schade

In Figure 2.11 an alternative curve of calculation of effective width b_e is given. The parameters of calculation are the type of cross section, the point of interest along the beam, the boundary conditions, the linear distribution of the load, the relations of the dimensions of the cross section, the ratio of width of flange to length of the beam and the ratio of width attached plating to distance L_0 of points along the beam, that the bending moment is zero. In case of the beam that are simply supported, L_0 equates to the length of the beam.

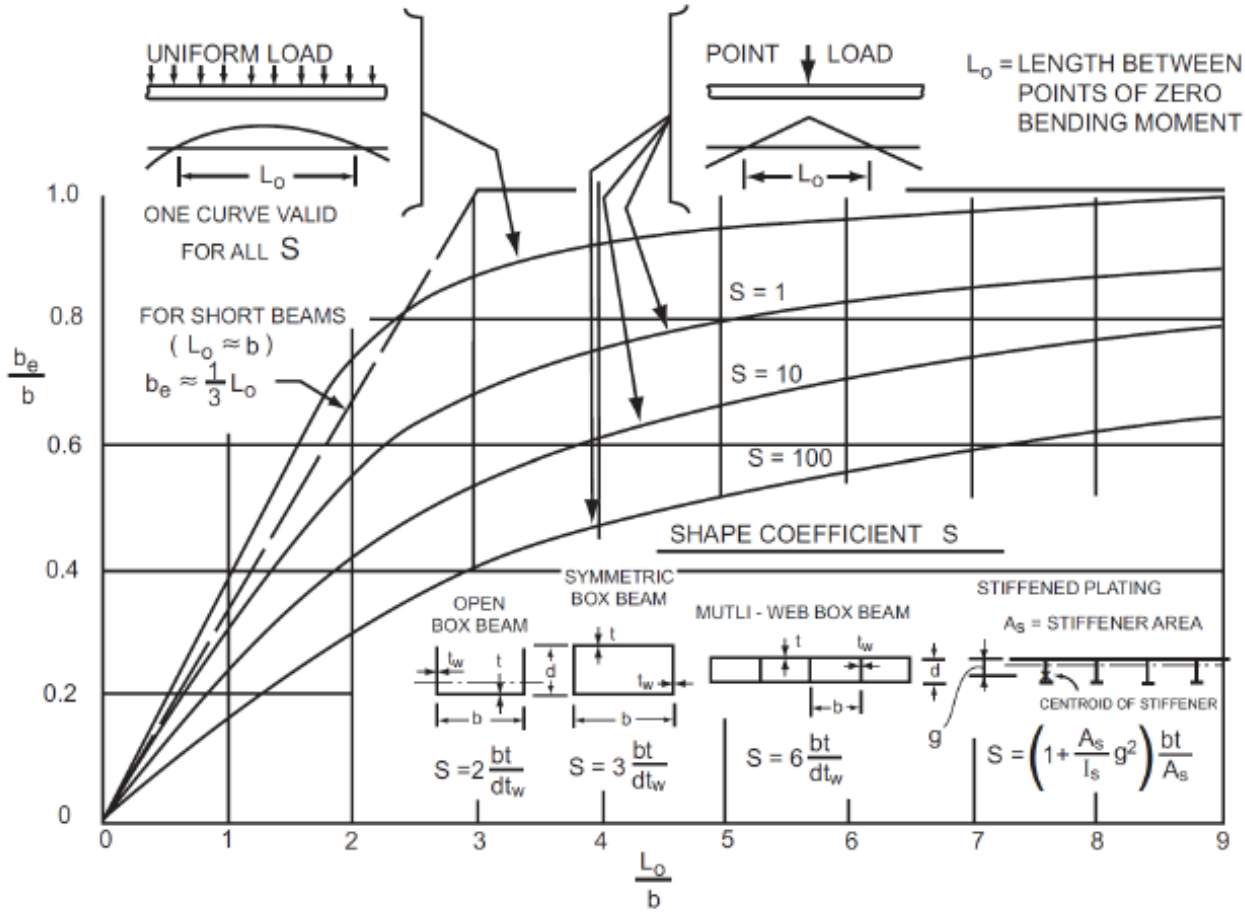

Figure 2.11: Shade curves

2.2 Finite element analysis

This subchapter discusses topics of finite element method for beams, shells and solids. In the finite element method, a structure is discretized into structural parts

called finite elements. The points where the finite elements are interconnected are known as nodes and the process in specifying the nodes is known as modeling. The whole collection of elements is termed mesh. Each node is associated to nodal forces and nodal displacements. A system of equilibrium equations between nodal forces and displacements can be formulated in matrix form for the whole structure, that is:

$$\{F\} = [K]\{U\} \tag{2.29}$$

The first step to obtain nodal displacements and forces with the finite element method is the determination of the global stiffness matrix $[K]$. This can be achieved with one of the following methodologies and principles:

a. Equilibrium
b. Total Potential Energy Principle
c. Principle of Virtual Work
d. Galerkin Weighted Residual

The concept of equilibrium method is to satisfy equilibrium for each element and for the system as a whole and it will be applied for beam elements. Energy methods can are used to design systems with a large number of degrees of freedom. The total potential energy principle applies only to linear elastic materials and it will be applied for shell and solid elements. The principle of virtual work and Galerkin weighted residual applies to any material behavior.

2.2.1 Beams

Beams can undertake tensile or compressive forces, transverse forces and bending moments. So, beam experience axial deformation, transverse deformations and rotations associated with bending moments and shear forces. In order to examine a slender structural member as a beam, there is the prerequisite that the length is much greater than the width and the height of the cross section. According to Euler-Bernoulli theory, the length between the supports must be at least ten times greater than the other two dimensions.

The beam element stiffness equation is derived using the method of equilibrium and bending theory based on Euler-Bernoulli assumptions. The assumptions are the followings:

a. The plane sections initially normal to the longitudinal axis of the beam remain plane and normal to the deflected axis after bending.
b. The deformed beam angles are small.
c. The deflections are small compare to the height of the beam.

Initially, we will consider a beam with two degrees of freedom per node that is the transverse displacement v_1 and rotation θ_1 for the first node and transverse displacement v_2 and rotation θ_2 for the second node (see Figure 2.12). Because the beam has four degrees of freedom, the element stiffness matrix will be 4x4.

Figure 2.12: Beam with four degrees of freedom

The formulation of stiffness matrix according to equilibrium method is now derived. The moment m at a cross section can be calculated as follows:

$$m = -EI\frac{d^2v}{dx^2} \tag{2.30}$$

The equilibrium condition for vertical forces gives that:

$$f_1 = f_2 \tag{2.31}$$

The equilibrium condition for moments gives that:

$$m_1 = m_2 + f_2 L \tag{2.32}$$

$$m(x) = m_1 - f_1 x \tag{2.33}$$

By substituting equation (2.30) into (2.33), we get that:

$$\frac{d^2v}{dx^2} = -\frac{1}{EI}(m_1 - f_1 x) \tag{2.34}$$

Integrating the equation (2.34) two times, we get that :

$$\frac{dv}{dx} = -\frac{m_1 x}{EI} + \frac{f_1 x^2}{2EI} + \theta_1 \tag{2.35}$$

$$v = -\frac{m_1 x^2}{2EI} + \frac{f_1 x^3}{6EI} + \theta_1 x + v_1 \tag{2.36}$$

By substituting $x = L$ into equations (2.35) and (2.36), we get that:

$$\left.\frac{dv}{dx}\right|_{x=L} = -\frac{m_1 x}{EI} + \frac{f_1 x^2}{2EI} + \theta_1 = \theta_2 \tag{2.37}$$

$$v|_{x=L} = -\frac{m_1 L^2}{2EI} + \frac{f_1 L^3}{6EI} + \theta_1 x + v_1 = v_2 \tag{2.38}$$

Solving equations (2.37) and (2.38), f_1 and m_1 can be calculated as follows:

$$f_1 = f_2 = \frac{12EI}{L^3}\left[(\theta_2 - \theta_1)\frac{L}{2} - (v_2 - v_1)\right] \tag{2.39}$$

$$m_1 = \frac{6EI}{L^2}\left[(\theta_2 + 2\theta_1)\frac{L}{3} - (v_2 - v_1)\right] \tag{2.40}$$

By substituting equation (2.40) into equation (2.33) we get that:

$$m_2 = \frac{6EI}{L^2}\left[-(2\theta_2 + \theta_1)\frac{L}{3} + (v_2 - v_1)\right] \tag{2.41}$$

The equation (2.29) can now be written as follows:

$$\begin{Bmatrix} f_1 \\ m_1 \\ f_2 \\ m_2 \end{Bmatrix} = \frac{EI}{L^3}\begin{bmatrix} 12 & 6L & -12 & 6L \\ 6L & 4L^2 & -6L & 2L^2 \\ -12 & -6L & 12 & -6L \\ 6L & 2L^2 & -6L & 4L^2 \end{bmatrix}\begin{Bmatrix} v_1 \\ \theta_1 \\ v_2 \\ \theta_2 \end{Bmatrix} \tag{2.42}$$

According to Timoshenko beam theory, the cross section is not perpendicular to the bending line. The model takes into account shear deformation. The relation between forces and displacements can be expressed as follows:

$$\begin{Bmatrix} f_1 \\ m_1 \\ f_2 \\ m_2 \end{Bmatrix} = \frac{EI}{L^3}\begin{bmatrix} 12 & 6L & -12 & 6L \\ 6L & (4+\Phi)L^2 & -6L & (2-\Phi)L^2 \\ -12 & -6L & 12 & -6L \\ 6L & (2-\Phi)L^2 & -6L & (4+\Phi)L^2 \end{bmatrix}\begin{Bmatrix} v_1 \\ \theta_1 \\ v_2 \\ \theta_2 \end{Bmatrix} \tag{2.43}$$

where $\Phi = 12EI/GA_SL^2$ and A_S is the shear coefficient of the cross section.

Considering a beam with three degrees of freedom per node that is axial and transverse displacement and rotation, the element as a whole has six degrees of freedom and the stiffness matrix will be 6x6 (see Figure 2.13).

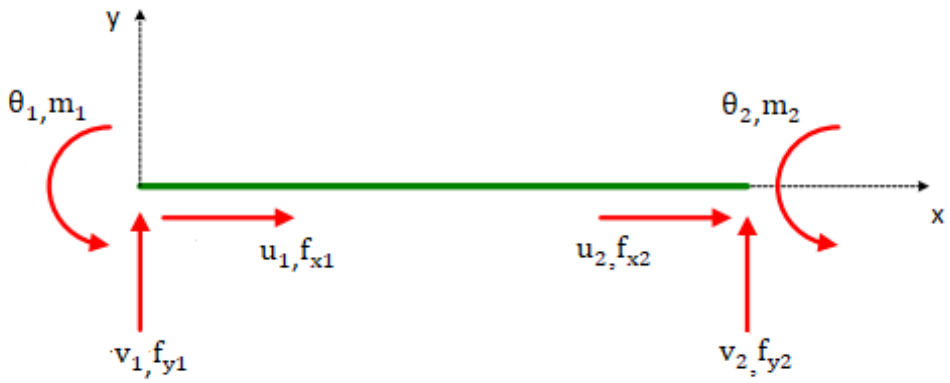

Figure 2.13: Beam with six degree of freedoms

The relationship between axial forces and displacements is:

$$f_{x1} = -\frac{EA}{L}(u_2 - u_1) \tag{2.44}$$

$$f_{x2} = \frac{EA}{L}(u_2 - u_1) \tag{2.45}$$

The equation (2.29) can now be written as follows:

$$\begin{Bmatrix} f_{x1} \\ f_{y1} \\ m_1 \\ f_{x2} \\ f_{y2} \\ m_2 \end{Bmatrix} = \frac{EI}{L^3}\begin{bmatrix} s^2 & 0 & 0 & -s^2 & 0 & 0 \\ 0 & 12 & 6L & 0 & -12 & 6L \\ 0 & 6L & 4L^2 & 0 & -6L & 2L^2 \\ -s^2 & 0 & 0 & s^2 & 0 & 0 \\ 0 & -12 & -6L & 0 & 12 & -6L \\ 0 & 6L & 2L^2 & 0 & -6L & 4L^2 \end{bmatrix}\begin{Bmatrix} u_1 \\ v_1 \\ \theta_1 \\ u_2 \\ v_2 \\ \theta_2 \end{Bmatrix} \tag{2.46}$$

where $s = \sqrt{AL/I}$

The relations between of the local system x-y and the global coordinate system X-Y will now be given.

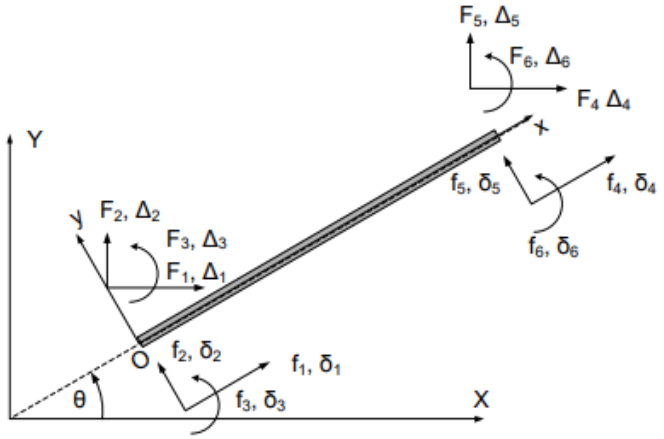

Figure 2.14: Inclined beam element

Nodal displacement in the local system can be expressed with respect to displacements in global system as given by:

$$\begin{Bmatrix} \delta_1 \\ \delta_2 \\ \delta_3 \\ \delta_4 \\ \delta_5 \\ \delta_6 \end{Bmatrix} = \begin{bmatrix} [r] & 0 \\ 0 & [r] \end{bmatrix} \begin{Bmatrix} \Delta_1 \\ \Delta_2 \\ \Delta_3 \\ \Delta_4 \\ \Delta_5 \\ \Delta_6 \end{Bmatrix} \tag{2.47}$$

where $[r] = \begin{bmatrix} \cos\theta & \sin\theta & 0 \\ -\sin\theta & \cos\theta & 0 \\ 0 & 0 & 1 \end{bmatrix}$

The relationship between the nodal forces can be expressed as follows:

$$\begin{Bmatrix} f_1 \\ f_2 \\ f_3 \\ f_4 \\ f_5 \\ f_6 \end{Bmatrix} = \begin{bmatrix} [r] & 0 \\ 0 & [r] \end{bmatrix} \begin{Bmatrix} F_1 \\ F_2 \\ F_3 \\ F_4 \\ F_5 \\ F_6 \end{Bmatrix} \tag{2.48}$$

The element stiffness matrix [K] expressed in the global coordinate system X-Y is related to [k], as follows:

$$[K] = [R]^T[k][R] \tag{2.49}$$

where $[R] = \begin{bmatrix} [r] & 0 \\ 0 & [r] \end{bmatrix}$

2.2.2 Plates and Shells

The main difference between plates and shells, which both are two dimensional structures, is the shape of their mid-surface. The mid-surface of plates is plane, while the mid-surface of shells is curved. The deformations of these two elements are expressed with reference to their mid-surface. Plates and shell structures are categorized to thin and thick. A plate is considered thin, if its thickness is fifteen times smaller than the shortest span length. The criterion for shell structures is the ratio of their thickness over the radius of curvature.

For finite element analysis, these elements should be connected to each other only at their nodal points. A suitable number of nodal points and proper shape functions can satisfy continuity requirements. The displacement distribution should also maintain internal or interelement compatibility and continuity of nodal displacements.

The method of total potential energy is now derived. Considering a structural system subjected to external loads, the internal forces produce work called strain energy and the external forces produce work called load potential. The strain energy W can be expressed as follows:

$$W = \frac{1}{2}\int \{\sigma\}^T\{\varepsilon\}dV \tag{2.50}$$

The load potential Ω is given by:

$$\Omega = -\int \{T\}^T\{u\}dA \tag{2.51}$$

where {T} are the external loads applied on the boundary surface.

The total potential energy U of the system is given by:

$$U = W + \Omega \tag{2.52}$$

The structural system is in equilibrium when the total potential energy is minimum, namely:

$$\frac{\partial U}{\partial u} = 0 \tag{2.53}$$

where $u(x)$ can be calculated by the summation of shape functions $N_i(x)$ multiplied by the nodal displacements u_i, namely:

$$u(x) = \sum_i N_i(x) u_i \tag{2.54}$$

For the linear case of axial deformation, the relation between strain and displacement can be expressed as follows:

$$\{\varepsilon\} = [B]\{u\} = \sum_i \frac{\partial N_i}{\partial x} \{u\} \tag{2.55}$$

The relation between stress and strain is given by:

$$\{\sigma\} = [C]\{\varepsilon\} \tag{2.56}$$

where the matrix $[C]$ contains the elastic constants. By substituting equations (2.52), (2.55) and (2.56) into equation (2.53), we get that:

$$\int [B]^T [C][B]\{u\} dV - \int \{T\}^T [N] dA = 0 \tag{2.57}$$

Thus, the expressions for the stiffness matrix $[k]$ and the force vector $\{f\}$ are:

$$[k] = \int [B]^T [C][B] dV \tag{2.58}$$

$$\{f\} = \int \{T\}^T [N] dA \tag{2.59}$$

The behavior of thin plates is based on the classical theory on plate bending of Kirchhoff. The assumptions of the theory are the following:

1. Deflections are small compared to plate thickness.
2. Slopes of the deflected mid-surface are small.
3. Mid-surface remains unstrained for bending.
4. Plane sections initially normal to mid-surface remain plain and normal to the deflected surface.
5. Transverse shear strains are negligible.
6. Stresses normal to mid-surface are negligible.

Considering a plate subjected to a distributed load p_z, due to the assumptions of plate bending theory, the stress-strain relations are given by:

$$\sigma_x = \frac{E}{1-\nu^2}\left(\varepsilon_x + \nu\varepsilon_y\right) \tag{2.60}$$

$$\sigma_y = \frac{E}{1-\nu^2}\left(\varepsilon_y + \nu\varepsilon_{yx}\right) \tag{2.61}$$

$$\tau_{xy} = G\,\gamma_{xy} \tag{2.62}$$

The relation between strain, curvature and displacement is given by:

$$\varepsilon_x = -z\kappa_x = -z\frac{\partial^2 w}{\partial x^2} \tag{2.63}$$

$$\varepsilon_y = -z\kappa_y = -z\frac{\partial^2 w}{\partial y^2} \tag{2.64}$$

$$\gamma_{xy} = -2\,z\,\kappa_{xy} = -2\,z\frac{\partial^2 w}{\partial x\,\partial y} \tag{2.65}$$

Using the method of potential energy, the load potential can now be expressed as follows:

$$\Omega = -\int \{T\}^T\{u\}dA = \Omega = -\int p_z\,w\,dA \tag{2.66}$$

The strain energy can be written:

$$W = \frac{1}{2}\int \{\sigma_x \quad \sigma_y \quad \tau_{xy}\} \begin{Bmatrix} \varepsilon_x \\ \varepsilon_y \\ \gamma_{xy} \end{Bmatrix} dV = \frac{1}{2}\int \{\kappa\}^T [C]\{\kappa\} dA \tag{2.67}$$

Where the matrix $[C]$ and $\{\kappa\}$ are given by:

$$[C] = \frac{Et^3}{12(1-\nu^2)} \begin{bmatrix} 1 & \nu & 0 \\ \nu & 1 & 0 \\ 0 & 0 & \frac{1}{2}(1-\nu) \end{bmatrix} \text{ and } \{\kappa\} = \begin{Bmatrix} -\kappa_x \\ -\kappa_y \\ -2\kappa_{xy} \end{Bmatrix}$$

The curvature-displacement can be expressed as follows:

$$\{\kappa\} = [B]w = \begin{bmatrix} -\frac{\partial^2}{\partial x^2} \\ -\frac{\partial^2}{\partial y^2} \\ -2\frac{\partial^2}{\partial x\, \partial y} \end{bmatrix} w \tag{2.68}$$

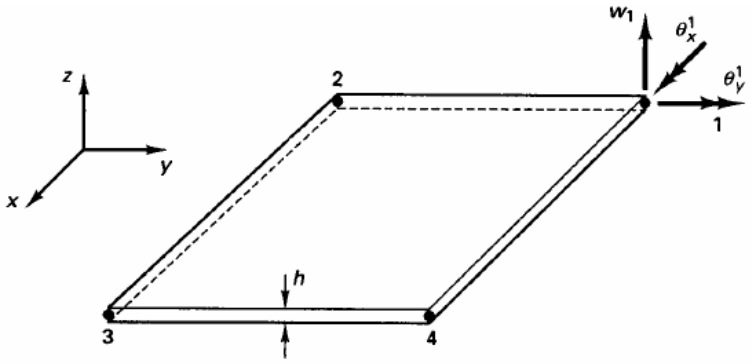

Figure 2.15: Nodal displacements and slopes for plate elements

A plate element has three degrees of freedom per node, the transverse deflection w and the rotations θ_x and θ_y about x and y axes. For a plate with four nodes, as depicted in Figure 2.15, the deformed shape can be approximated as follows:

$$w(x,y) = \sum_i N_i(x,y)u_i = [N]\{u\} \tag{2.69}$$

where the nodal displacements u_i are:

$$\{u\}^T = \{w_1 \quad \theta_{1x} \quad \theta_{1y} \quad w_2 \quad \theta_{2x} \quad \theta_{2y} \quad w_3 \quad \theta_{3x} \quad \theta_{3y} \quad w_4 \quad \theta_{4x} \quad \theta_{4y}\} \quad (2.70)$$

The simplest type of plate element is three triangular element. The polynomial approximation for w is:

$$w(x,y) = c_1 + c_2x + c_3y + c_4x^2 + c_5xy + c_6y^2 + c_7y^3 + c_8(x^2y + xy^2) + c_9y^3 \quad (2.71)$$

The displacement distribution of the three node triangular plate element is a complete polynomial. However, the continuity requirements are violated across the element boundaries.

The four node rectangular plate element has twelve degrees of freedom. The polynomial approximation for w is:

$$w(x,y) = c_1 + c_2x + c_3y + c_4x^2 + c_5xy + c_6y^2 + c_7x^3 + c_8x^2y + c_9y^2x + c_{10}y^3 + c_{11}x^3y + c_{12}y^3x \quad (2.72)$$

The displacement distribution of the four node rectangular plate element is not a complete polynomial and continuity requirements are violated.

The four node rectangular plate element of sixteen degrees of freedom, is an improved version, as it meets the convergence criteria and the continuity requirements. The extra degree of freedom per node is $\frac{\partial^2 w}{\partial x\, \partial y}$. The polynomial approximation can be written as follows:

$$w(x,y) = c_1 + c_2x + c_3y + c_4x^2 + c_5xy + c_6y^2 + c_7x^3 + c_8x^2y + c_9y^2x + c_{10}y^3 + c_{11}x^3y + c_{12}x^2y^2 + c_{13}y^3x + c_{14}x^3y^2 + c_{15}x^2y^3 + c_{16}x^3y^3 \quad (2.73)$$

The behavior of thick plates is based on Mindlin plate theory. According to this theory shear strains γ_{xz} and γ_{yz} are not ignored. The assumptions 4 and 5 of Kirchhoff theory are not valid. The relation between stress and strain include the out-of-plane shear strain γ_{xz} and γ_{yz} and can be expressed as follows:

$$\tau_{xz} = G\,\gamma_{xz} \quad (2.74)$$

$$\tau_{yz} = G\,\gamma_{yz} \tag{2.75}$$

The relation between strain and displacement is expressed by:

$$\varepsilon_x = -z\frac{\partial\theta_x}{\partial x} = -z\kappa_x \tag{2.76}$$

$$\varepsilon_y = -z\frac{\partial\theta_y}{\partial y} = -z\kappa_y \tag{2.77}$$

$$\gamma_{xy} = -z\left(\frac{\partial\theta_x}{\partial y} + \frac{\partial\theta_y}{\partial x}\right) = -z\kappa_{xy} \tag{2.78}$$

$$\gamma_{xz} = -\theta_y + \frac{\partial w}{\partial x} \tag{2.79}$$

$$\gamma_{yz} = -\theta_x + \frac{\partial w}{\partial y} \tag{2.80}$$

For the equation (2.67), $[C]$ and $\{\kappa\}$ can be calculated as follows:

$$[C] = \frac{Et^3}{12(1-\nu^2)}\begin{bmatrix} 1 & \nu & 0 & 0 & 0 \\ \nu & 1 & 0 & 0 & 0 \\ 0 & 0 & \beta & 0 & 0 \\ 0 & 0 & 0 & \beta & 0 \\ 0 & 0 & 0 & 0 & \beta \end{bmatrix} \text{ where } \beta = \frac{1-\nu}{\nu}, \quad \{\kappa\} = \begin{Bmatrix} -\kappa_x \\ -\kappa_y \\ -\kappa_{xy} \\ -\gamma_{xz} \\ -\gamma_{yz} \end{Bmatrix}$$

The shell analysis is based on a combination of membrane-flexure theory. According to the membrane theory, a shell structure experiences only axial and shear stresses. Transverse shear stresses and bending moments are ignored. A shell element has five degrees of freedom per node, as shown in Figure 2.16. The behavior of thin shells is based to classical theory of bending, while the behavior of thick shell is based on Mindlin theory.

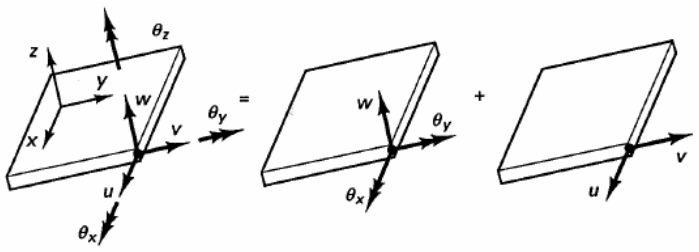

Figure 2.16: Nodal displacements and slopes for shell elements

2.2.3 Solids

General three dimensions structures require the use of solid finite elements. Solid elements are used to determine a three dimensional stress-strain state. Some of the most representative solid elements are 4-node tetrahedron, 5-node pyramid and 8-node hexahedron (see Figure 2.17). Each node of solid elements, has three degrees of freedom, u, v and *w* displacements.

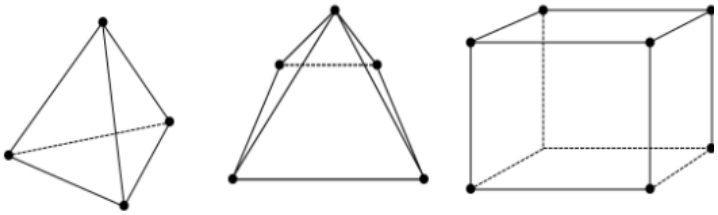

Figure 2.17: Representative solid elements

The concept of isoparametric elements is used to calculate the shape functions. Considering a solid element with eight nodes and dimensions $2a, 2b$ and $2c$, the coordinates of a local system placed at the centroid of the element (x_0, y_0, z_0) are given by:

$$\xi = \frac{x - x_0}{a}, \qquad \eta = \frac{y - y_0}{b}, \qquad \zeta = \frac{z - z_0}{c} \tag{2.81}$$

The displacement functions can be expressed by:

$$u(\xi, \eta, \zeta) = c_1 + c_2\xi + c_3\eta + c_4\zeta + c_5\xi\eta + c_6\eta\zeta + c_7\xi\zeta + c_8\xi\eta\zeta \tag{2.82}$$

$$v(\xi, \eta, \zeta) = c_9 + c_{10}\xi + c_{11}\eta + c_{12}\zeta + c_{13}\xi\eta + c_{14}\eta\zeta + c_{15}\xi\zeta + c_{16}\xi\eta\zeta \tag{2.83}$$

$$w(\xi, \eta, \zeta) = c_{17} + c_{18}\xi + c_{19}\eta + c_{20}\zeta + c_{21}\xi\eta + c_{22}\eta\zeta + c_{23}\xi\zeta + c_{24}\xi\eta\zeta \tag{2.84}$$

The shape function N_i is given by:

$$N_i = \frac{1}{8}(1 - \xi_i\xi)(1 - \eta_i\eta)(1 - \zeta_i\zeta) \tag{2.85}$$

The displacement functions can be expressed in terms of shape functions and nodal coordinates as follows:

$$\begin{Bmatrix} u \\ v \\ w \end{Bmatrix} = \begin{bmatrix} N_1 & 0 & 0 & N_2 & 0 & 0 & \dots & N_8 & 0 & 0 \\ 0 & N_1 & 0 & 0 & N_2 & 0 & \dots & 0 & N_8 & 0 \\ 0 & 0 & N_1 & 0 & 0 & N_2 & \dots & 0 & 0 & N_8 \end{bmatrix} \begin{Bmatrix} u_1 \\ v_1 \\ w_1 \\ \vdots \\ u_8 \\ v_8 \\ w_8 \end{Bmatrix} \tag{2.86}$$

For the solid element, the equivalent nodal force vector {f} may be the summation of body forces $\{f\}_b$ and surface forces $\{f\}_s$:

$$\{f\} = \{f\}_b + \{f\}_s \tag{2.87}$$

$$\{f\}_b = \int \begin{Bmatrix} W_x \\ W_y \\ W_z \end{Bmatrix}^T [N] dV \ , \qquad \{f\}_S = \int \begin{Bmatrix} p_x \\ p_y \\ p_z \end{Bmatrix}^T [N] dA \tag{2.88}$$

where p_x, p_y and p_z is the distributed load which is applied to the surface and W_x, W_y and W_z are the components of the body force.

3. Stress analysis of stiffened panels

3.1 Analytical calculation

An alternative analytical solution for the stress distribution for a plate-beam combination is now derived (in this chapter it will be referred as analytical solution 1). The field of shear stresses in a cross section, can be calculated as follows:

$$\tau(s) = \frac{q(s)}{t_{el}} \tag{3.1}$$

where $q(s)$ is the distribution of shear flow and t_{el} the thickness of the element (flange or web). The relation between shear stresses and strains is given by:

$$\tau(s) = G\,\gamma(s) \tag{3.2}$$

where G is the shear modulus. As depicted in Figure 3.1, the shear strain can be expressed as follows:

$$\gamma(s) = \frac{\partial e}{\partial s} \tag{3.3}$$

By substituting equation (3.2) into equation (3.3) and integrating over the variable s, we get that:

$$e = \frac{1}{G}\int \tau(s)ds \tag{3.4}$$

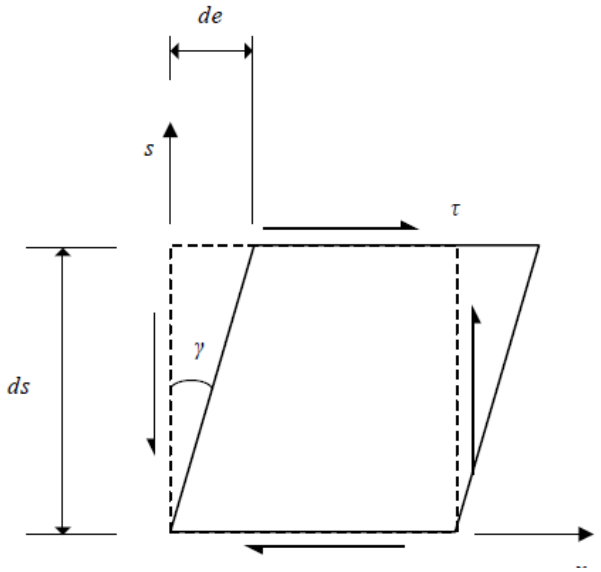

Figure 3.1: Geometric definition of shear strain

The axial strain ε_s can be defined as:

$$\varepsilon_s = \frac{\partial \mathrm{e}}{\partial \mathrm{x}} \tag{3.5}$$

Applying Hooke's law ($\sigma = E\varepsilon$) and substituting equation (3.4) into equation (3.5), we get that:

$$\sigma_\mathrm{s}(\mathrm{s}) = \frac{\mathrm{E}}{\mathrm{G}}\frac{\partial}{\partial \mathrm{x}}\left(\int \tau(\mathrm{s})\mathrm{ds}\right) \tag{3.6}$$

Substituting equation (3.1) into (3.6), we get that:

$$\sigma_\mathrm{s}(\mathrm{s}) = \frac{\mathrm{E}}{\mathrm{G}}\frac{\partial \mathrm{V}}{\partial \mathrm{x}}\left(\int \frac{\mathrm{Q}}{\mathrm{I_y t_{el}}}\mathrm{ds}\right) \tag{3.7}$$

Considering that $G = E/2(1-\nu)$ σ_s can be expressed as follows:

$$\sigma_s(s) = \frac{2(1-\nu)w}{I_y}\int \frac{Q}{t_{el}}ds \tag{3.8}$$

The equation (3.8) describes the axial stress field which is developed due to shear lag and is added to axial stress field due to pure bending. However, the addition of these two stress fields, does not result to a field that achieves equilibrium of forces and moments. In order to consider shear lag phenomenon and achieve static equilibrium, we need to subtract a uniform axial stress field ${\sigma_s}^{Axial}$ and a linear axial stress field ${\sigma_s}^{Bending}$. These axial stresses can be expressed as follows:

$${\sigma_\mathrm{s}}^{\mathrm{Axial}} = \frac{\int \sigma_\mathrm{s}\mathrm{dA}}{\mathrm{A}} = \frac{2(1-\nu)\mathrm{w}}{\mathrm{I_y A}}\int\int \frac{\mathrm{Q}}{\mathrm{t_{el}}}\mathrm{ds\,dA} \tag{3.9}$$

$${\sigma_\mathrm{s}}^{\mathrm{Bending}} = \frac{\int \sigma_\mathrm{s}\,\mathrm{z\,dA}}{\mathrm{I_y}} = \frac{2(1-\nu)\,\mathrm{w\,z}}{\mathrm{I_y I_y}}\int\int \frac{\mathrm{Q}}{\mathrm{t_{el}}}\mathrm{ds\,z\,dA} \tag{3.10}$$

The real stress field can be calculated as follows:

$$\sigma_{real} = \sigma_b + \sigma_s - {\sigma_\mathrm{s}}^{\mathrm{Axial}} - {\sigma_\mathrm{s}}^{\mathrm{Bending}} \tag{3.11}$$

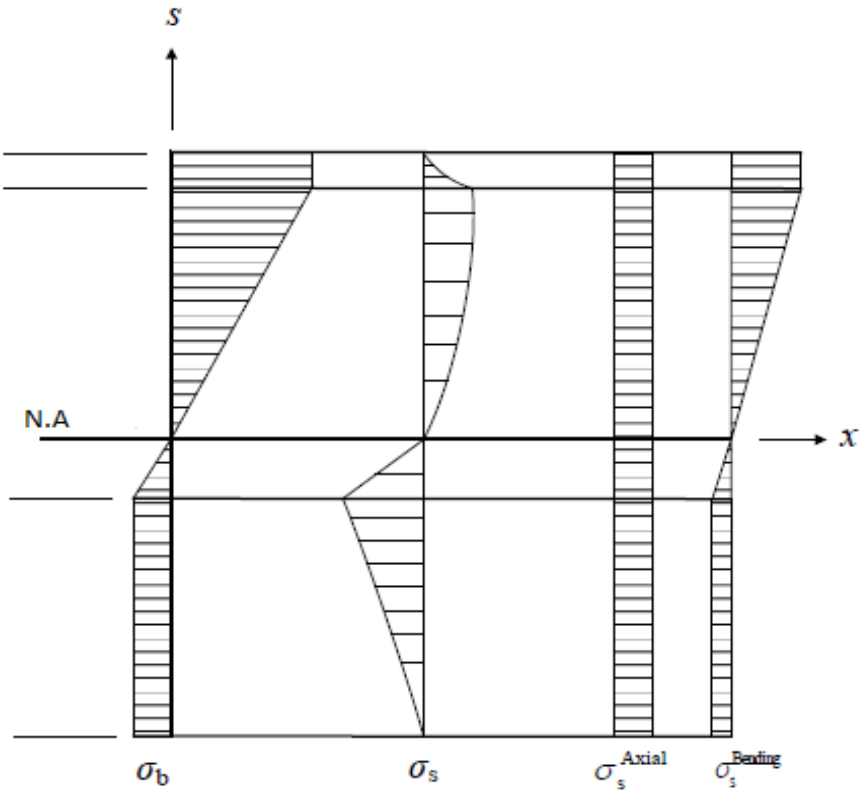

Figure 3.2: Components of axial stress field

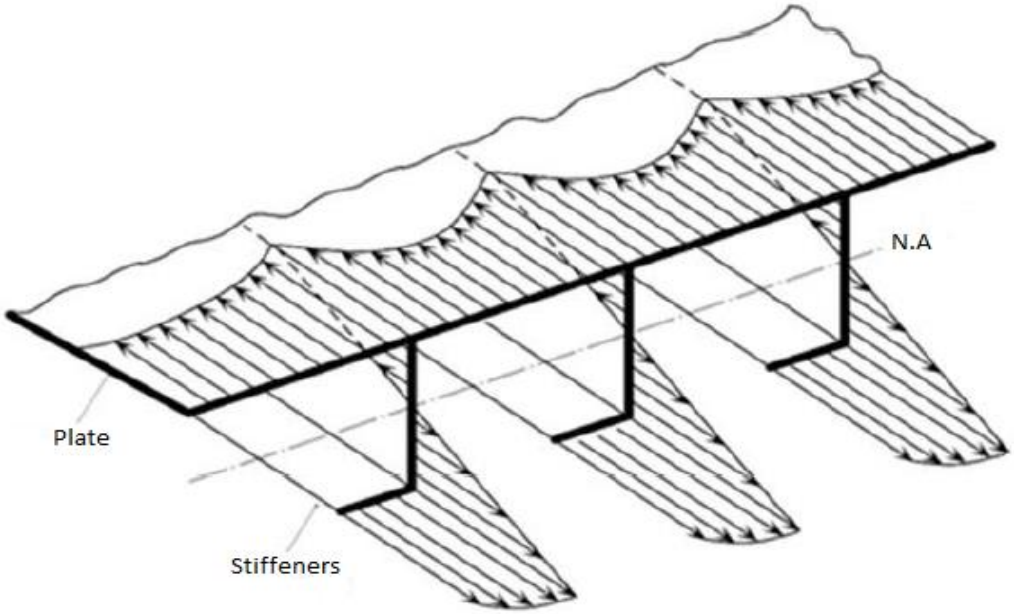

Figure 3.3: Real distribution of axial stress field due to shear lag

3.2 Numerical implementation of analytical solutions

Initially, for a one-way stiffened panel, with $L = 3650mm$, that is subjected to uniform pressure load, with $p = 0.1\,MPa$ and the boundary conditions to be fixed supports, the stress field will be calculated with different theoretical modeling strategies. It is noted that the representative repetitive section can be considered the effective cross section of a beam. For the calculations, the Poisson's ratio is $\nu = 0.3$.

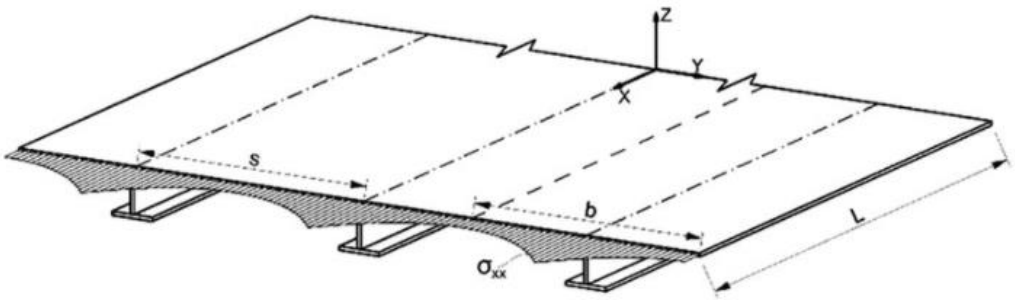

Figure 3.4: One-way stiffened panel with repetitive section

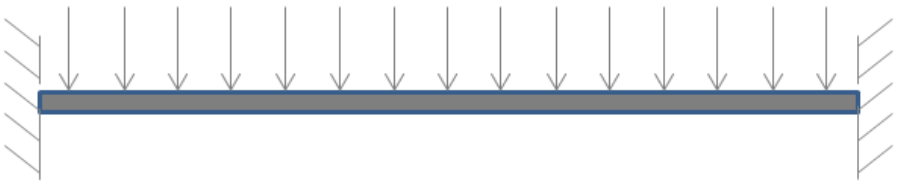

Figure 3.5: Beam subjected to uniform loads

The dimensions of the cross section are the following:

- Web height: $wh = 300mm$
- Web thickness: $wt = 15mm$
- Top width: $tfw = 200mm$
- Top thickness: $tft = 18mm$
- Bottom width: $bfw = 800mm$
- Bottom thickness: $bft = 20mm$

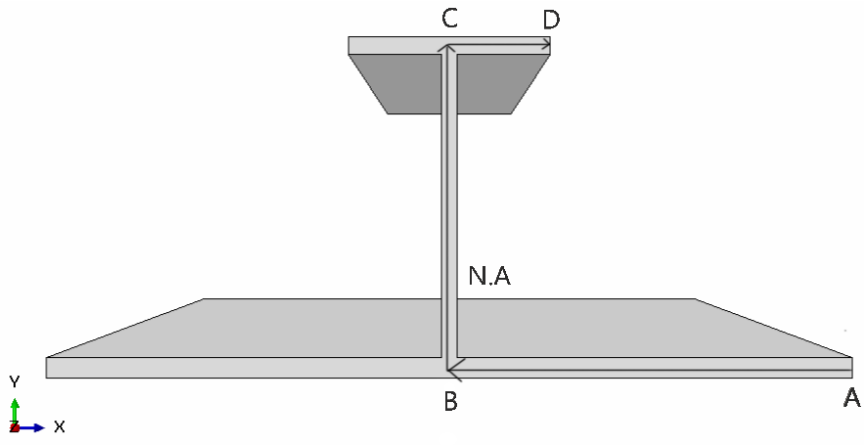

Figure 3.6: Cross section of the beam

According to the analytical solution 1, the real stress distribution will now be calculated using the equation (3.11) (for $x = L/2$). For fixed supports, the bending moment along the beam can be expressed as follows:

$$M\left(\frac{L}{2}\right) = \frac{wL^2}{24}$$

Bending stress σ_b:

$$\sigma_b = \frac{Mz}{I} = \frac{wL^2 z}{24I}$$

$$w = p * bfw = 80\ MPa * mm$$

Top Flange (C-D) $\rightarrow \sigma_b = 29.98\ MPa$

Bottom Flange (A-B) $\rightarrow \sigma_b = -10.48 MPa$

Axial stress σ_s:

$$\sigma_s = \frac{2(1-\nu)w}{I} \int \frac{Q}{t_{el}} ds$$

Above neutral axis:

For $0 \leq s \leq 241.47$:

$$\sigma_s = \frac{2(1-\nu)w}{I} \int_0^S \left(\frac{18 * 200 * 241.47}{15}\right) + 0.5(241.47 - s)(241.47 + s) ds$$

For s=241.47 (C) → $\sigma_s = 5.64$ MPa

For 241.47≤ s ≤ 341.47 :

$$\sigma_s = 5.64 + \frac{2(1-\nu)w}{I}\int_{241.47}^{S}(341.47 - s) * 241.47\ ds$$

for s=341.47 (D) → $\sigma_s = 6$ MPa

Below neutral axis:

For 0 ≤ s ≤ 77.53 :

$$\sigma_s = \frac{2(1-\nu)w}{I}\int_{0}^{S}\left(\frac{20 * 800 * 77.53}{15}\right) + 0.5(77.53 - s)(77.53 + s)ds$$

for s=77.53 (B) → $\sigma_s = -1.98$ MPa

For 77.53≤ s ≤ 477.53 :

$$\sigma_s = 1.982 + \frac{2(1-\nu)w}{I}\int_{77.53}^{S}(477.53 - s) * 77.53\ ds$$

for s=477.53 (A) → $\sigma_s = -3.85$ MPa

Axial stress ${\sigma_s}^{Axial}$:

$${\sigma_s}^{Axial} = \frac{2(1-\nu)w}{IA}\iint\frac{Q}{t_{el}}dsdA$$

Above neutral axis :

$$A = \frac{2(1-\nu)w}{IA}\left[\int_{0}^{241.47}15\left(\int_{0}^{241.47}\left(\frac{18 * 200 * 241.47}{15}\right) + 0.5(241.47 - s)(241.47 + s)ds\right)ds + 2\int_{241.47}^{341.47}18\left(\int_{241.47}^{341.47}(341.47 - s) * 241.47\ ds\right)ds\right]$$

Below neutral axis :

$$B = \frac{2(1-\nu)w}{IA}\left[\int_0^{77.53} 15\left(\int_0^{241.47}\left(\frac{20*800*77.53}{15}\right)\right.\right.$$
$$\left.+ 0.5(77.53-s)(77.53+s)ds\right)ds$$
$$\left.+ 2\int_{77.53}^{477.53} 20\left(\int_{77.53}^{477.53}(477.53-s)*77.53\,ds\right)ds\right]$$

$\sigma_s{}^{Axial} = A + B = 2.24$ MPa

Bending stress $\sigma_s{}^{Bending}$:

$$\sigma_s{}^{Bending} = \frac{2(1-\nu)wz}{I^2}\iint \frac{Q}{t_{el}}dszdA$$

$$\sigma_s{}^{Bending} = \frac{2(1-\nu)wz}{I^2}\left[\int_0^{241.47} 15\,s\left(\int_0^{241.47}\left(\frac{18*200*241.47}{15}\right)\right.\right.$$
$$\left.+ 0.5(241.47-s)(241.47+s)ds\right)ds$$
$$+ 2\int_{241.47}^{341.47} 18*241.47\left(\int_{241.47}^{341.47}(341.47-s)*241.47\,ds\right)ds$$
$$+\int_0^{77.53} 15\,s\left(\int_0^{241.47}\left(\frac{20*800*77.53}{15}\right)\right.$$
$$\left.+ 0.5(77.53-s)(77.53+s)ds\right)ds$$
$$\left.+ 2\int_{77.53}^{477.53} 20*77.53\left(\int_{77.53}^{477.53}(477.53-s)*77.53\,ds\right)ds\right]$$

Top Flange (C-D) → $\sigma_b = 3.51$ MPa

Bottom Flange (A-B) → $\sigma_b = -1.23$ MPa

In the following tables, the stresses from the analytical solution 1 and from Schade are presented. It is also presented the relative percentage change considering as reference the stresses from the Euler bending theory.

Cross section	σ_{real} [MPa] (from the analytical solution 1)	$\frac{\sigma_{real} - \sigma_{Euler}}{\sigma_{Euler}} 100\%$
A	-10.09	-3%
B	-11.87	13.2%
C	30.02	0.1%
D	29.72	-0.8%

Table 3.1: Stresses according to the analytical solution 1

Cross section	σ_{real} [MPa] (from Schade)	$\frac{\sigma_{real} - \sigma_{Euler}}{\sigma_{Euler}} 100\%$
A	-12.39	18.2%
B	-12.39	18.2%
C	30.33	1.1%
D	30.33	1.1%

Table 3.2: Stresses according to the analytical solution of Schade

3.3 Application of stiffness method

In order to compare the direct stiffness method with the analytical solutions, a code in Matlab was written. The user can choose between Euler and Timoshenko beam and the total number of the elements of the beam. Each element has two degrees of freedom per node that is the transverse displacement v_1 and rotation θ_1 for the first node and transverse displacement v_2 and rotation θ_2 for the second node. The stiffness matrix is calculated by the equations (2.42) and (2.43). The Timoshenko shear coefficient is 0.44 and the modulus of elasticity E=207 GPa. In order to succeed convergence of the stresses, at least 25 elements must be used. The stress is given by $\sigma = -Ez\frac{\partial^2 w}{\partial x^2}$ where the deflection of each element can be calculated as follows:

$$w(x) = v_1\left[1 - 3\left(\frac{x}{L}\right)^2 + 2\left(\frac{x}{L}\right)^3\right] + \theta_1\left[\frac{x}{L} - 2\left(\frac{x}{L}\right)^2 + 2\left(\frac{x}{L}\right)^3\right]L +$$
$$+ v_2\left[3\left(\frac{x}{L}\right)^2 - 2\left(\frac{x}{L}\right)^3\right] + \theta_2\left[-\left(\frac{x}{L}\right)^2 + \left(\frac{x}{L}\right)^3\right]L$$

In the following tables the stresses for Euler and Timoshenko beam from the application of direct stiffness method are presented, with the relative percentage change for each case.

Cross section	σ_{real} [MPa] from stiffness method for Euler beam	$\frac{\sigma_{real} - \sigma_{Euler}}{\sigma_{Euler}} 100\%$
A	-10.83	3.3%
B	-10.83	3.3%
C	30.99	3.3%
D	30.99	3.3%

Table 3.3: Stresses from direct stiffness method for Euler beam

Cross section	σ_{real} [MPa] from stiffness method for Timoshenko beam	$\frac{\sigma_{real} - \sigma_{Euler}}{\sigma_{Euler}} 100\%$
A	-10.07	-3.9%
B	-10.07	-3.9%
C	28.81	-3.9%
D	28.81	-3.9%

Table 3.4: Stresses from direct stiffness method for Timoshenko beam

3.4 Modeling in commercial FE software

A description of the elements that were used in Abaqus, will now be given.

Beam elements

Timoshenko beams B31 and B32 were used. These beams allow for transverse shear deformation. Abaqus assumes that the transverse shear behavior of Timoshenko beams is linear elastic with fixed modulus and thus independent of the response of the beam section to axial stretch and bending. B31 is a 2-node linear beam and B32 a 3-node quadrative beam with 6 active degrees of freedom per node. The default stress output points, if a beam section is integrated during analysis, are 1, 5, 9 and 13 as depicted in Figure (3.8).

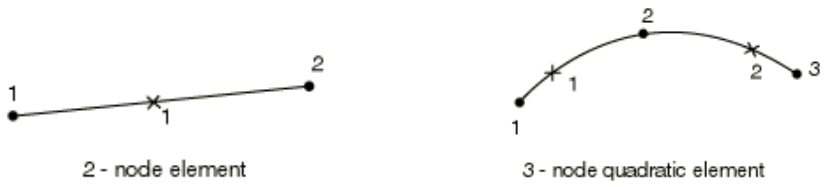

Figure 3.7: B31 & B32 elements

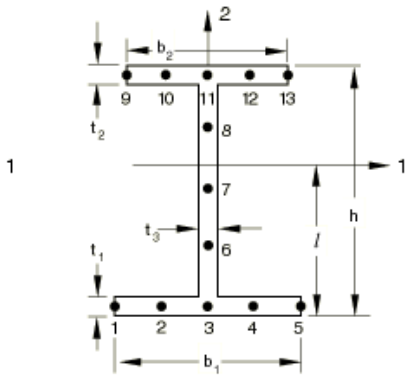

Figure3.8: Cross section of I profile

Shell elements

Conventional shells S4 and S8R were used. These shell elements descretize a body by defining the geometry at a reference surface. S4 is a 4-node general-purpose shell and S8R an 8-node doubly curved thick shell with reduced integration with 6 active

degrees of freedom per node. Reduced integration usually provides more accurate results and significantly reduces running time.

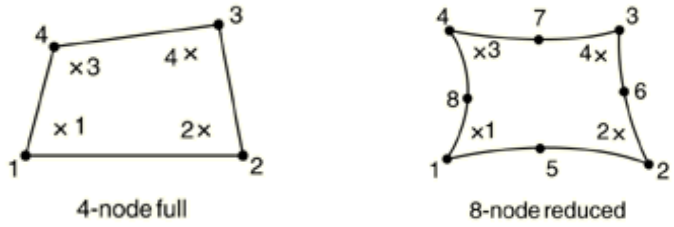

Figure 3.9: S4 & S8R elements

Solid elements

Three dimensional solid elements C3D8 and C3D20R were used. C3D8 is an 8-node linear brick element and C3D20R a 20-node quadratic brick with reduced integration. Each of them has 3 degrees of freedom per node. Reduced integration uses a lower-order integration to form the element stiffness. C3D20R has 8 integration points.

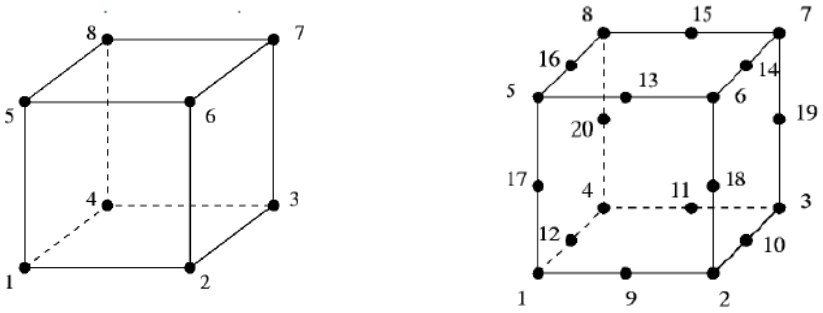

Figure 3.10: C3D8 & C3D20R elements

Initially, a beam was created, that consisted of 25 B31 elements. The stresses, for $x = L/2$, at the cross section were presented in the following table:

Cross section	σ_{real} [MPa] from Abaqus	$\frac{\sigma_{real} - \sigma_{Euler}}{\sigma_{Euler}} 100\%$
A	-9.67	-7.7%
B	-9.67	-7.7%
C	30.13	0.5%
D	30.13	0.5%

Table 3.5: Stresses from Abaqus with B31 elements

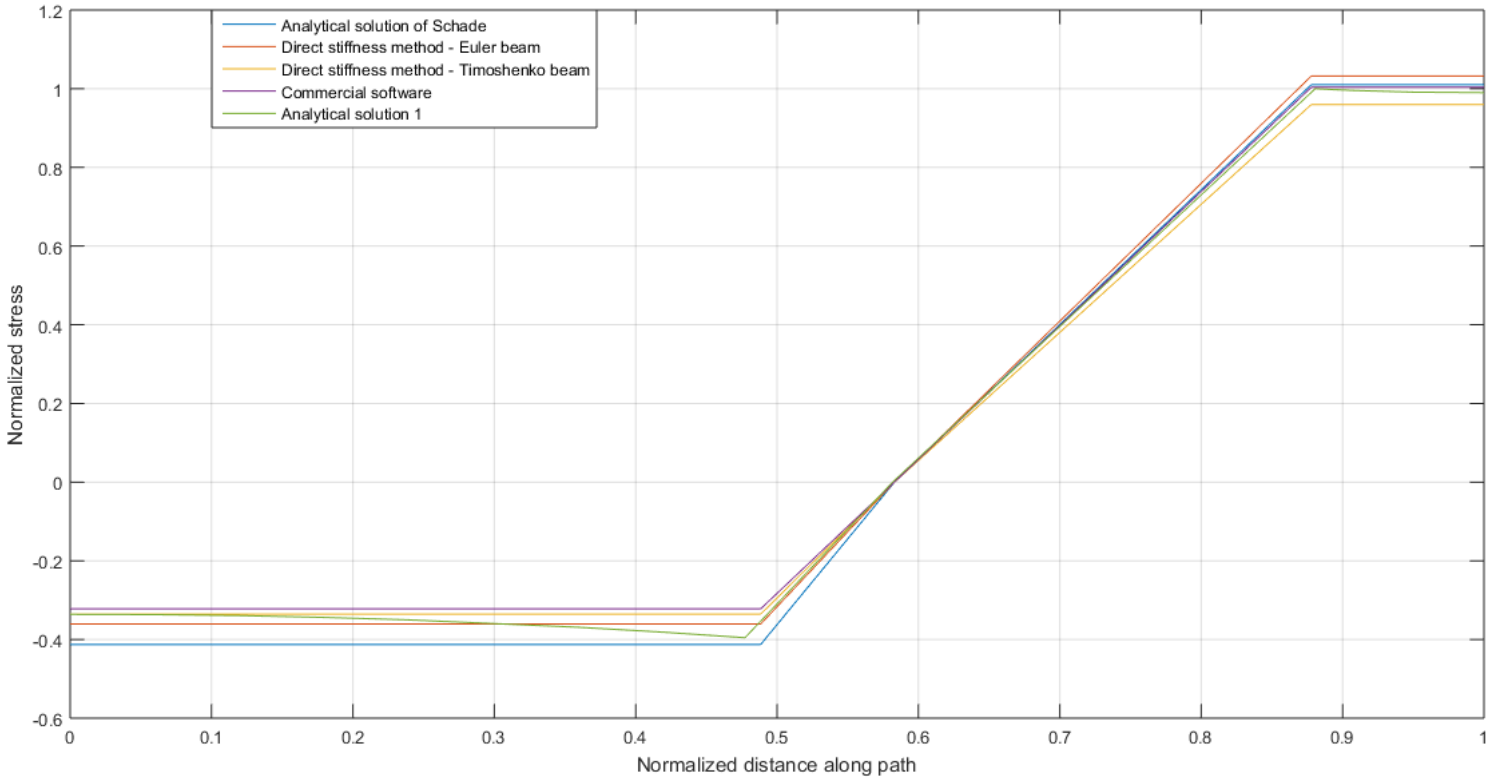

Figure 3.11: Comparison of the stress field for the beam

In Figure 3.11, the comparison of the stress field for the path A-B-C-D is depicted. The stresses are devided by the maximum stress from the analytical solution 1. For the bottom flange, analytical solution of Schade gives the maximum stresses. For the top flange, the Euler beam with the direct stiffness method, has the maximum stresses. The results of the commercial software converge with the direct stiffness method with Timoshenko beam, as B31 is a Timoshenko beam.

As detailed below, a stiffened panel in one direction was modeled, with length $L = 3650$ mm , width $B = 3200$ mm and thickness $t = 20$ mm. The plate is fixed circumferential. The uniform pressure, the modulus of elasticity and the dimensions of the stiffeners are the same as the previous case. The models were created with C3D8, C3D20R, S4, S8R, S4&B31 and S8R&B32 elements. The aim was to compare the results of Abaqus with the analytical solution 1 in order to choose the appropriate element for the calculation of secondary stresses. Each element was modeled with 20, 50 and 100 mm size of mesh. In the below figures, the comparison of the stresses is depicted for the cross section (A-B-C-D) of the second stiffener for $x = L/2$ and $x = 0$ for 100 mm size of mesh.

Shells: S4 and S8R

In the following figures, the distribution of the stresses with direction parallel to the length of the stiffeners for S4 and S8R elements is depicted. In figure 3.14 and 3.15 the stresses of these elements are compared with the analytical solution 1 along the path (A-B-C-D) of the cross section for $x = L/2$ and for $x = 0$ with 100 mm size of mesh. The stresses are normalized as they are divided by the maximum stress if analytical solution 1. It is clarified that the calculated stresses concern the intermediate longitudinal stiffener.

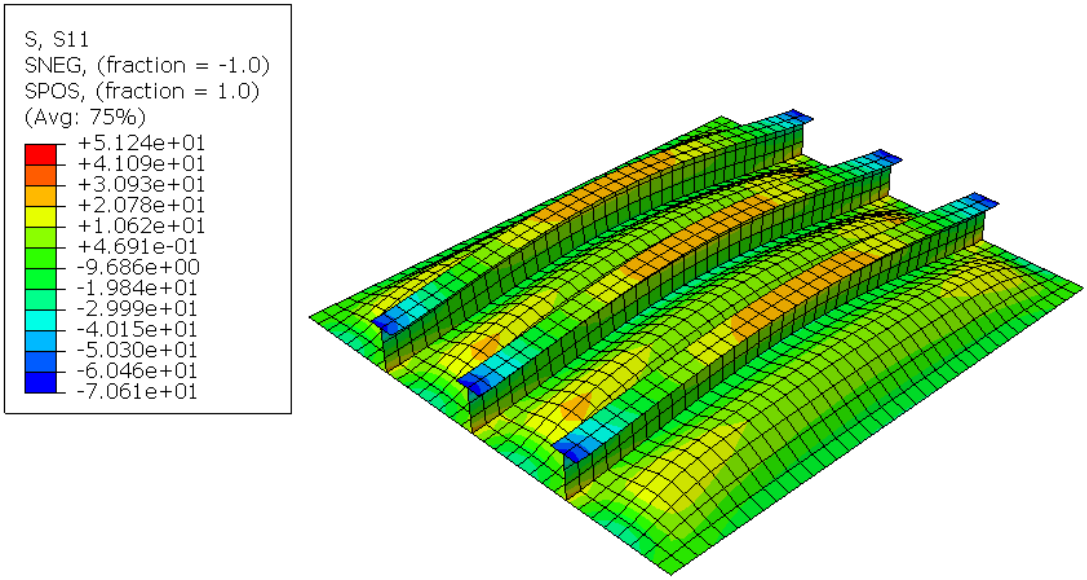

Figure 3.12: Stress field for S4 element

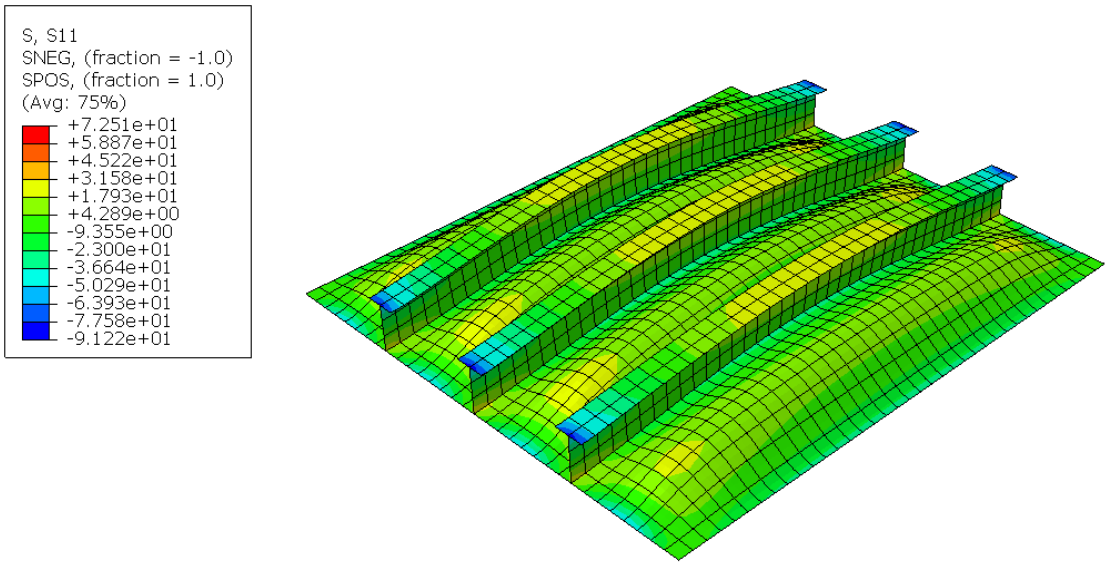

Figure 3.13: Stress field for S8R element

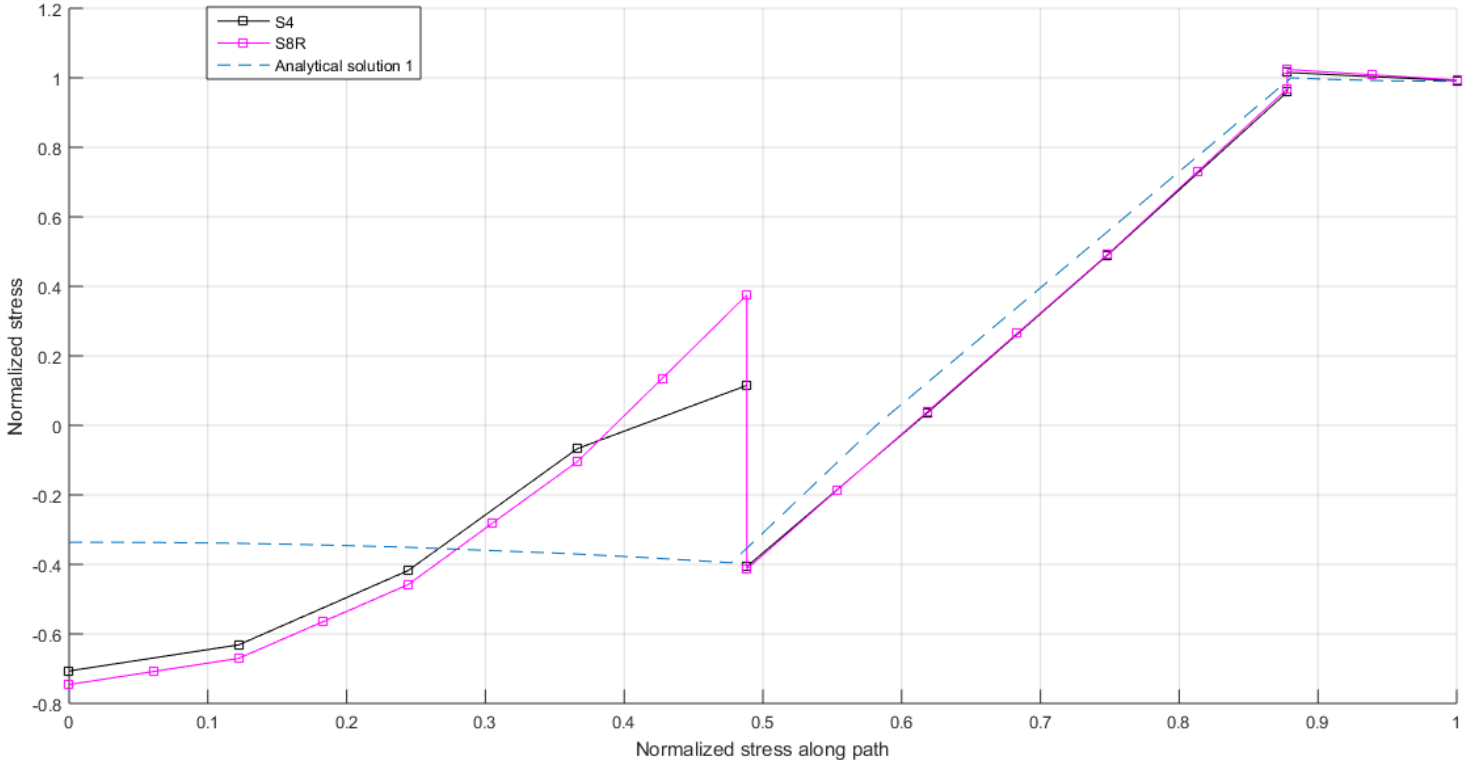

Figure 3.14: Normalized stress for shell elements for $\boldsymbol{x = L/2}$

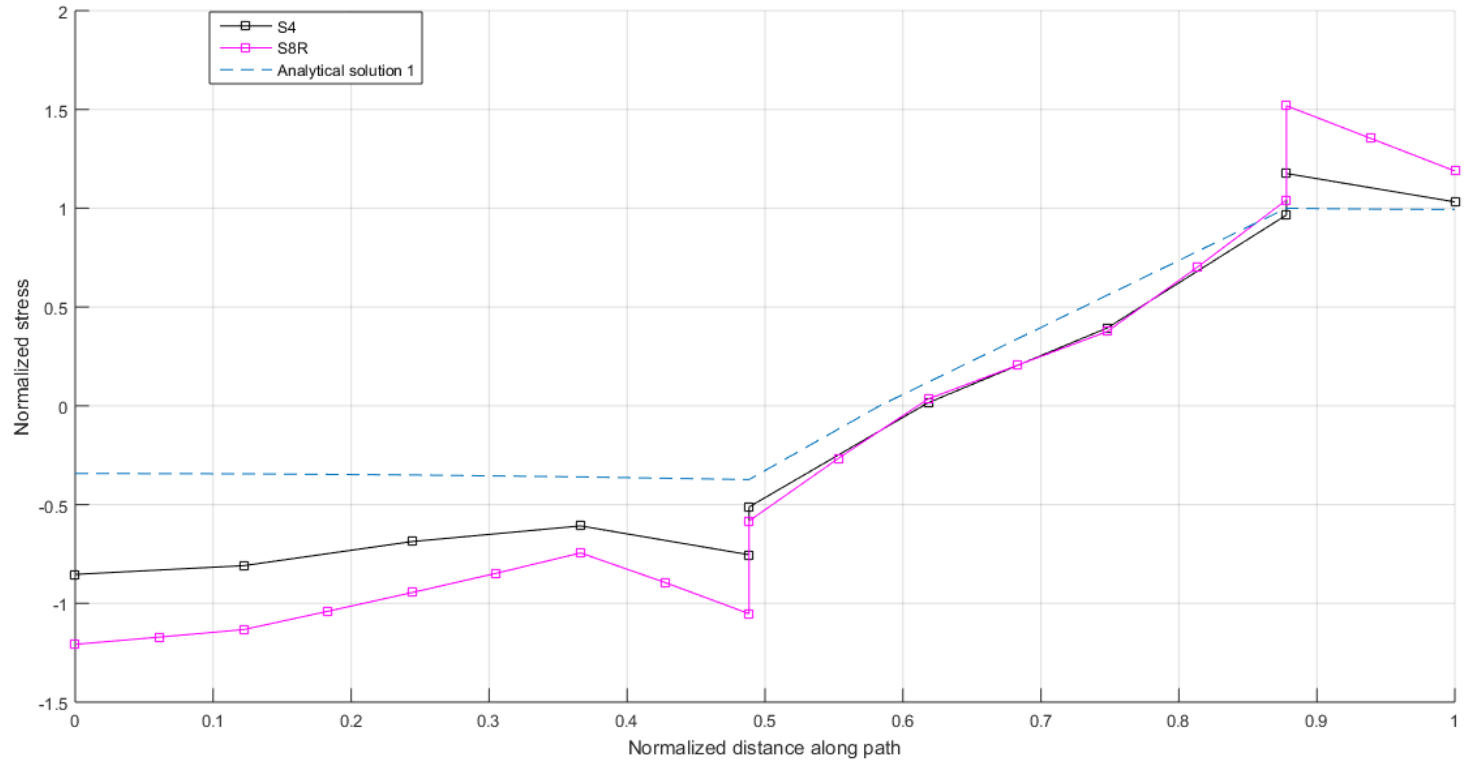

Figure 3.15: Normalized stress for shell elements for $\boldsymbol{x = 0}$

From the comparison with the analytical solution 1, it can be concluded that for shell elements, only the stresses of web and flange approximate the theoretical results. Moreover, on the boundaries the above elements overestimate the stresses.

Solids: C3D8 and C3D20R

The following figures depict the stresses parallel to the longitudinal stiffeners for solid elements for the cross section (A-B-C-D) of the intermediate stiffener.

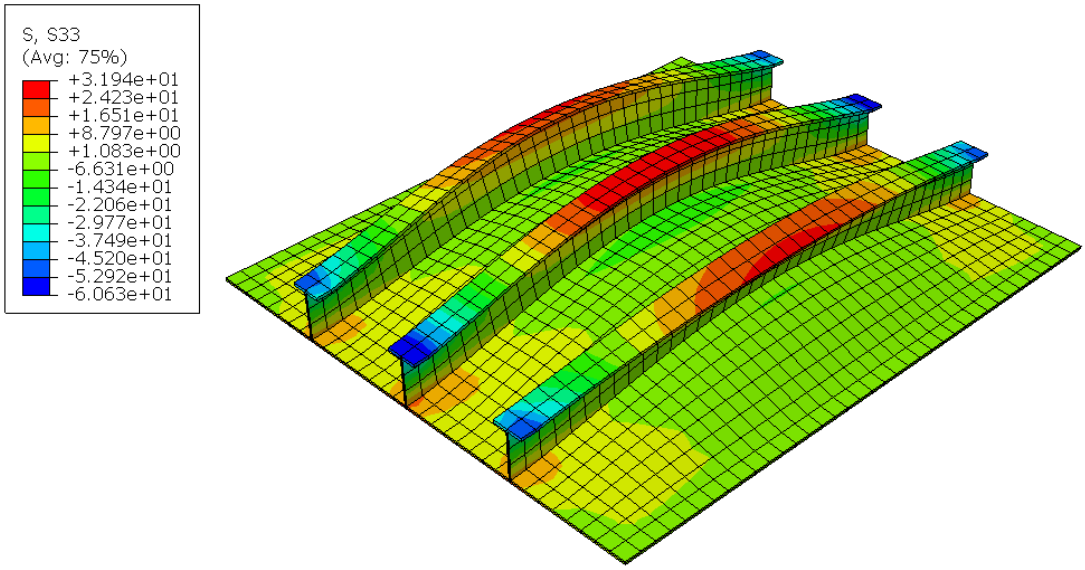

Figure 3.16: Stress field for C3D8 element

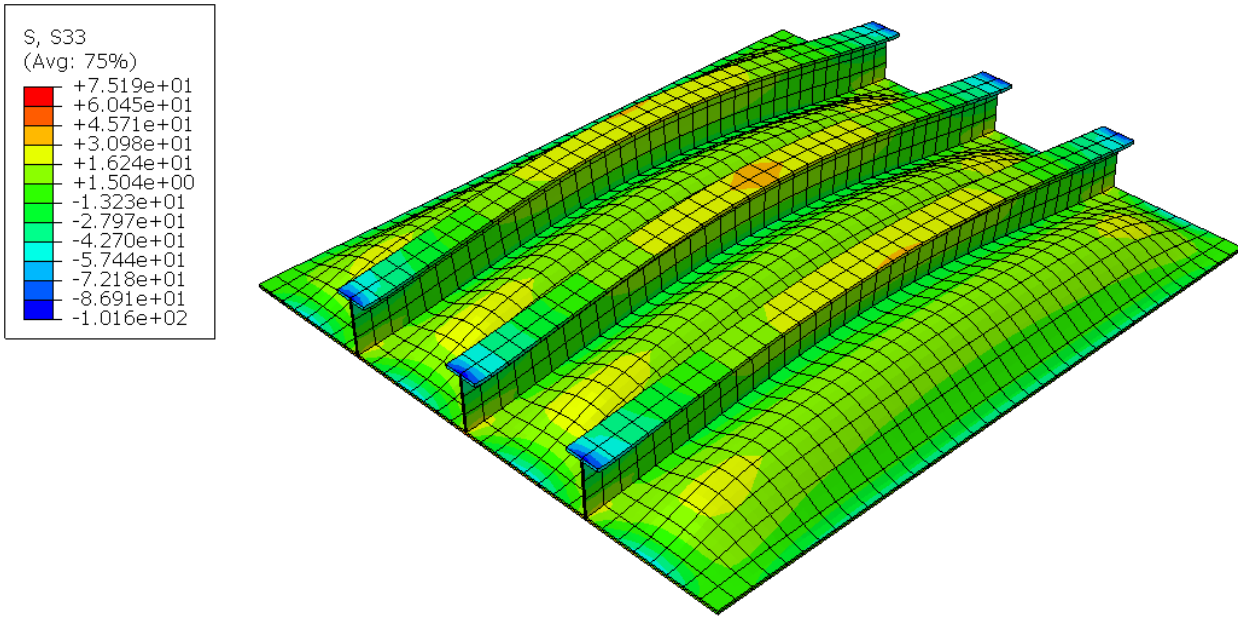

Figure 3.17: Stress field for C3D20R element

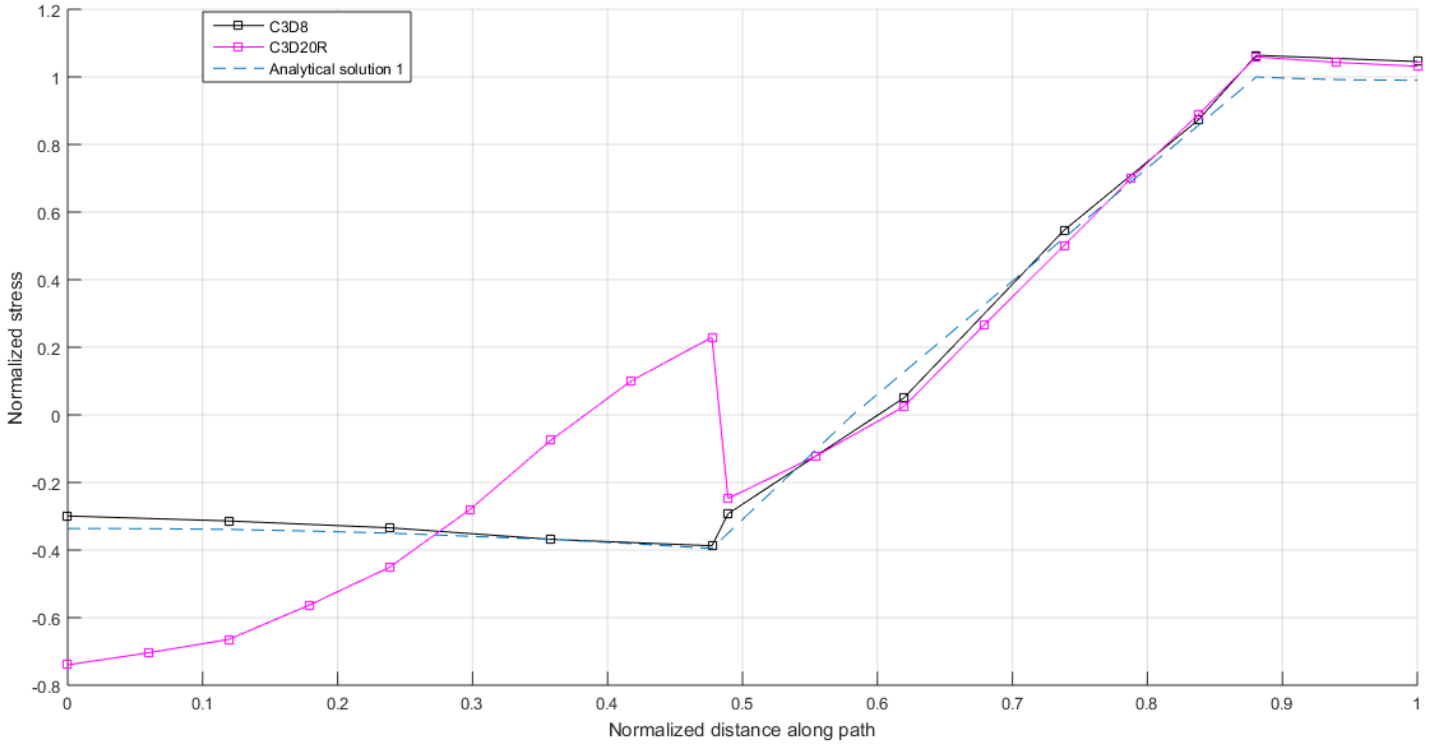

Figure 3.18: Normalized stress for solid elements for $\boldsymbol{x = L/2}$

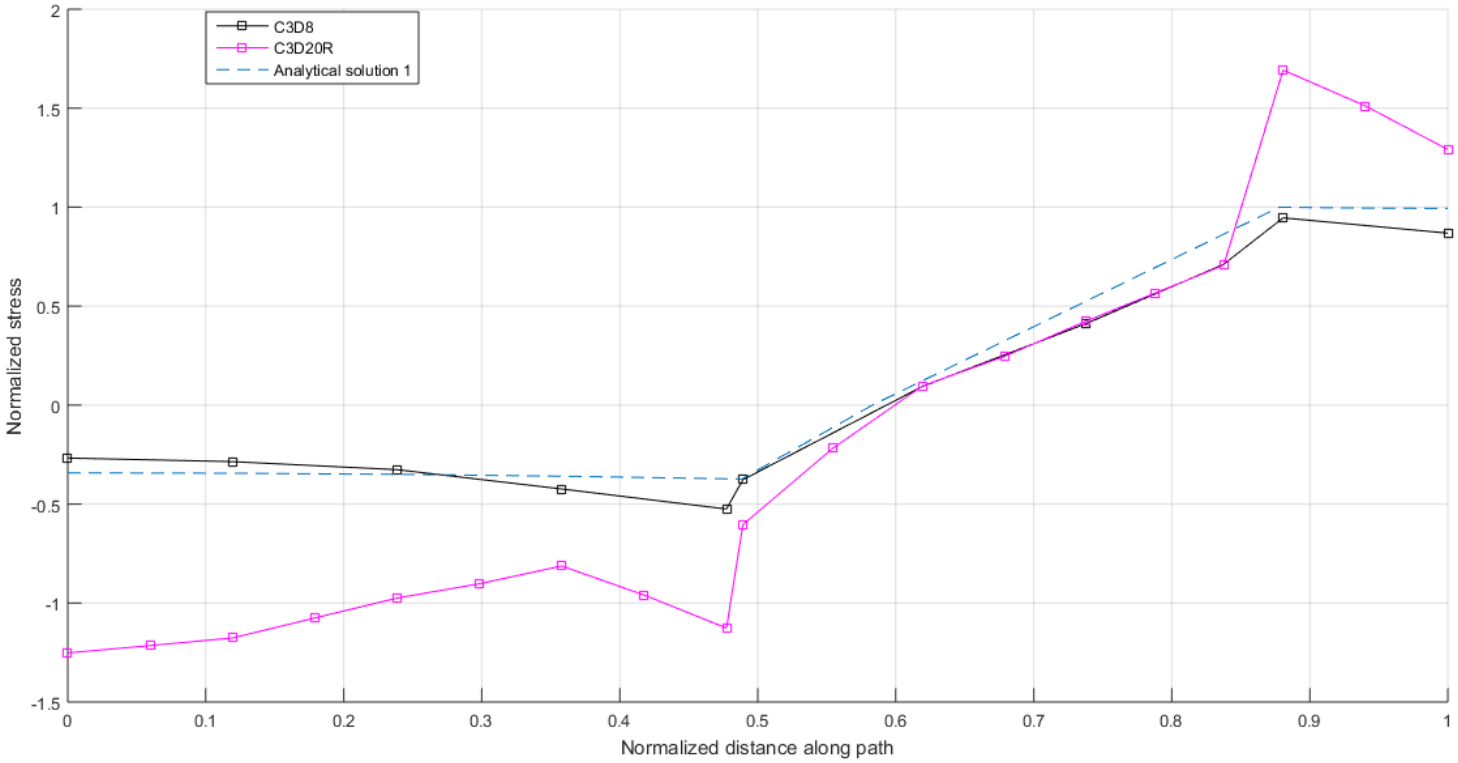

Figure 3.19: Normalized stress for solid elements for $\boldsymbol{x = 0}$

From the above solid elements, C3D8 is more appropriate for the calculation of the secondary stresses, even though the stresses are underestimated on the boundary conditions.

Shells with beams:S4&B31 and S8R&B32

The results for a model with plate as shell element and longitudinal stiffeners as beam elements are presented in the following figures.

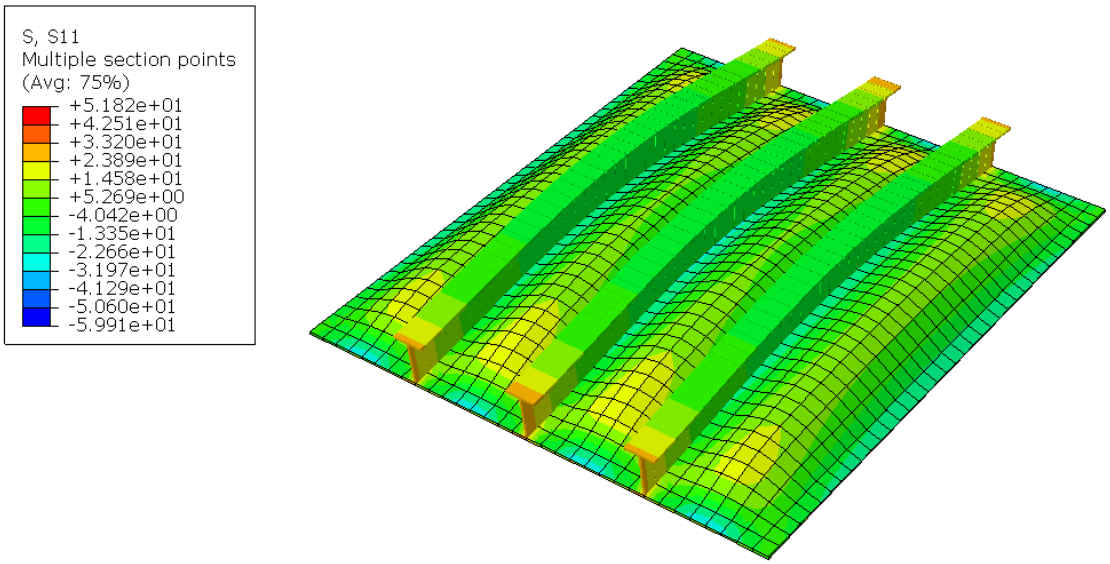

Figure 3.20: Stress field for S4 & B31 elements

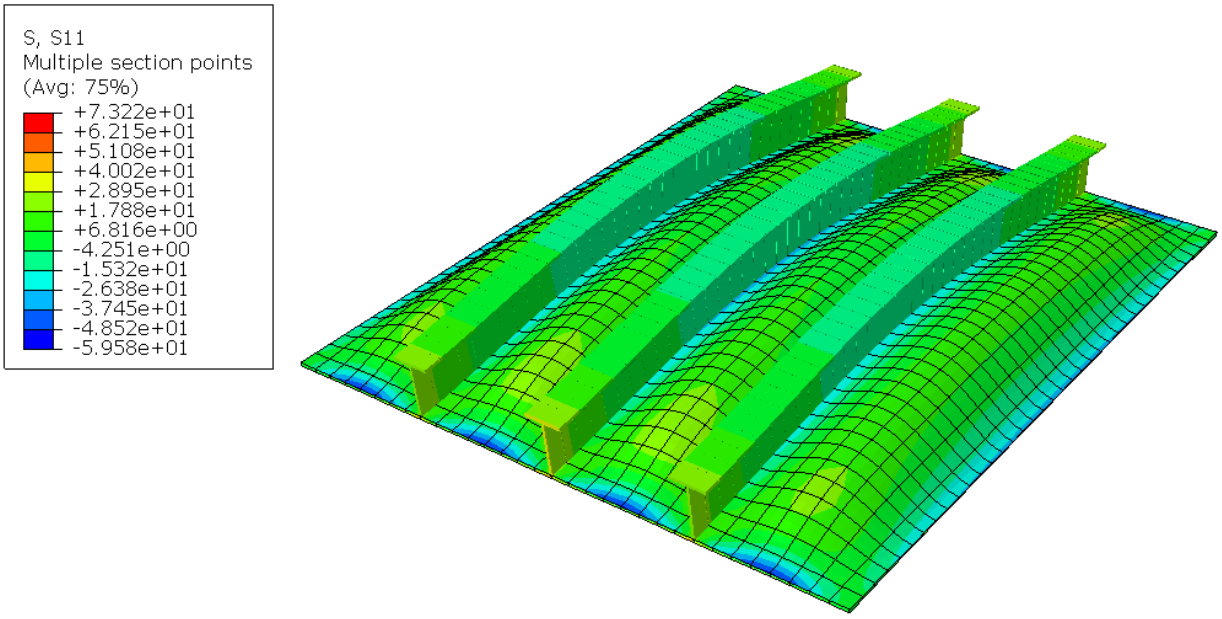

Figure 3.21: Stress field for S8R & B32 elements

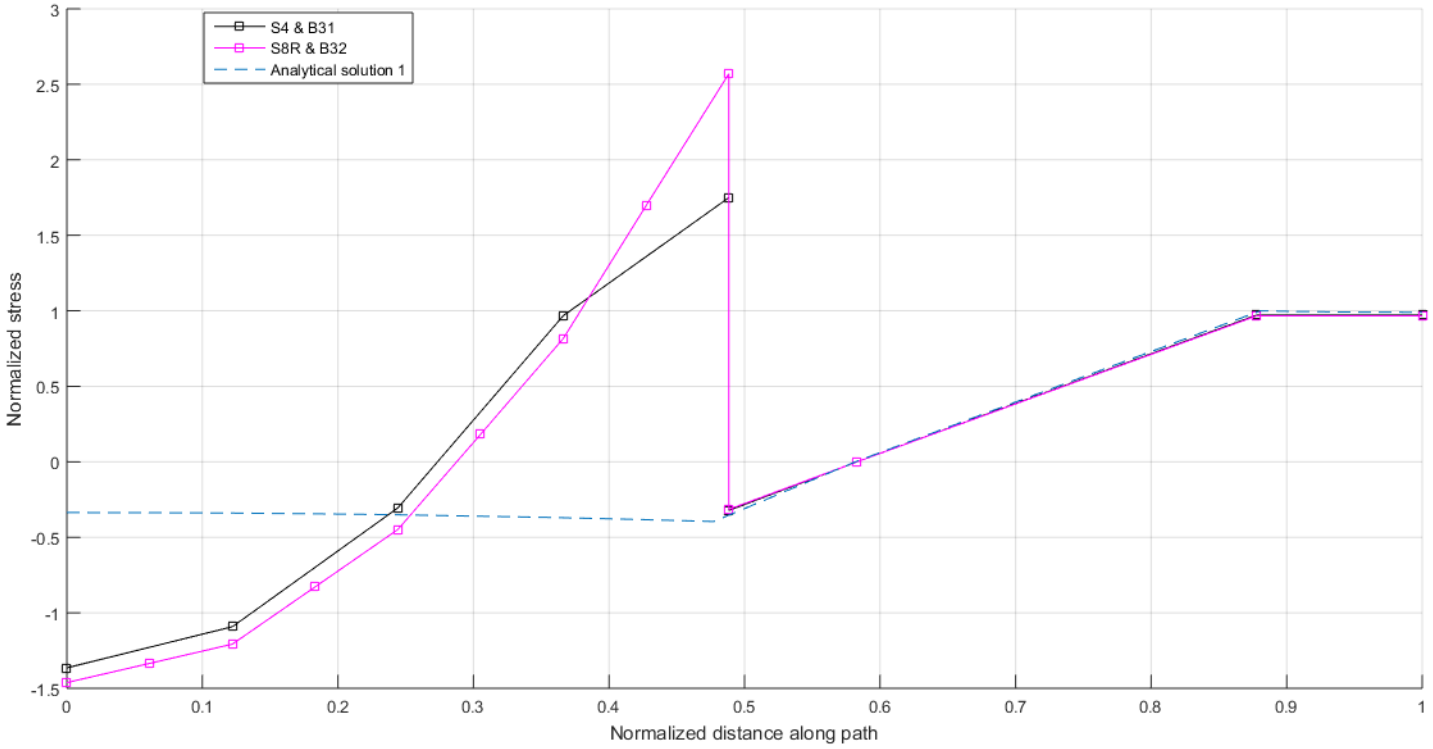

Figure 3.22: Normalized stress for shell & beam elements for $\boldsymbol{x = L/2}$

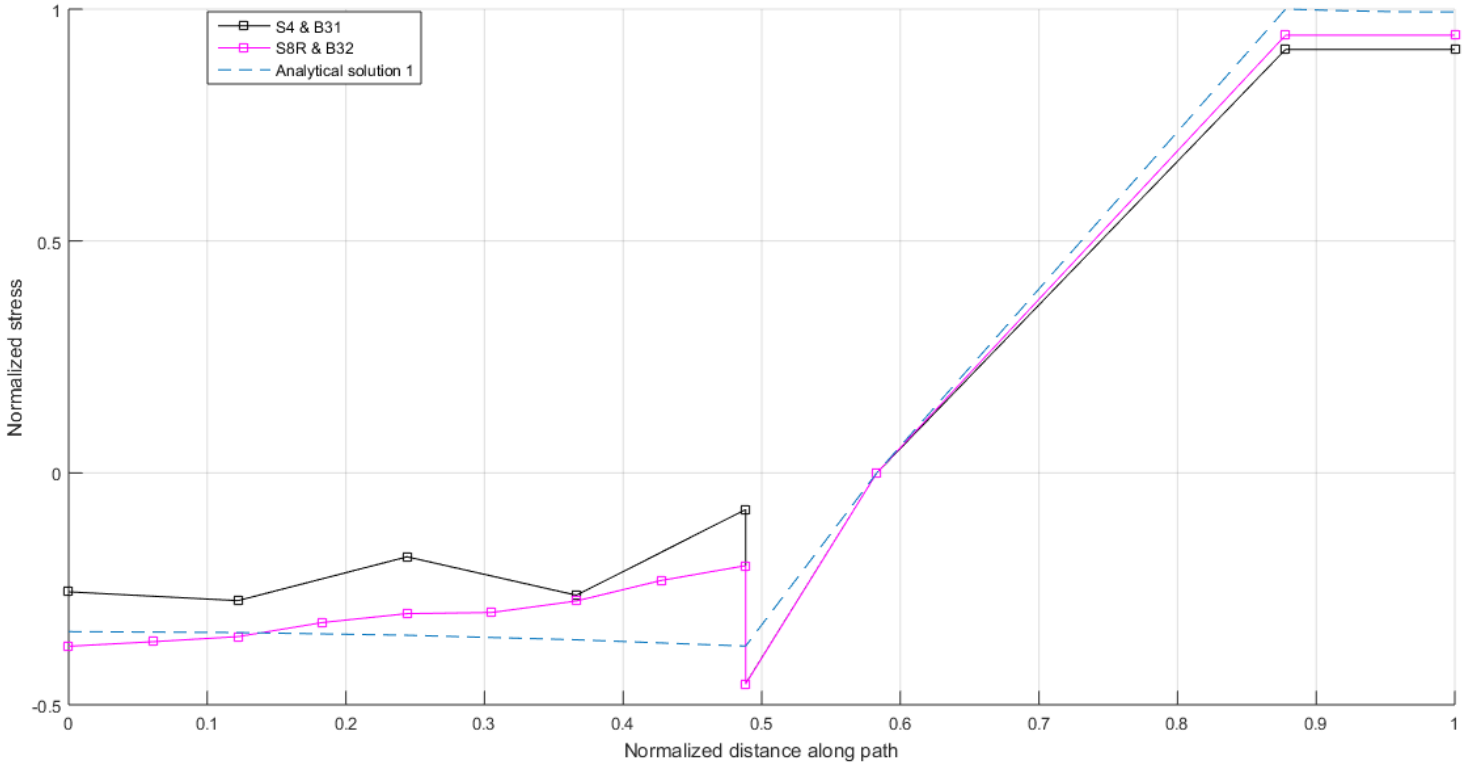

Figure 3.23: Normalized stress for shell & beam elements for $\boldsymbol{x = 0}$

From figure 3.22 and 3.23, it can be concluded that both B31 and B32 elements approximate to the analytical solution 1. However, they underestimate the stresses in the flange because they are 1-D elements and the effect of the shear lag phenomenon cannot be calculated.

In the following diagrams, the results of the stresses along the flange (C-D) for different size of mesh for C3D8, B31 and B32 elements are depicted. The stresses are divided by the maximum stress of the analytical solution 1 (C) and concern the intermediate longitudinal stiffener. As depicted in the following figures, reducing the mesh size from 100 to 20 mm for C3D8 element, the numerical calculations converge to the theoretical. However, on the boundary conditions, with fine mesh the stresses fluctuate along the flange. As regards beam elements, both for B31 and B32 element, from coarse to fine size of mesh the deviance of stresses is reduced between the numerical and theoretical results. For the other elements that mentioned before, it was not observed any remarkable change concerning the size of mesh.

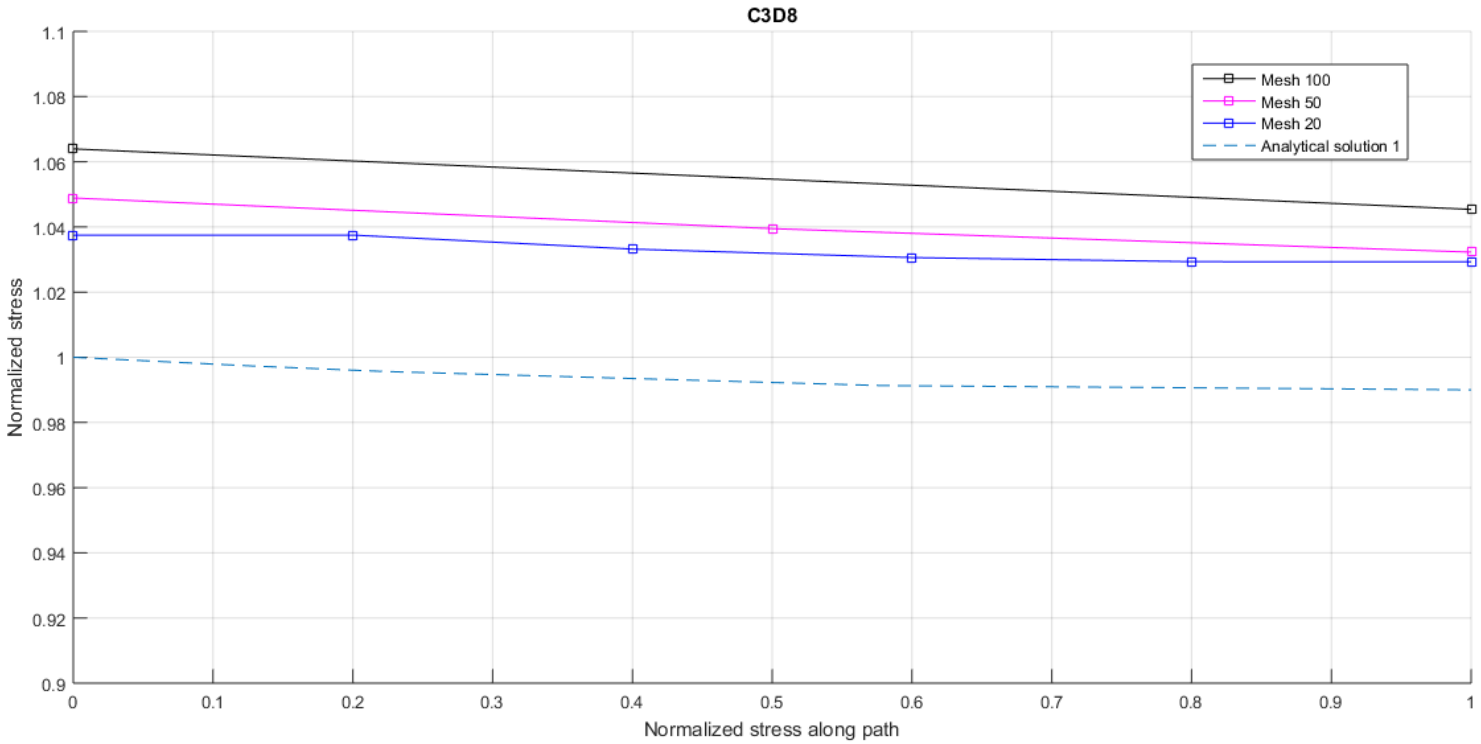

Figure 3.24: Comparison of mesh size for C3D8 element for $\boldsymbol{x = L/2}$

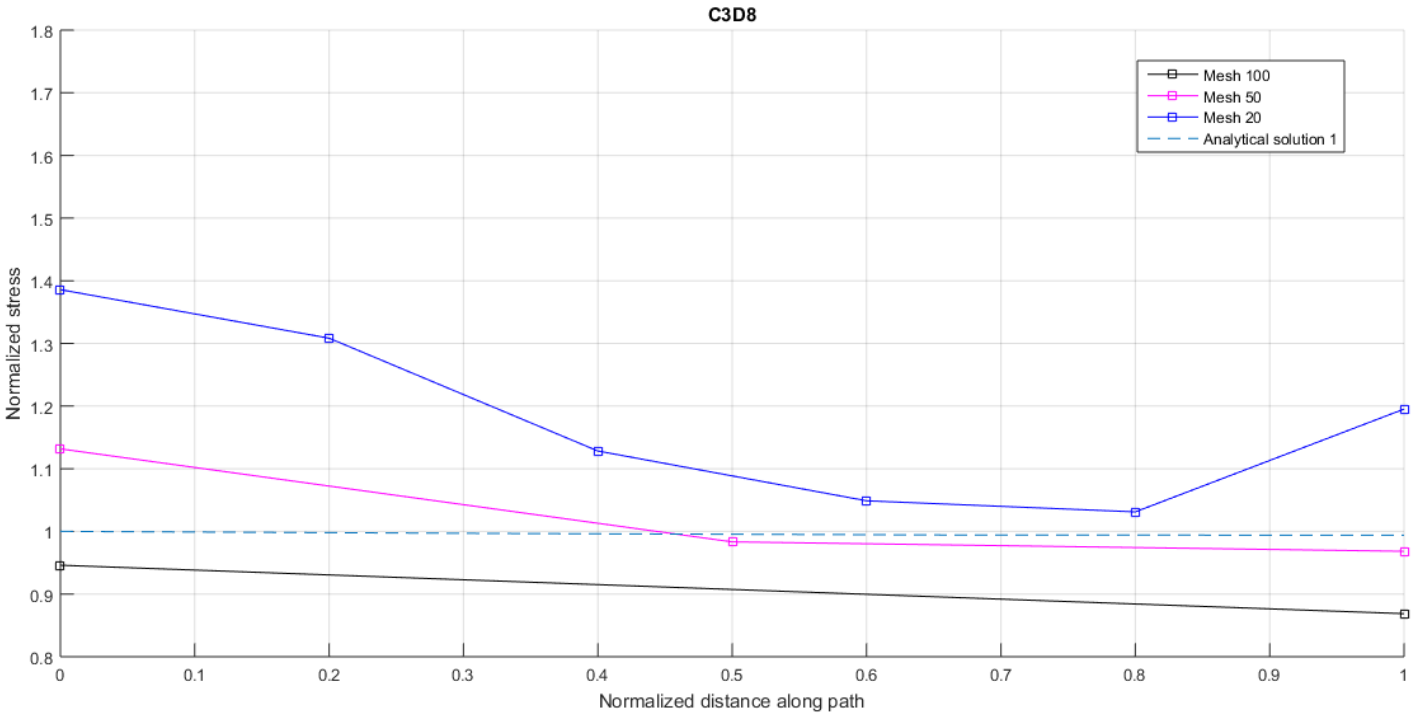

Figure 3.25: Comparison of mesh size for C3D8 element for $\boldsymbol{x = 0}$

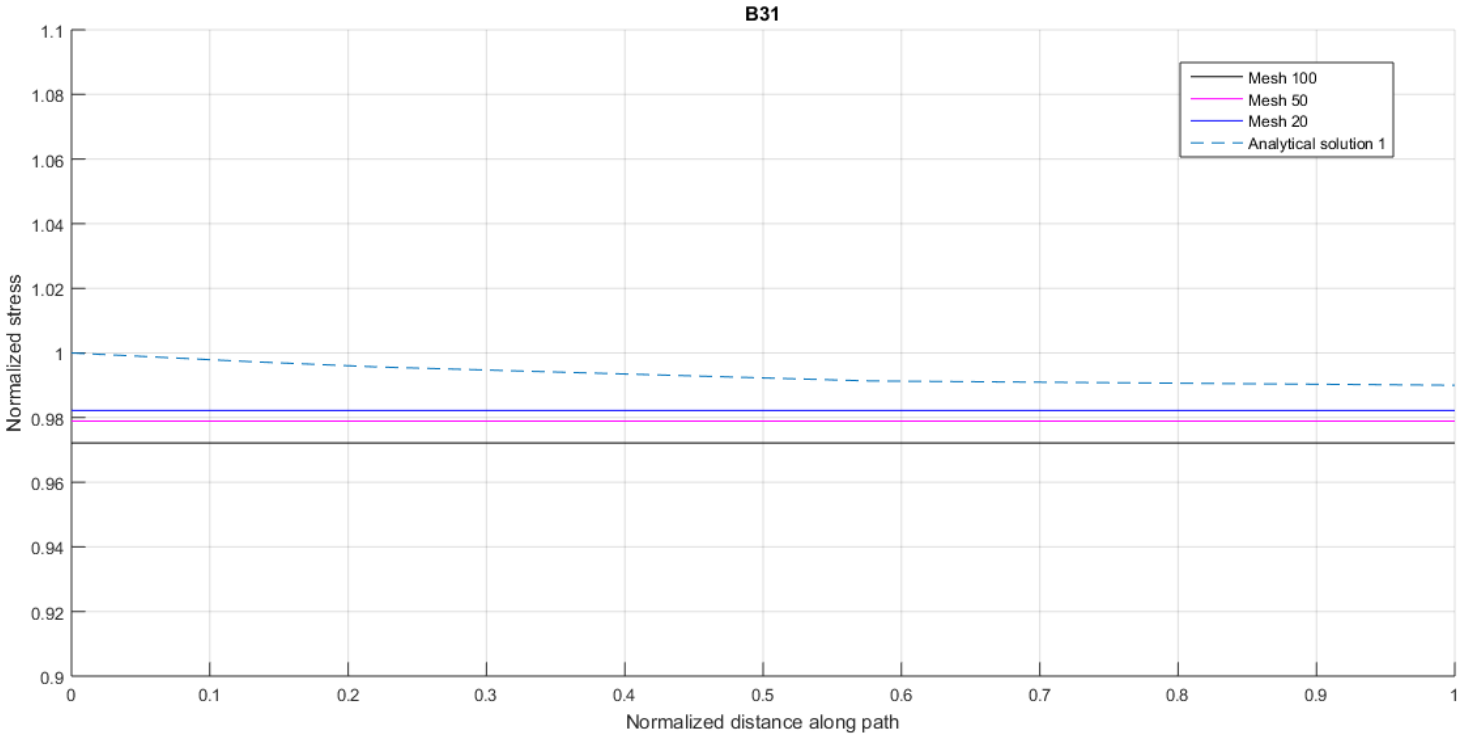

Figure 3.26: Comparison of mesh size for B31 element for $\boldsymbol{x = L/2}$

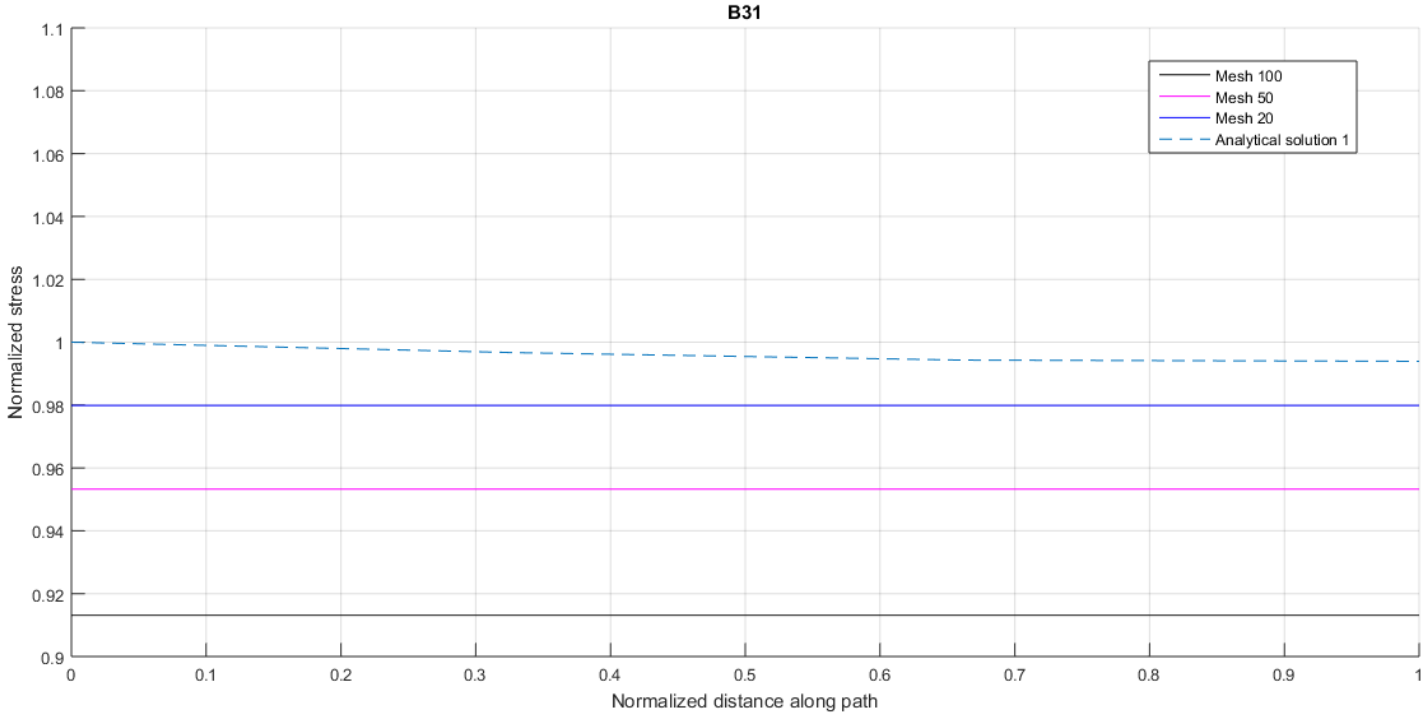

Figure 3.27: Comparison of mesh size for B31 element for $\boldsymbol{x = 0}$

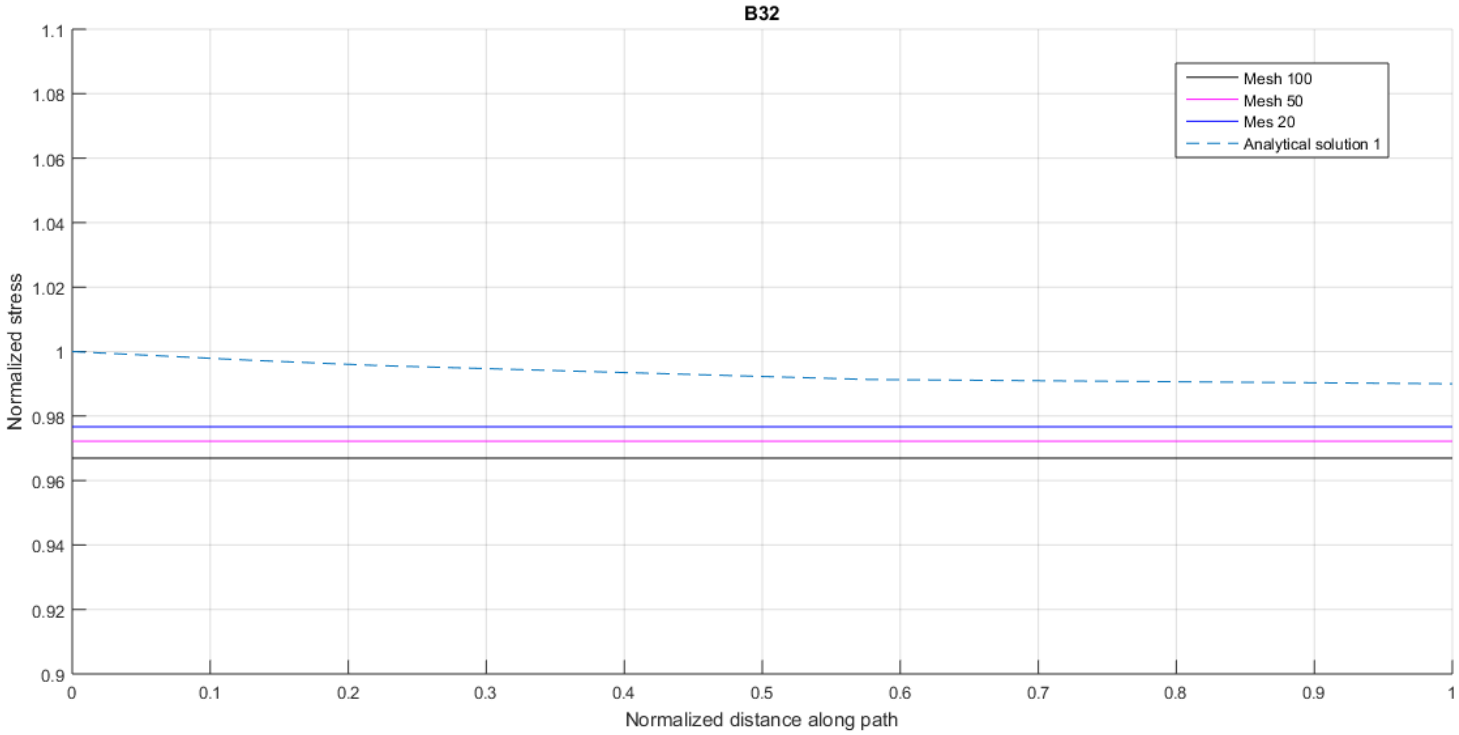

Figure 3.28: Comparison of mesh size for B32 element for $\boldsymbol{x = L/2}$

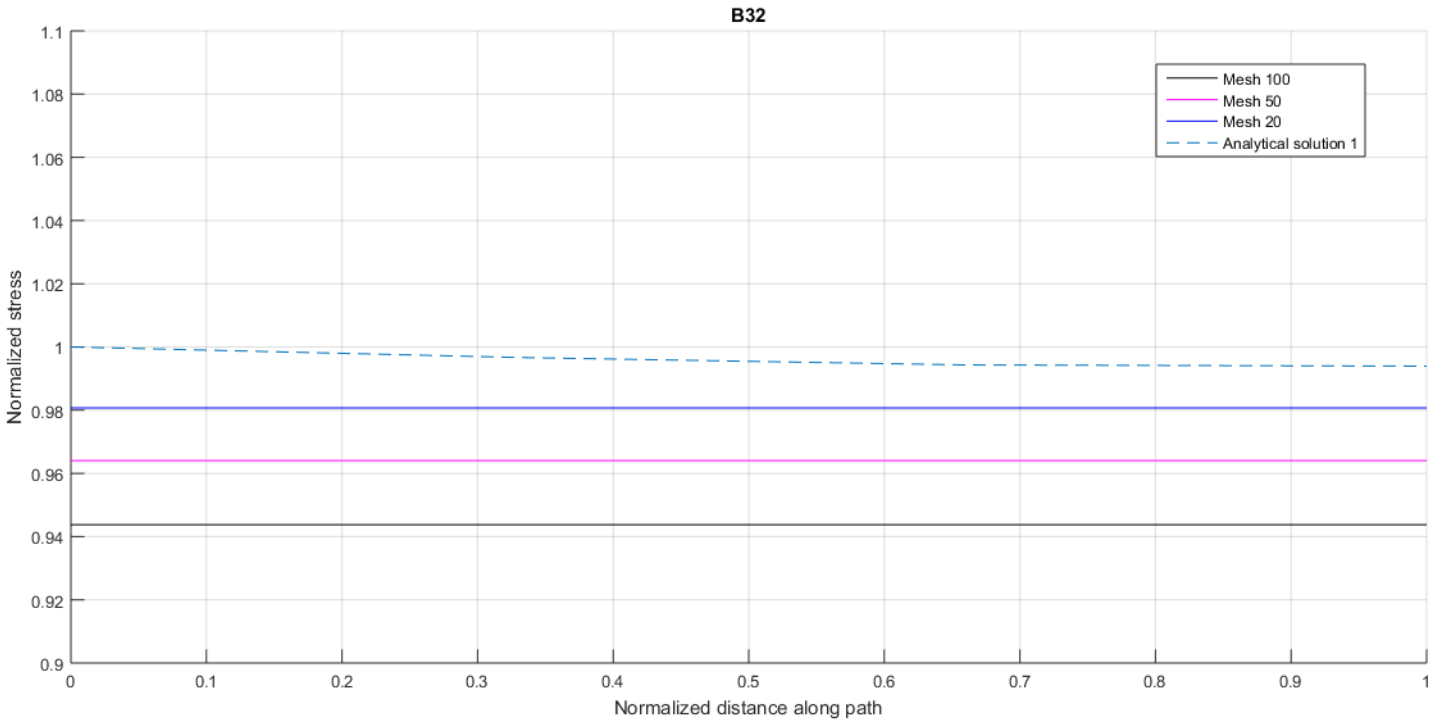

Figure 3.29: Comparison of mesh size for B32 element for $\boldsymbol{x = 0}$

From the above diagrams we can observe that the C3D8 element is suitable to examine the secondary stresses, and by reducing the size of mesh, the results converge to the analytical solution. However, this element is not appropriate to examine the tertiary stresses, namely the stresses that are developed due to the bending of the plate between of the stiffeners. Shell elements seem to be appropriate, for analysis of secondary stresses, only to the web and to the top flange. It is clear that the plate is polluted by tertiary stresses. Moreover, the beam elements give a good approach compared with the analytical solution, but because they are 1-D elements the shear lag phenomenon is not considered and the stresses are underestimated. However, they are the only elements that give a good approach at the boundaries and with a fine mesh, the results converge with the analytical solution.

3.5 Application to real ship scantlings

At this point, stiffeners with the attached plate from ships scantling will be examined, in order to compare the variation of the effective width versus the ratio of

stiffener spacing to the beam span from analytical solutions of Shade, Paik, Miller and CSR. There will be examined T, L and flat bar profiles.

For T and L profiles, the dimensions are the following:

Width of plate [mm]	Thickness of plate [mm]	Height of web [mm]	Thickness of web [mm]	Width of flange [mm]	Thickness of flange [mm]
800	20	300	15	200	18
600	12	200	10	50	10
750	20	280	14	90	14
900	28	340	15	110	15
650	12	240	12	70	12
700	15	300	15	100	15
800	18	380	17	130	17
900	25	425	18	150	18
760	16	350	15	150	15
830	19	430	18	150	18

Table 3.1: Dimensions of T and L profiles

For flat bar profiles, the dimensions are the following:

Width of plate [mm]	Thickness of plate [mm]	Height of web [mm]	Thickness of web [mm]
800	20	300	15
600	12	200	10
750	20	280	14
900	28	340	15
650	12	240	12
700	15	300	15
800	18	380	17
900	25	425	18
760	16	350	15
830	19	430	18

Table 3.2: Dimensions of flat bar profiles

The above profiles are from a range of stiffeners that are used in bulk carriers and tankers. Firstly, for the above profiles, the results of the analytical solution 1 were pictured in the below figure. With the method of least squares, which is a standard approach in regression analysis, the envelope of the lines can be described by the following 4th degree polynomial equations:

- For the lower line:

$$y = -0.21x^4 + 0.87x^3 - 1.1x^2 + 0.038x + 1$$

with residual $\|r\| = \sqrt{\sum |r_k|^2} = 0.002$

where $|r_k|$ the difference between the value of the analytical solution 1 and the 4th polynomial degree for each point

- For the upper line:

$$y = -0.31x^4 + 0.93x^3 - 0.89x^2 + 0.026x + 1$$

with $\|r\| = \sqrt{\sum |r_k|^2} = 0.001$

It is clarified that $y = b_e/b$ and $x = b/L$.

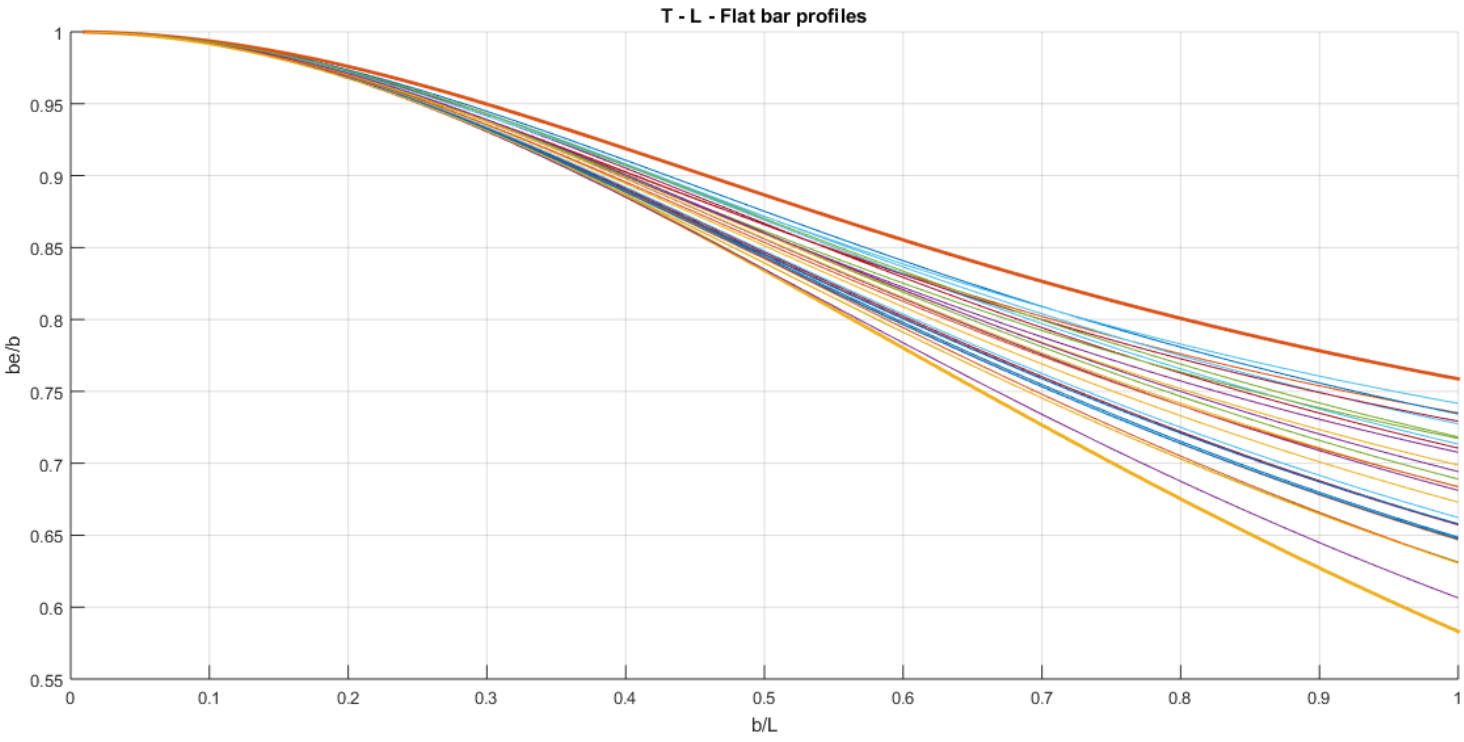

Figure 3.30: Analytical solution 1 for ship scantlings

In the following diagrams, the residuals of the 4th degree polynomial are presented for the lower and upper line.

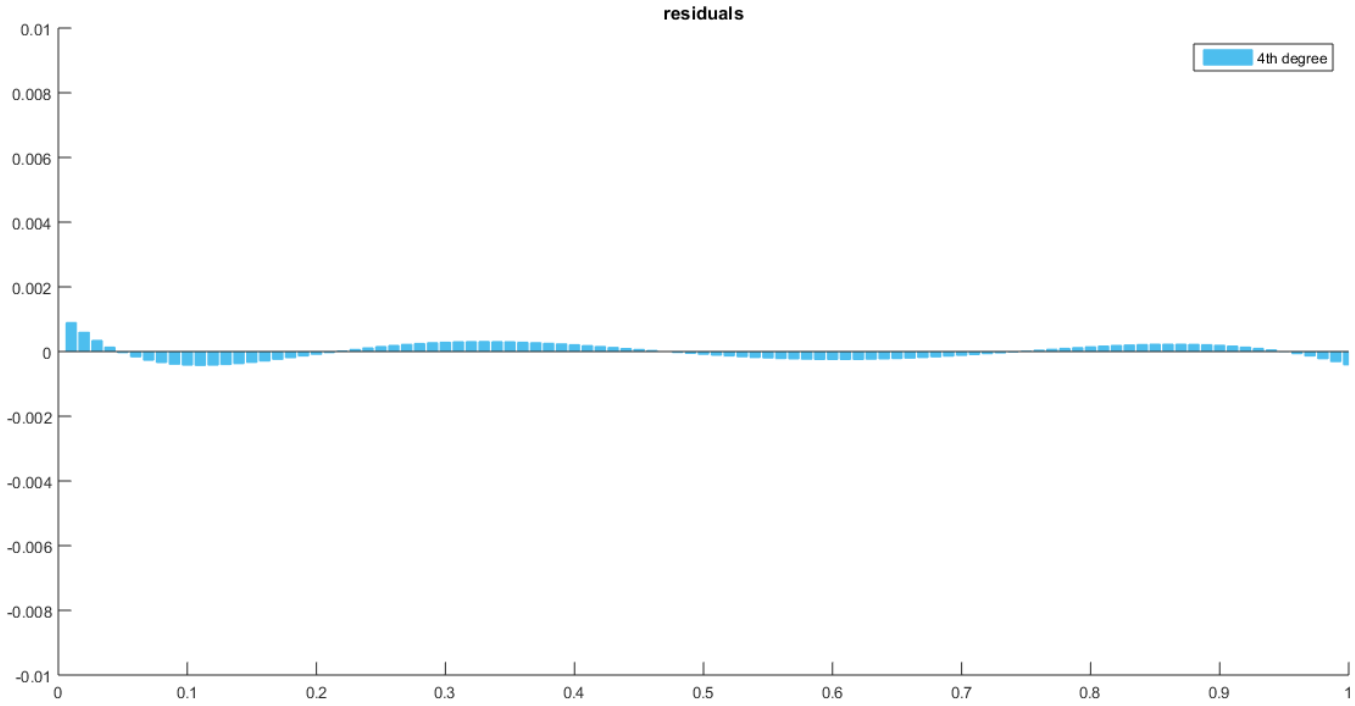

Figure 3.31: Residuals of the 4th degree polynomial for the lower line

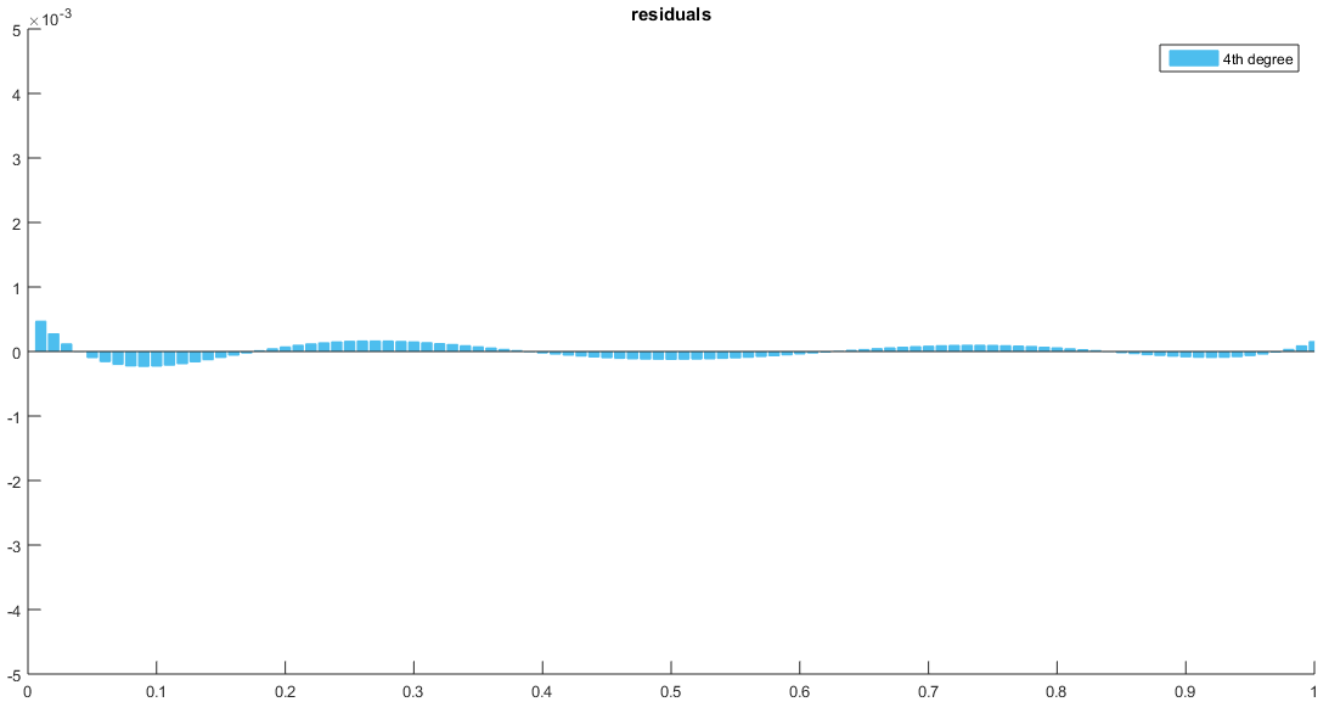

Figure 3.32: Residuals of the 4th degree polynomial for the upper line

It is noted that the equation of CSR is the following:

$$b_e = b * \min\left[\frac{1.12}{1+\frac{1.75}{\left(\frac{L}{b\sqrt{3}}\right)^{1.8}}}, 1\right] \quad \text{for } \frac{L}{b\sqrt{3}} \geq 1$$

$$b_e = 0.407\frac{L}{\sqrt{3}} \quad \text{for } \frac{L}{b\sqrt{3}} < 1$$

In the below figures, the comparison of the different methods is pictured for each profile separately. In each case, the solid lines represent the solution 1 and the envelope of these lines is described by the following 4th degree polynomial equations:

For T profile the envelope of lines of analytical solution 1 is the following:

- For the lower line:

$y = -0.21x^4 + 0.87x^3 - 1.1x^2 + 0.038x + 1$

with residual $\|r\| = \sqrt{\sum |r_k|^2} = 0.002$

- For the upper line:

$y = -0.32x^4 + x^3 - x^2 + 0.032x + 1$

with residual $\|r\| = \sqrt{\sum |r_k|^2} = 0.001$

For L profile the envelope of lines of analytical solution 1 is the following:

- For the lower line:

$y = -0.32x^4 + 1.1x^3 - 1.2x^2 + 0.04x + 1$

with residual $\|r\| = \sqrt{\sum |r_k|^2} = 0.001$

- For the upper line:

$y = -0.33x^4 + x^3 - x^2 + 0.031x + 1$

with residual $\|r\| = \sqrt{\sum |r_k|^2} = 0.002$

For Flat-bar profile the envelope of lines of analytical solution 1 is the following:

- For the lower line:

$y = -0.37x^4 + 1.1x^3 - 1.1x^2 + 0.033x + 1$

with residual $\|r\| = \sqrt{\sum |r_k|^2} = 0.001$

- For the upper line:

$y = -0.31x^4 + 0.93x^3 - 0.89x^2 + 0.026x + 1$

with residual $\|r\| = \sqrt{\sum |r_k|^2} = 0.001$

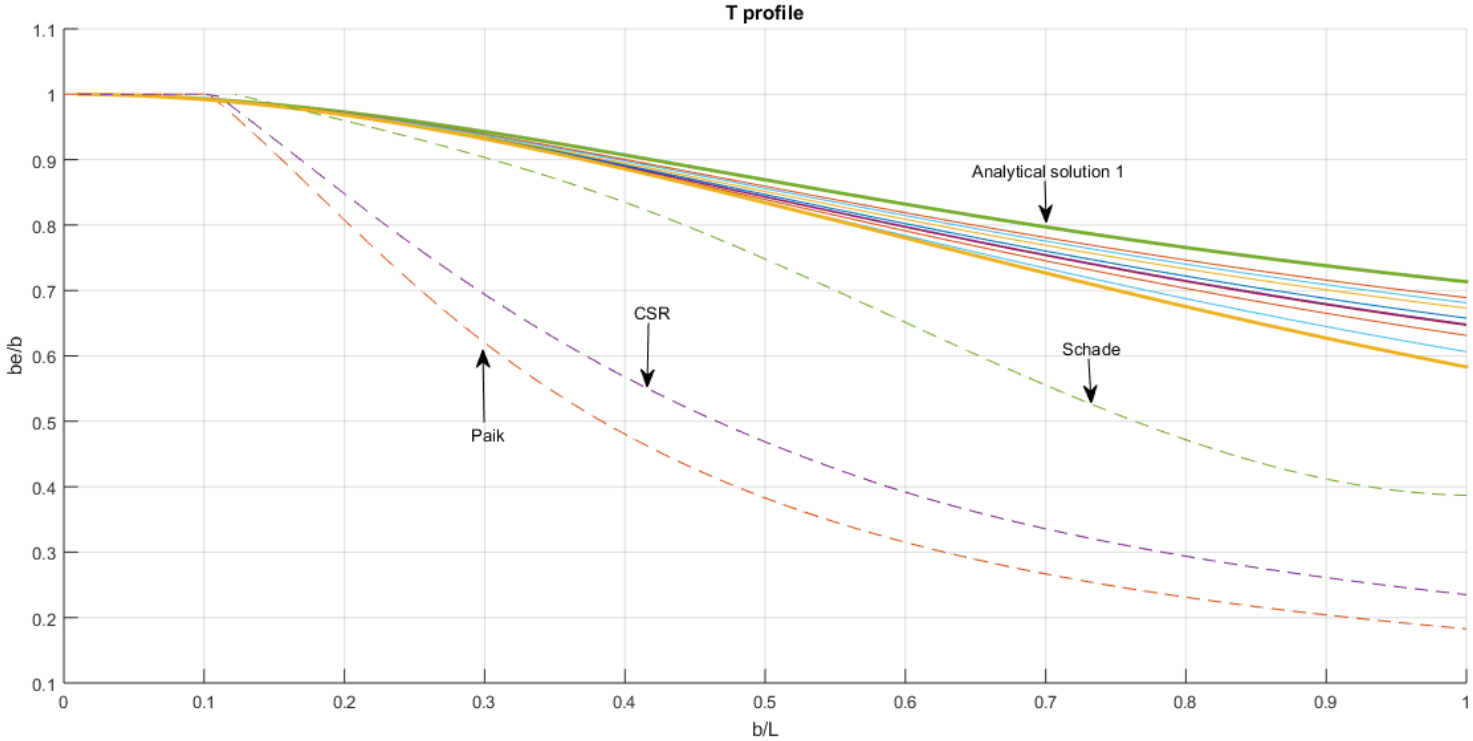

Figure 3.33: Effective width according to analytical solution 1, Paik, Schade and CSR of T profile

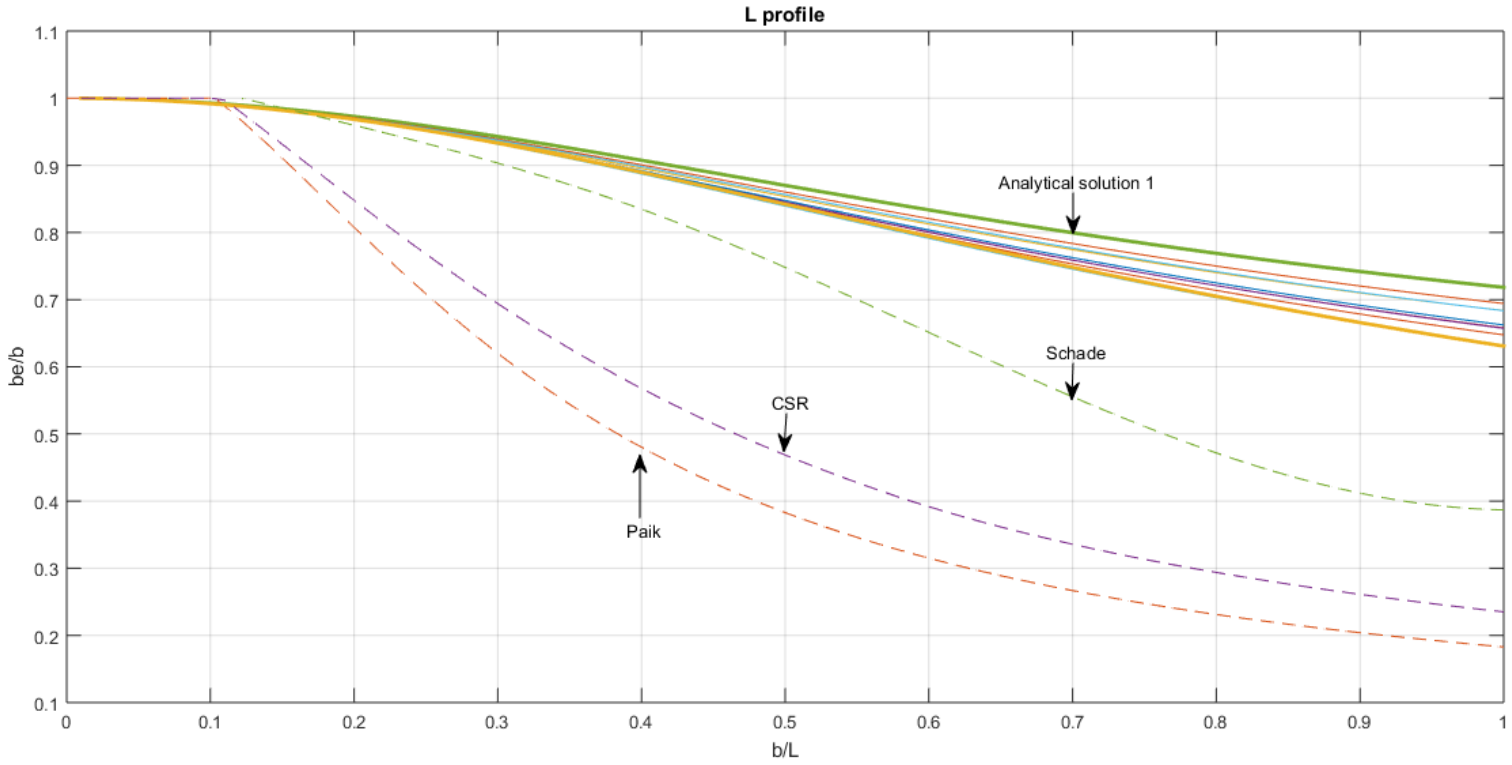

Figure 3.34: Effective width according to analytical solution 1, Paik, Schade and CSR of L profile

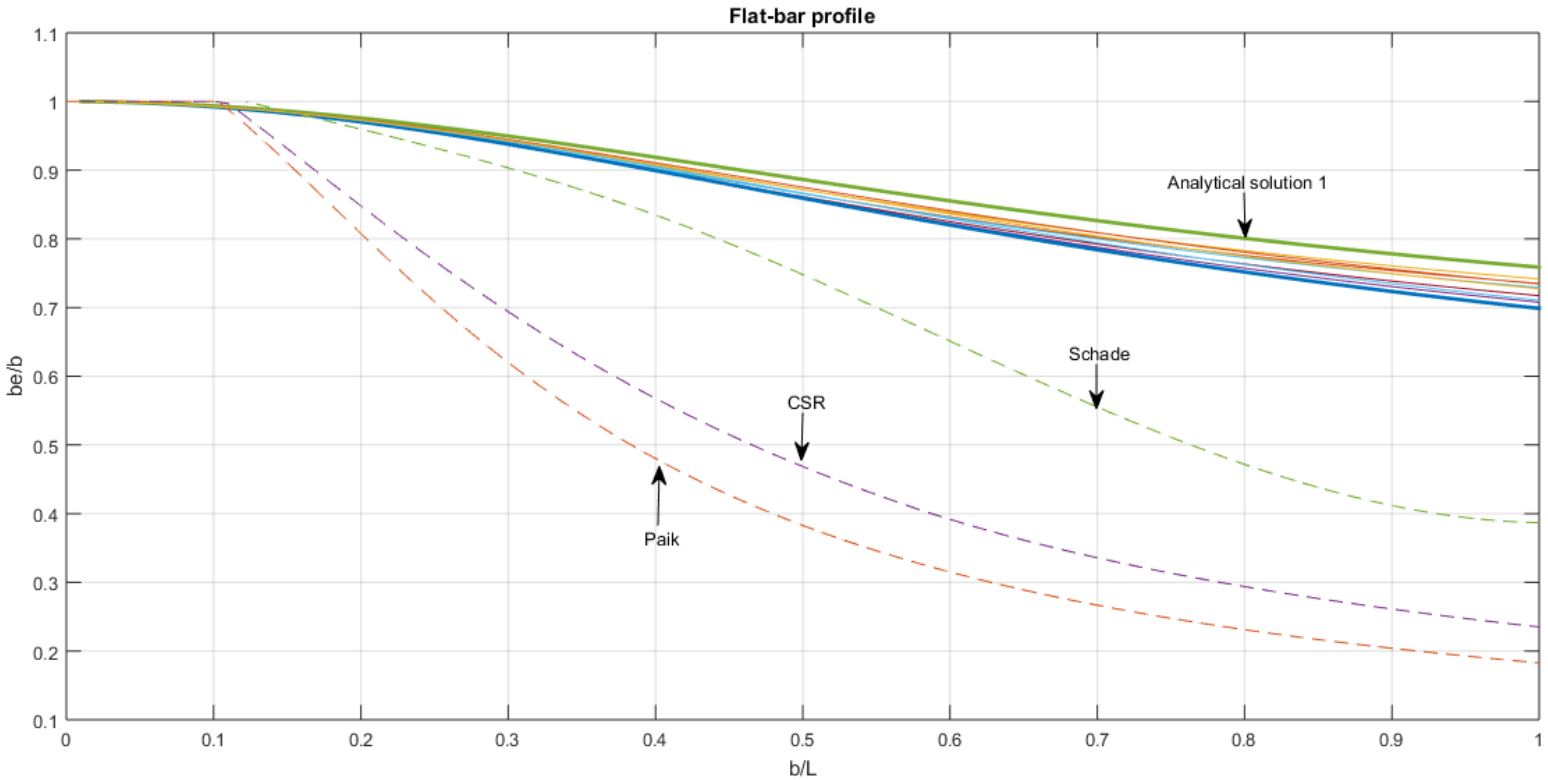

Figure 3.35: Effective width according to analytical solution 1, Paik, Schade and CSR of Flat-bar profile

In conclusion, for simply supported conditions, the method of Paik gives the smallest values of the ratio b_e/b in comparison with the other three methods, which means that is the safest and the most conservative method for the stresses of the attached plate of T, L and flat bar profiles.

4. Stress analysis of cross-stiffened panels

4.1 From 2D to 1D: Analytical calculations-Assumptions

At shipbuilding industry, the cross-stiffened panels are found mainly in passenger and RORO ships. This chapter deals with a modeling strategy for cross-stiffened panels which are subjected to uniform pressure loads and concerns the analysis of the secondary stresses of the longitudinal stiffeners.

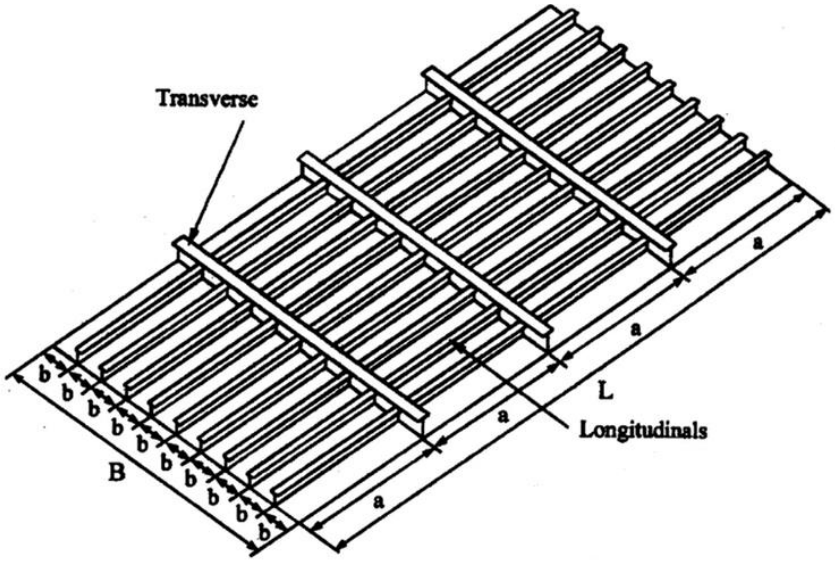

Figure 4.1: Cross-stiffened panels

For stiffened panels in one direction, on the boundaries where the longitudinal and transverse girders are found, it is considered that the support is simple or fixed due to the stiffness of the girder. It is clarified that for the simple support the deflection and the moment is zero and the slope has a non zero value in comparison with the fixed support where the deflection and the slope is zero and the moment has a non zero value. The scope of this chapter is to estimate the boundary conditions that the transverse stiffeners impose to the longitudinal stiffeners. The bending of the longitudinal stiffeners is examined along with the attached plate. For the determination of the boundary conditions, only the secondary stresses are examined. The idea is that the secondary stresses of the stiffeners are related with one coefficient, which in the following pages will be referred as *k*, depending on the boundary conditions. Thus, calculating the secondary stresses of a longitudinal

stiffener between two transverse stiffeners with a commercial software of finite element analysis, we will be able to correlate the coefficient *k* with the type of support. The coefficient *k* will now be defined for simple and fixed supports.

Simply supported beam:

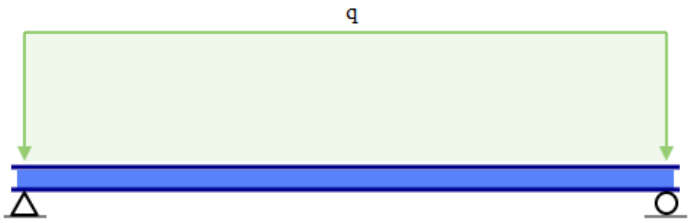

Figure 4.2: Simply supported beam

Let consider a simply supported beam with length *a* and width *b*. From the equilibrium equation $\Sigma F_y = 0$ we get that the reaction forces at supports are $qa/2$. Thus, the shear force *Q* and the bending moment *M* are the following:

$$Q(x) = \frac{qa}{2} - qx \tag{4.1}$$

$$M(x) = \int_0^x Q(\xi)d\xi = \frac{qa}{2}x - \frac{q}{2}x^2 \tag{4.2}$$

The maximum bending moment is at $x = a/2$ because at this position $dM/dx = 0$. By substituting $x = a/2$ into equation (4.2) we get that :

$$M_{max} = \frac{qa^2}{8} \tag{4.3}$$

In the following figure, the first distribution depicts the bending moment and the second depicts the shear force along a simply supported beam.

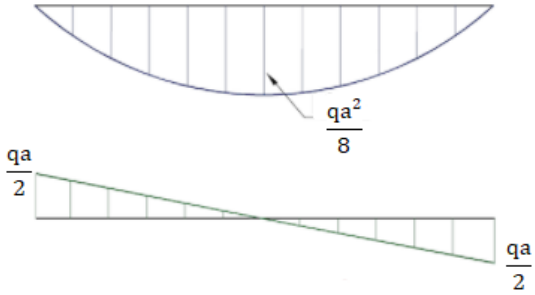

Figure 4.3: Bending moment and shear force distribution of simply supported beams

Considering that $q = p * b$ the maximum stress can be expressed as follows:

$$\sigma_{max} = \frac{M_{max}}{I} z_{max} = \frac{pa^2 b z_{max}}{8I} \quad (4.4)$$

Fixed supported beam:

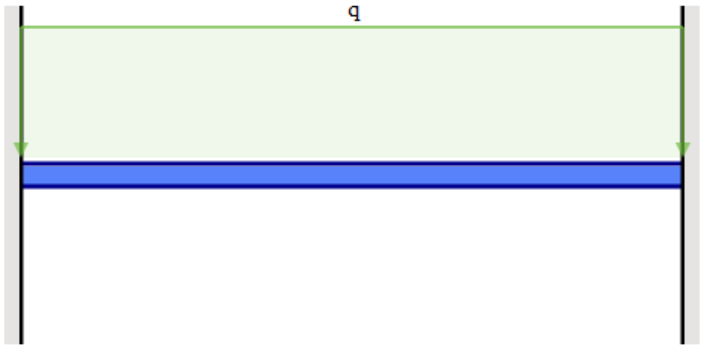

Figure 4.4: Fixed supported beam

Let consider a simply supported beam with length *a* and width *b*. From the equilibrium equations $\Sigma F_y = 0$ and $\Sigma M = 0$ we get that the reaction forces at supports are $qa/2$ and the reaction moments M_F. Thus, the bending moment can be expressed as follows:

$$M(x) = -\frac{qx^2}{2} + \frac{qax}{2} - M_F \quad (4.5)$$

From the elastic curve equation, we get that:

$$\frac{d^2w(x)}{dx^2} = -\frac{M(x)}{EI} \tag{4.6}$$

where w(x) is the deflection of the beam. The boundary conditions are the following:

- $w|_{x=0} = 0$ (4.7)
- $w|_{x=a} = 0$ (4.8)
- $\frac{dw}{dx}\Big|_{x=0} = 0$ (4.9)
- $\frac{dw}{dx}\Big|_{x=a} = 0$ (4.10)

By substituting equations (4.7)-(4.10) into equation (4.6) we that:

$$M_F = \frac{qa^2}{12} \tag{4.11}$$

Thus, the bending moment can be expressed as:

$$M(x) = -\frac{qx^2}{2} + \frac{qax}{2} - \frac{qa^2}{12} \tag{4.12}$$

The maximum bending moment is at $x = 0$ with value:

$$M_{max} = \frac{qa^2}{12} \tag{4.13}$$

In the following figure, the first distribution depicts the bending moment and the second depicts the shear force along a fixed supported beam.

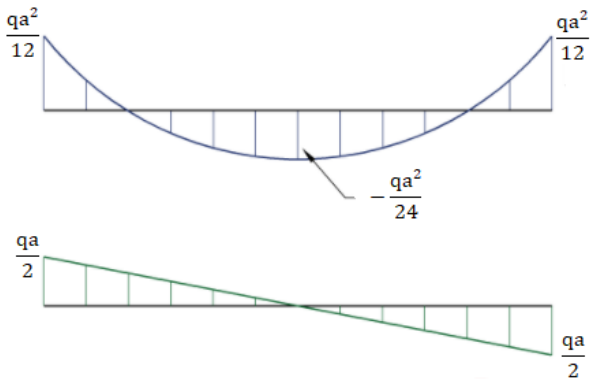

Figure 4.5: Bending moment and shear force distribution of fixed supported beams

The maximum stress can now be expressed as follows:

$$\sigma_{max} = \frac{M_{max}}{I} z_{max} = \frac{pa^2 b z_{max}}{12I} \quad (4.14)$$

From the equation (4.4) and (4.14) we get that the formula of the maximum stress is:

$$\sigma_{max} = \frac{pa^2 b z_{max}}{kI} \quad (4.15)$$

with *k* to be equal with 8 for simply supported beam and 12 for fixed supported beam. In order to visualize this, let consider a beam with torsional springs as supports, as depicted in the following figure. When $k = 8$ then the spring stiffness is zero and when $k = 12$ then the spring stiffness is infinite.

Figure 4.6: Beam with torsional springs as supports

Thus, designing a model with cross-stiffened panel in the finite element analysis software, the stresses can be computed and by substituting them to the equation (4.15) the coefficient *k* can be calculated. The parameters of the model are the pressure load, the number of the longitudinal and transverse stiffeners, the distance *a* of the transverse stiffeners (which is the length of the longitudinal stiffeners), the distance *b* between the longitudinal stiffeners (which is the width of the attached plate of the longitudinal stiffeners), the thickness t_{el} of the plate and the dimensions of longitudinal and transverse stiffeners. It is clarified that the moment of inertia of equation (4.15) concerns the longitudinal stiffener along with the attached plate. Our scope is to find the relation between the inertia moment of transverse stiffeners and the coefficient *k.* In order to succeed reliable results, we need to run the model for a range of the parameters that were mentioned previously. The choice of the values of the parameters and the number that the model will be run, will be determined from the central composite design, that is analyzed below.

4.2 Design of experiment and test matrix

Central composite design is appropriate for calibrating full quadratic models. It consists of a full factorial design with a central point and additional axial points at a specific distance from its centre. There are three types of central composite design: circumscribed, inscribed and faced. For our case, we will use the faced design.

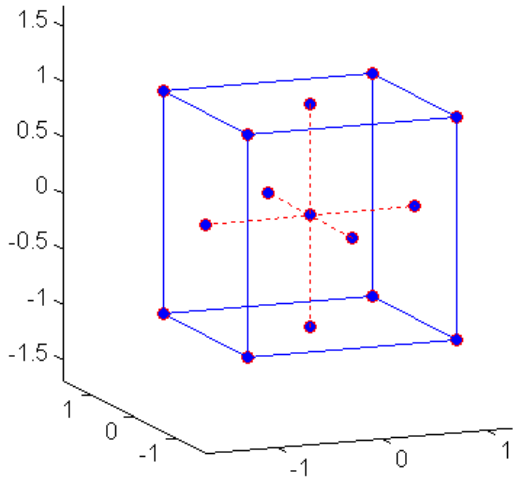

Figure 4.7: Central Composite Faced

For our case, the range of the values of the variables will be determined from the range of the values that are used to real ship scantlings. The variables of the problem are the following:

- X_1: The distance between two consecutive longitudinal stiffeners
- X_2: The distance between two consecutive transverse stiffeners
- X_3: The thickness of the plate
- X_4: The profile of the cross section of the longitudinal stiffeners

Considering that *n* represents the number of the variables, the total number of design points is equal to $2^n + 2n + 1 = 25$. The range of the values for the variable X_1 is from 600 to 900 mm, for the variable X_2 from 1800 to 5400 mm and for the variable X_3 from 12 to 28 mm. For the variable X_4 the following T profiles are examined: (200x10 + 50x10), (280x14 + 90x14) and (340x15 + 110x15). The test matrix of the four variables is the following:

X_1	X_2	X_3	X_4
-1	-1	-1	-1
-1	-1	-1	$+1$
-1	-1	$+1$	-1
-1	-1	$+1$	$+1$
-1	$+1$	-1	-1
-1	$+1$	-1	$+1$
-1	$+1$	$+1$	-1
-1	$+1$	$+1$	$+1$
$+1$	-1	-1	-1
$+1$	-1	-1	$+1$
$+1$	-1	$+1$	-1
$+1$	-1	$+1$	$+1$
$+1$	$+1$	-1	-1
$+1$	$+1$	-1	$+1$
$+1$	$+1$	$+1$	-1
$+1$	$+1$	$+1$	$+1$
-1	0	0	0
$+1$	0	0	0
0	-1	0	0
0	$+1$	0	0
0	0	-1	0
0	0	$+1$	0
0	0	0	-1
0	0	0	$+1$
0	0	0	0

Table 4.1: Test matrix of central composite faced

Applying the above test matrix to the range of the variables that was described previously, the values of each experiment are the following:

X_1[mm]	X_2[mm]	X_3[mm]	X_4[mm × mm]
600	1800	12	$200 \times 10 + 50 \times 10$
600	1800	12	$340 \times 15 + 110 \times 15$
600	1800	28	$200 \times 10 + 50 \times 10$
600	1800	28	$340 \times 15 + 110 \times 15$
600	5400	12	$200 \times 10 + 50 \times 10$
600	5400	12	$340 \times 15 + 110 \times 15$
600	5400	28	$200 \times 10 + 50 \times 10$
600	5400	28	$340 \times 15 + 110 \times 15$
900	1800	12	$200 \times 10 + 50 \times 10$
900	1800	12	$340 \times 15 + 110 \times 15$
900	1800	28	$200 \times 10 + 50 \times 10$
900	1800	28	$340 \times 15 + 110 \times 15$
900	5400	12	$200 \times 10 + 50 \times 10$
900	5400	12	$340 \times 15 + 110 \times 15$
900	5400	28	$200 \times 10 + 50 \times 10$
900	5400	28	$340 \times 15 + 110 \times 15$
600	3600	20	$280 \times 14 + 90 \times 14$
900	3600	20	$280 \times 14 + 90 \times 14$
750	1800	20	$280 \times 14 + 90 \times 14$
750	5400	20	$280 \times 14 + 90 \times 14$
750	3600	12	$280 \times 14 + 90 \times 14$
750	3600	28	$280 \times 14 + 90 \times 14$
750	3600	20	$200 \times 10 + 50 \times 10$
750	3600	20	$340 \times 15 + 110 \times 15$
750	3600	20	$280 \times 14 + 90 \times 14$

Table 4.2: The values of the variable for the model

For each of the above 25 cases the stresses, thus the coefficient *k*, will be calculated for five different cross sections of transverse stiffeners in order to find a relation between the second moment of inertia of transverse stiffeners and the coefficient *k*.

Namely, for the longitudinal stiffeners with T profile and dimensions $200 \times 10 + 50 \times 10$, the stresses will be calculated for the following transverse stiffeners of T profile [mm × mm]:

- $200 \times 10 + 50 \times 10$
- $270 \times 13 + 85 \times 13$
- $330 \times 15 + 110 \times 15$
- $375 \times 16 + 130 \times 16$
- $425 \times 18 + 150 \times 18$

For the longitudinal stiffeners with $280 \times 14 + 90 \times 14$ dimensions and T profile, the stresses will be calculated for the following transverse stiffeners of T profile [mm × mm]:

- $280 \times 14 + 90 \times 14$
- $320 \times 15 + 105 \times 15$
- $360 \times 16 + 120 \times 16$
- $390 \times 17 + 140 \times 17$
- $425 \times 18 + 150 \times 18$

For the longitudinal stiffeners with $340 \times 15 + 110 \times 15$ dimensions and T profile, the stresses will be calculated for the following transverse stiffeners of T profile [mm × mm]:

- $340 \times 15 + 110 \times 15$
- $360 \times 16 + 120 \times 16$
- $380 \times 17 + 130 \times 17$
- $400 \times 17 + 140 \times 17$
- $425 \times 18 + 150 \times 18$

The dimensions of the transverse stiffeners were chosen considering that the second moment of inertia of longitudinal stiffeners is smaller than the second moment of inertia of transverse stiffeners. It is clarified that the above transverse stiffeners have different second moment of inertia.

For each case, all structural elements comply with the applicable slenderness and proportion requirements according to CSR. Specifically, the net thickness satisfies the following criteria:

$$t_p \geq \frac{b}{C}\sqrt{\frac{R_{eH}}{235}} \tag{4.16}$$

where b is the breadth of the plate, R_{eH} is the specified minimum yield stress of the material and for all the structural elements is considered 235 N/mm^2 and $C = 100$.

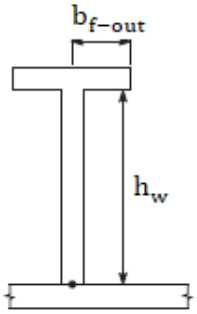

Figure 4.8: T bar profile of stiffeners

The net thickness of stiffener web plate satisfies the following criterion:

$$t_w \geq \frac{h_W}{C_w}\sqrt{\frac{R_{eH}}{235}} \tag{4.17}$$

The net thickness of flange satisfies the following criterion:

$$t_f \geq \frac{b_{f-out}}{C_f}\sqrt{\frac{R_{eH}}{235}} \tag{4.18}$$

The total flange breath satisfies the following criterion:

$$b_f \geq 0.25 h_W \tag{4.19}$$

where $C_W = 75$ and $C_f = 12$ are slenderness coefficients. As depicted in figure 4.8 h_W is the depth of stiffener web and b_{f-out} is the maximum distance from mid thickness of the web to the flange edge.

The minimum value of the net moment of inertia of the stiffener with the effective width of attached plate is given by:

$$I_{st} \geq Cl^2 A_{eff} \frac{R_{eH}}{235} \tag{4.20}$$

where A_{eff} is the net sectional area of stiffener including attached plate and C ,the slenderness coefficient, is 1.43 for longitudinal stiffeners and 0.72 for transverse stiffeners.

4.3 Modeling in commercial Finite Element software

For each model in the finite element software, four transverse stiffeners with distance equal to a (X_2 variable) and three longitudinal stiffeners with distance equal to b (X_1 variable) will be used. The plate is fixed supported. The value of the pressure is equal to 0.1 MPa, of the modulus of elasticity equal to 207 GPa and of the Poisson's ratio equal to 0.3. The mesh size is 50 mm. The plate was modeled with S4 shell elements and the stiffeners with B31 beam elements. The longitudinal stiffener that was examined, was in the middle of X-Y plane in order to have minimization of the effect of the boundary conditions. It is clarified that for each case, the maximum stress S_{11}along the longitudinal stiffener between the two transverse stiffeners, with the stress to be parallel with the direction of longitudinal stiffeners, will be substituted into equation (4.15).

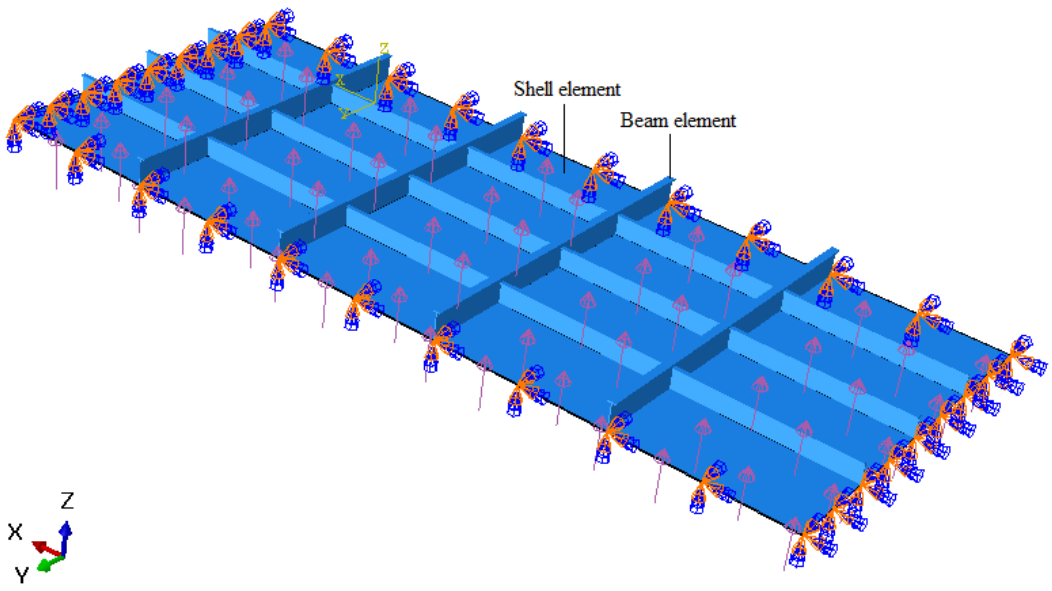

Figure 4.9: Boundary conditions for cross-stiffened panel in Abaqus

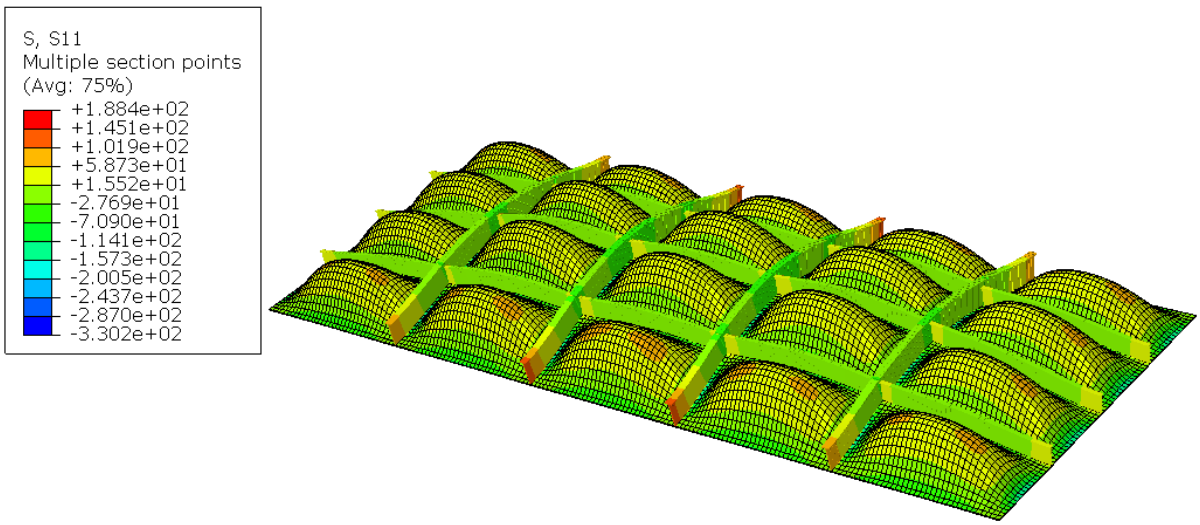

Figure 4.10: Stresses with direction parallel to the length of the plate

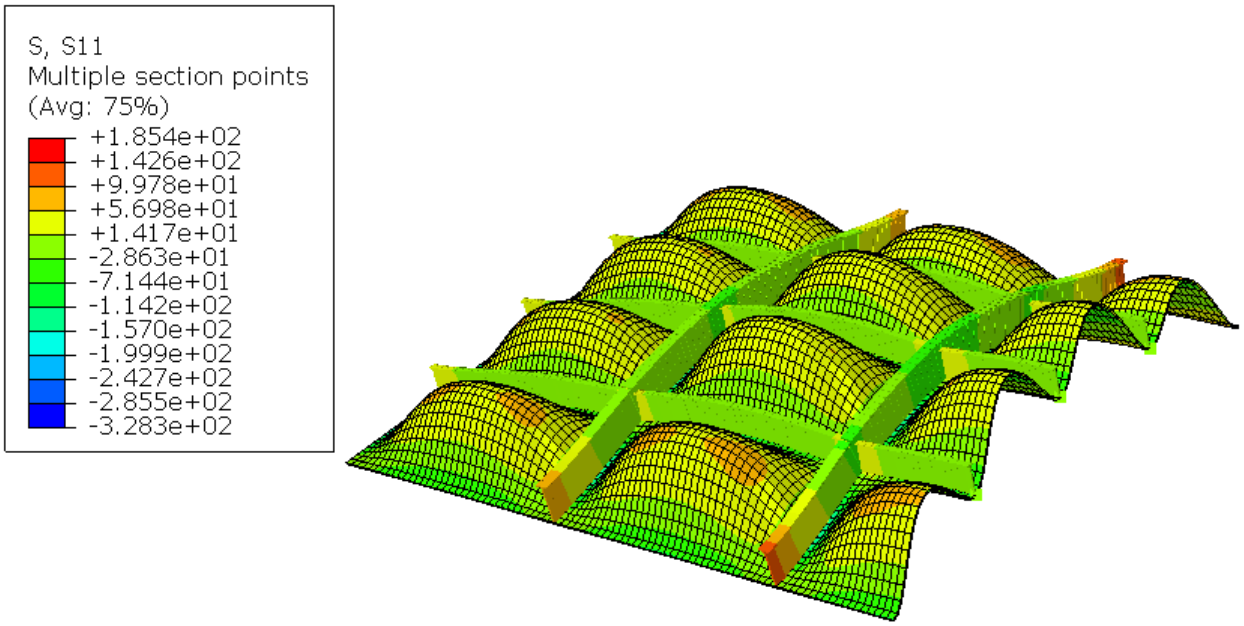

Figure 4.11: Cut view at the middle length of the plate

In figure 4.9, it is depicted the pressure loads and the boundary conditions and with annotations the beam and shell elements. In figures 4.10 and 4.11 it is depicted the distribution of the stress with direction parallel to the undeformed longitudinal stiffeners. The longitudinal stiffener that was examined, is the intermediate that is depicted in cut view in figure 4.11. In the following diagrams the distribution of beam stress and the magnitude of deflection are presented.

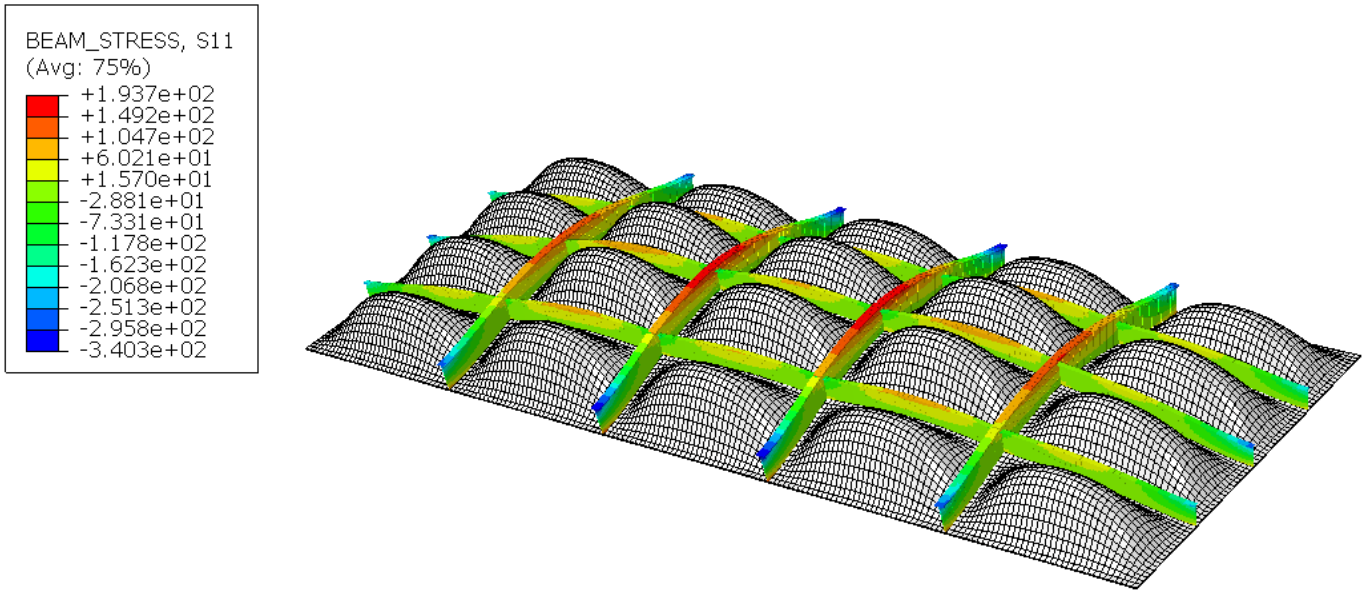

Figure 4.12: Beam stress of longitudinal and transverse stiffeners

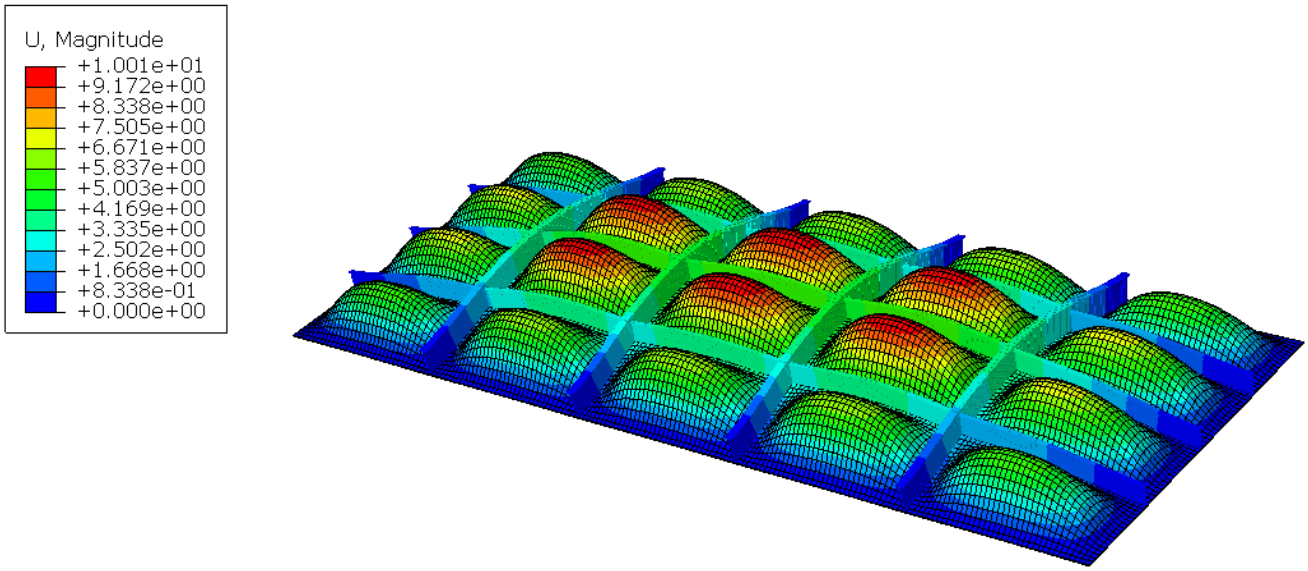

Figure 4.13: Magnitude of the deflection

4.4 Application to real ship scantlings – Results

Below, for each case the mean and standard deviation of *k* are presented. The analytical results for each are found in the appendix. Given that for each case, the value of *k* is calculated for five different values of second moment of inertia of transverse stiffeners, the mean (μ) and the standard deviation (σ) are given by the following formulas:

$$\mu = \frac{\sum_i X_i}{N} \tag{4.21}$$

$$\sigma = \sqrt{\frac{\sum_i (X_i - \mu)^2}{N}} \tag{4.22}$$

where X_i the values of k for each case, and $N = 5$ the number of the values.

Case	Mean (μ)	Standard deviation (σ)
1	12.57	0.32
2	13.73	0.69
3	14.16	0.74
4	15.56	0.85
5	11.8	0.03
6	8.88	0.05
7	18.95	1.33
8	12.91	0.11
9	13.06	0.52
10	11.19	1.31
11	15.09	0.56
12	12.33	1.64
13	11.76	0.06
14	11.46	0.08
15	14.26	0.97
16	11.94	0.04
17	11.93	0.02
18	11.92	0.03
19	14.53	0.92
20	11.8	0.02
21	11.59	0.1
22	12.31	0.08
23	12.28	0.13
24	11.75	0.02
25	11.89	0.04

Table 4.3: Mean and standard deviation of *k* for each case

For all the cases, the value of *k* is not smaller than 8. Thus, we can consider that for longitudinal stiffeners with values of second moment of inertia from 1.1×10^7 to 8.8×10^7 mm^4 and for transverse stiffeners with values from 1.1×10^7 to $21.3 \times 10^7 mm^4$, the most safe and conservative value for the coefficient *k* is 8. It can also be considered that the increase of the second moment of inertia of transverse stiffeners for each case does not affect the value of the coefficient. In the following figure, the values of the 125 points are depicted. The Y axis refers to the second moment of inertia of transverse stiffeners.

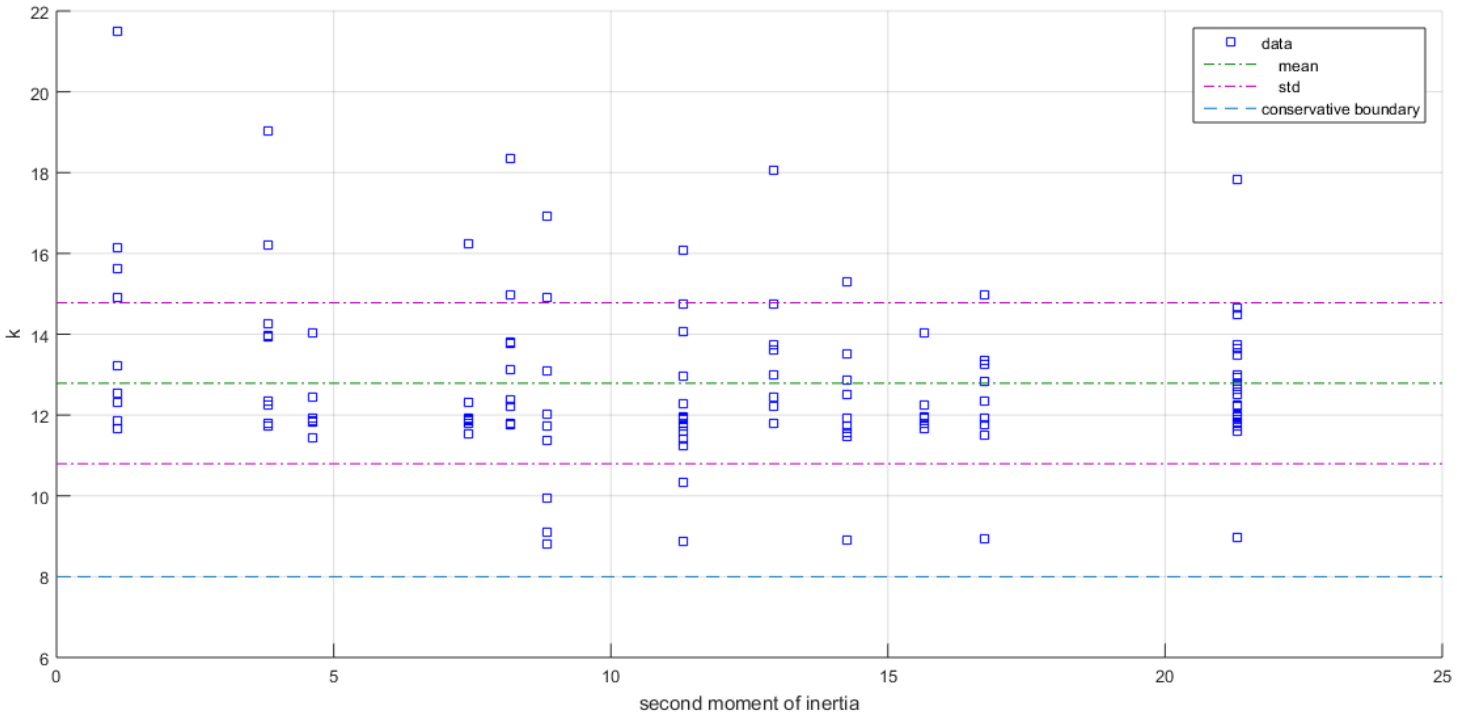

Figure 4.14: Results for k in relation with second moment of inertia of transverse stiffeners

In the following figures, the histogram and the probability distribution of values of *k* are presented. The probability distribution can be approximated by the probability density function of *t location-scale* distribution with the following formula:

$$f_X(x) = \frac{\Gamma\left(\frac{\nu+1}{2}\right)}{\sigma\sqrt{\nu\pi}\,\Gamma\left(\frac{\nu}{2}\right)}\left[\frac{\nu + \left(\frac{x-\mu}{\sigma}\right)^2}{\nu}\right]^{-(\nu+1)} \tag{4.23}$$

where μ is the location parameter and is equal to 12.16, σ is the scale parameter and is equal to 0.77, ν is the shape parameter and is equal to 1.36 and $\Gamma(\cdot)$ is the gamma function and its formula is given by:

$$\Gamma(x) = \int_0^{\infty} e^{-t} t^{x-1} dt \tag{4.24}$$

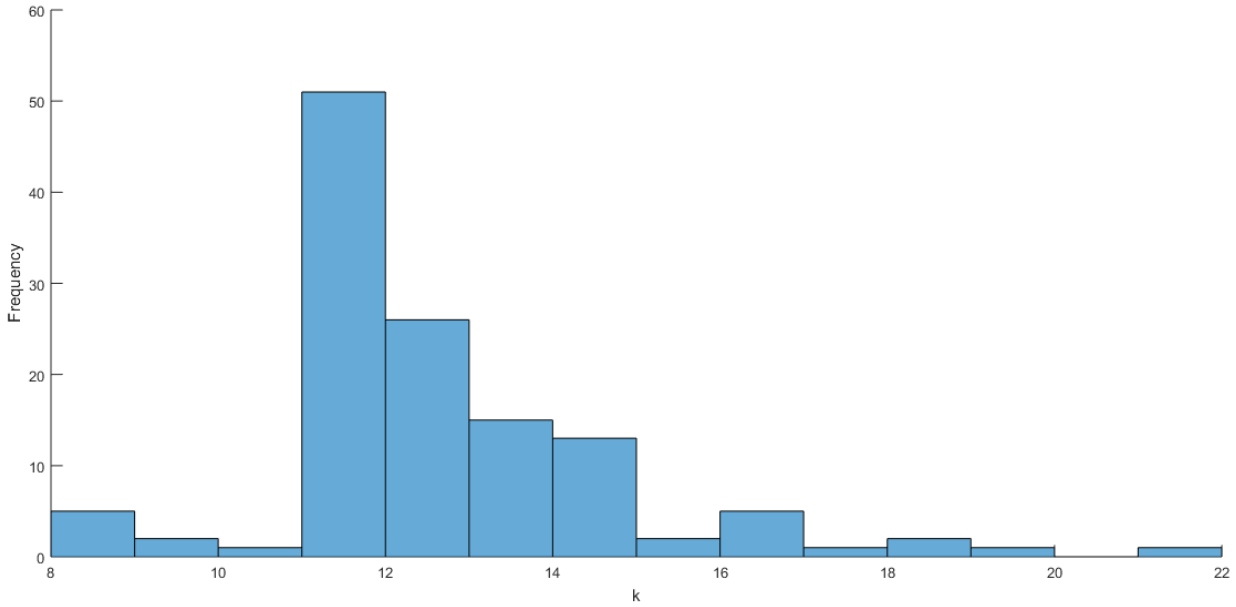

Figure 4.15: Histogram for the values of *k*

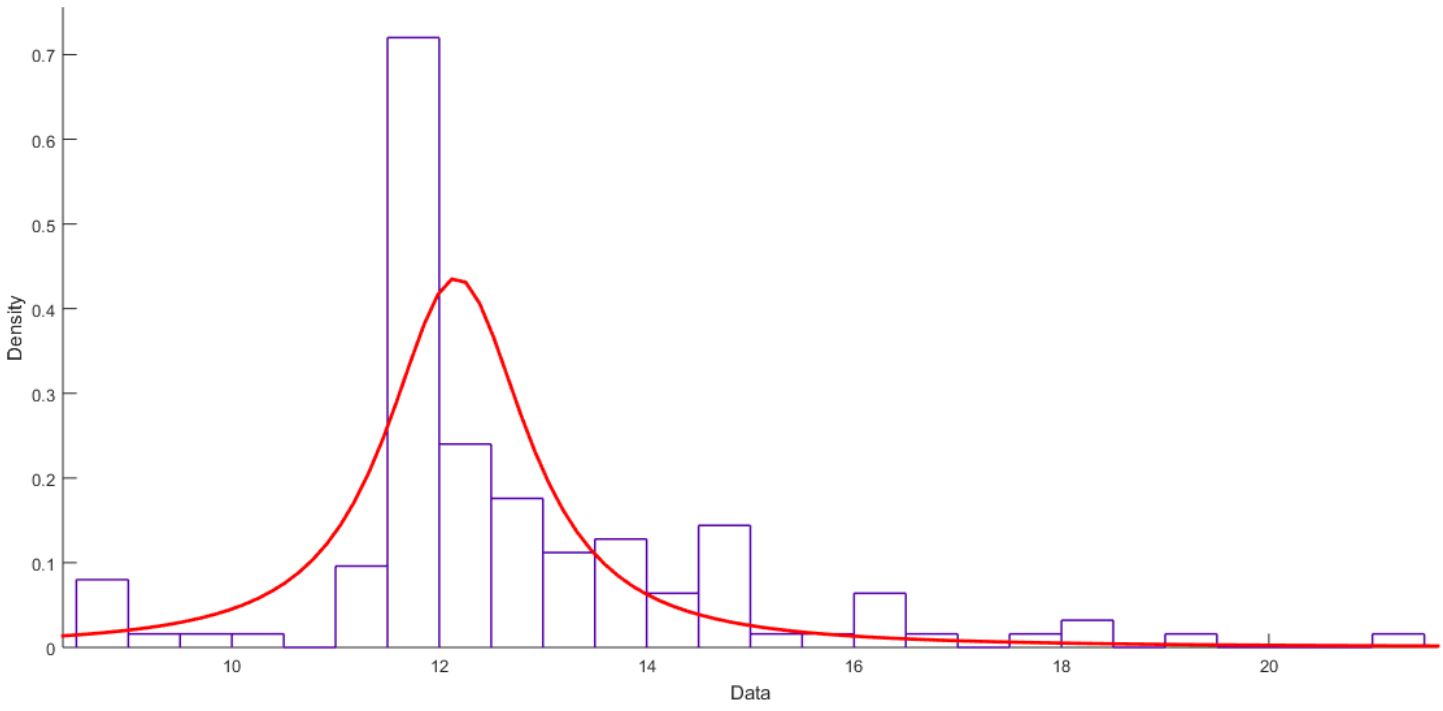

Figure 4.16: The *t location-scale* distribution for the values of *k*

In the following figure, the box plot for the values of *k* is depicted. It is shown that in most cases the effect of the second moment of inertia of transverse stiffeners is negligible.

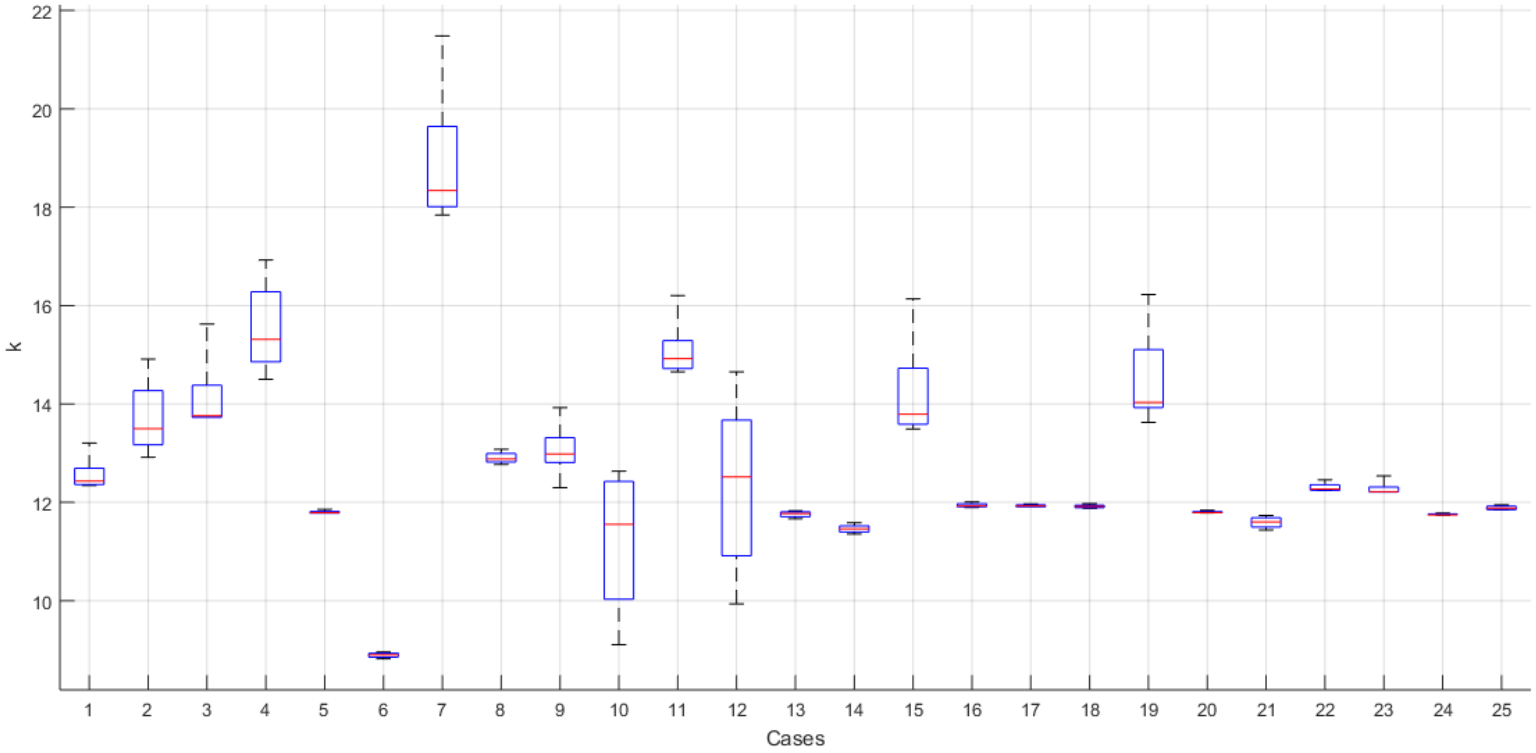

Figure 4.17: Box plot for the values of *k*

In the following table, the values of *k* are given in relation with 3 variables. The variable in the third column is the second moment of inertia of longitudinal stiffeners along with the attached plate. The effect of the second moment of inertia of transverse stiffeners is considered negligible from 1.1×10^7 to $21.3 \times 10^7 \text{mm}^4$. For variables within the limits that were mentioned before, coefficient *k* can be calculated using trilinear interpolation.

X_1	X_2	I	k
600	1800	4.1	12.34
600	1800	25.62	12.92
600	1800	5.18	13.73
600	1800	33.85	14.5
600	5400	4.1	11.78
600	5400	25.62	8.82
600	5400	5.18	17.84
600	5400	33.85	12.77
900	1800	4.39	12.29
900	1800	28.85	9.11
900	1800	5.42	14.65
900	1800	36.54	9.93
900	5400	4.39	11.67
900	5400	28.85	11.37
900	5400	5.42	13.49
900	5400	36.54	11.89
600	3600	17.15	11.91
900	3600	18.56	11.88
750	1800	17.96	13.63
750	5400	17.96	11.78
750	3600	15.49	11.44
750	3600	19.72	12.24
750	3600	4.84	12.21
750	3600	32.12	11.73
750	3600	17.96	11.84

Table 4.4: The value of *k* in relation with $\mathbf{X_1}$, $\mathbf{X_2}$ and I

5. Generic conclusions

For stiffened panels that are subjected to uniform pressure loads, the Euler-Bernoulli beam theory underestimate the secondary stresses due to the shear lag phenomenon. Analytical solutions of Paik, Schade and Miller considering this phenomenon provide a method to calculate the secondary stresses. The most safe and conservative is the solution of Paik for T, L and Flat-bar profiles. Direct stiffness method also underestimates the stress field either using Euler or Timoshenko beam. For the modeling of a stiffened panel in a finite element software solid elements give a stress field with small deviances from the analytical solutions for the secondary stresses, apart from the boundaries, and reducing the mesh size the numerical results converge to the theoretical elements. Beam elements are 1-D elements which also underestimate the stress field. Shell elements are not suggested for secondary stress analysis.

For a cross-stiffened panel, given that the dimensions of the panel concern ship scantlings, the longitudinal stiffeners can be considered as simply supported between two transverse stiffeners. Moreover, the second moment of inertia of transverse stiffeners has small effect to the secondary stress field of the longitudinal stiffeners and as a result the type of support is not related with the second moment of inertia of transverse stiffeners.

References

Anderson, M., & Whitcomb, P. *DOE Simplified* (3rd ed.).

Beer, F. P., Johnston, E. R., DeWolf, J. T., & Mazurek, D. F. (2012). *ΜΗΧΑΝΙΚΗ ΤΩΝ ΥΛΙΚΩΝ* (6η ed.). (Τ. Καλβουρίδης, & Σ. Καρτσοβίτη, Trans.) Θεσσαλονίκη: Εκδόσεις ΤΖΙΟΛΑ.

Gere, J. M., & Goodno, B. J. (2012). *Mechanics of Materials* (8th ed.). Stamford: Cengage Learning.

Guedes Soares, C., & Das, P. K. (2009). *Analysis and Design of Marine Structures.* London: Taylor & Francis Group.

HETENYI, M. (1946). *BEAMS ON ELASTIC FOUNDATION - THEORY WITH APPLICATIONS IN THE FIELDS OF CIVIL AND MECHANICAL ENGINEERING.* ANN ARBOR: THE UNIVERSITY OF MICHIGAN PRESS.

Hughes, O. F., & Paik, J. K. (2010). *SHIP STRUCTURAL ANALYSIS AND DESIGN.* New Jersey: The Society of Naval Architects and Marine Engineers.

IACS. (2019). *Common Structural Rules for Bulk carriers and Oil Tankers*.

Okumoto, Y., Takeda, Y., Mano, M., & Okada, T. (2009). *Design of Ship Hull Structures - A Practical Guide for Engineers.* Berlin: Springer.

Paik, J. K., & Thayamballi, A. K. (2003). *Ultimate Limit State Design of Steel - Plated Structures.* Wiley.

Pietraszkiewikz, W., & Kreja, I. (2010). *Shell Structures - Theory and Applications.* London: Taylor & Francis Group.

SIMULIA Abaqus 2016. (n.d.).

Spyrakos, C. C., & Raftoyiannis, J. (1997). *LINEAR AND NONLINEAR FINITE ELEMENT ANALYSIS IN ENGINEERING PRACTICE.* Pittsburgh: Algor Publishing Division.

Ανυφαντής, Κ. Ν. (2020). *Στατική Ναυπηγικών Κατασκευών.* Αθήνα: Ε.Μ.Π.

Καρύδης, Π. Α. (2017). *Η Μεταλλική Κατασκευή του Πλοίου - Θέματα Τοπικής Αντοχής* (2η ed.). Αθήνα: Αυτοέκδοση.

Προβατίδης, Χ. Γ. (2016). *Πεπερασμένα Στοιχεία στην Ανάλυση Κατασκευών* (2η ed.). Θεσαλλονίκη: Εκδόσεις ΤΖΙΟΛΑ.

Appendix

Appendix A

Code of Direct Stiffness Method

```
E=207000;
v=0.3;
L=3650;
I=371068740.80221;
F=292000;
AS=17593;
G=E/(2*(v+1));
eulertim=input('Euler or Timoshenko? Press 0 for Euler , 1 for Timoshenko')
if eulertim==0
 FTIM=0;
elseif eulertim==1
 FTIM=12*E*I/(G*AS*(L^2));
end
l=0;
danaf=2;
d=input('dwste arithmo dokariwn')
L=L/d;
K=(E*I/(L^3))*[12,6*L,-12,6*L;6*L,(4+FTIM)*(L^2),-6*L,(2-FTIM)*(L^2);-12,-6*L,12,-
6*L;6*L,(2-FTIM)*(L^2),-6*L,(4+FTIM)*(L^2)];
while danaf~=d
     danaf=danaf+1;
     l=l+2;
end
for i=5:1:6+l
            for j=5:1:6+l
                K(i,j)=0;
            end
end
for i=1:1:6+l
            for j=1:1:6+l
                A(i,j)=0;

            end
end
for i=1:1:6+l
            for j=1:1:6+l
                if (i<=4) && (j<=4)
                    A(i+2,j+2)=K(i,j);

                end
            end
end
S=K+A;
if d~=2
    for c=1:1:(d-2)
        K=A;
        for i=1:1:6+l
            for j=1:1:6+l
                A(i,j)=0;
            end
        end
        for i=1:1:6+l
            for j=1:1:6+l
                if (i<=(4+l)) && (i>=(4-l)) && (j<=(4+l)) && (j>=(4-l))
                     A(i+2,j+2)=K(i,j);
                end
            end
        end
        S=S+A;
    end

end
```

```
MHTRWOAKAMPSIAS=S;
for ii=1:1:(6+l)
    if mod(ii,2)==0
        C(ii)=0;
    else
        C(ii)=(F/(d-1));
    end
end
C(1)=0;
C(2)=0;
C(5+l)=0;
C(6+l)=0;
EXDUNAMEIS=C';
MIKROSPINAKAS=S;
MIKROSPINAKAS(1,:)=0;
MIKROSPINAKAS(1,1)=1;
MIKROSPINAKAS(2,:)=0;
MIKROSPINAKAS(2,2)=1;
MIKROSPINAKAS(5+l,:)=0;
MIKROSPINAKAS(5+l,5+l)=1;
MIKROSPINAKAS(6+l,:)=0;
MIKROSPINAKAS(6+l,6+l)=1;
ANTISTROFOS=inv(MIKROSPINAKAS);
METATOPISEIS=ANTISTROFOS*EXDUNAMEIS
SYNOLIKESDYNAMEIS=MHTRWOAKAMPSIAS*METATOPISEIS;
ADIDRASEIS=SYNOLIKESDYNAMEIS-EXDUNAMEIS;
w=1;
for i=1:2:(l+3)
    tasi(w)=77.527*E*( (-1*METATOPISEIS(i+1)/L)  + (1*METATOPISEIS(i+3)/L));
    w=w+1;
end
```

Code for the calculation of b_e for T profiles

```
%analytiki sxesi apo Paik
k=1;
for z=0:10^(-3):1
    if z<=0.1
        w(k)=1;
        j(k)=z;
        k=k+1;
    else
        w(k)=(4*sinh(pi.*z).*sinh(pi.*z))./(pi*1.3*(2.7*sinh(2*pi.*z)-2.6*pi.*z).*z);
        j(k)=z;
        k=k+1;
    end
end
hold on
plot(j,w,'--')
%telos paik

grid on
tfw=150;
tft=18;
wh=430;
wt=15;
bfw=830;
bft=19;
A=(tfw*tft)+(wh*wt)+(bfw*bft);
zbot=((bfw*bft*bft/2)+(wh*wt*(bft+wh/2))+(tft*tfw*(bft+wh+tft/2)))/A;
ztop=(wh+bft+tft)-zbot;
zsbot=zbot-(bft/2);
zstop=ztop-(tft/2);
I=((1/12)*bfw*bft^3)+(bft*bfw*(bft/2-zbot)^2)+((1/12)*wt*wh^3)+(wt*wh*((bft+wh/2)-
zbot)^2)+((1/12)*tfw*tft^3)+(tft*tfw*((bft+wh+tft/2)-zbot)^2);
d=1;
for ii=0.01:0.01:1
%synthhkes edrasis
L=bfw/ii;
%ypologismos sb
sb=(0.1*bfw*(L^2)*zbot)/(8*I);

%ypologismos ss
fun=@(x)(bft*bfw*zsbot/wt)+0.5.*(zsbot-x).*(zsbot+x);
q=integral(fun,0,zsbot);
ss=((2*0.7*0.1*bfw)/I)*q;

%ypologismos ssaxial
%1os oros
fun=@(x) (tft*tfw*zstop/wt)+0.5.*(zstop-x).*(zstop+x);
q=integral(fun,0,zstop);
q1= wt*q*(zstop);
%2os oros
fun=@(x) zstop.*(zstop+(tfw/2)-x);
q=integral(fun,zstop,zstop+(tfw/2));
q2=2*tft*q*(tfw/2);
%3os oros
fun=@(x) (bft*bfw*zsbot/wt)+0.5.*(zsbot-x).*(zsbot+x);
q=integral(fun,0,zsbot);
q3=wt*q*zsbot;
%4os oros
fun=@(x) zsbot.*(zsbot+(bfw/2)-x);
q=integral(fun,zsbot,zsbot+(bfw/2));
q4=2*bft*q*(bfw/2);
```

```
%prosthesi twn tessarwn orwn
ssax=(q1+q2+q3+q4)*(1.4*0.1*bfw/(I*A));

%ypologismos ssbending
%1os oros
fun=@(x) (tft*tfw*zstop/wt)+0.5.*(zstop-x).*(zstop+x);
q=integral(fun,0,zstop);
fun=@(x) wt*q.*x;
q1=integral(fun,0,zstop);
%2os oros
fun=@(x) zstop.*(zstop+(tfw/2)-x);
q=integral(fun,zstop,zstop+(tfw/2));
q2=2*tft*zstop*q*(tfw/2);
%3os oros
fun=@(x) (bft*bfw*zsbot/wt)+0.5.*(zsbot-x).*(zsbot+x);
q=integral(fun,0,zsbot);
fun=@(x) wt*q.*x;
q3=integral(fun,0,zsbot);
%4os oros
fun=@(x) zsbot.*(zsbot+(bfw/2)-x);
q=integral(fun,zsbot,zsbot+(bfw/2));
q4=2*bft*zsbot*q*(bfw/2);
%prosthesi twn tessarwn orwn
ssb=(q1+q2+q3+q4)*(1.4*0.1*bfw*zbot/(I^2));

%ypologismos smax
smax=sb-ss+ssax+ssb;


%oloklirwma gia be
syms x
f=zsbot.*(zsbot+(bfw/2)-x);
fint=-int(f,x,zsbot);
fintt=smax-(1.4*0.1*bfw/I).*fint;
olokl=int(fintt,x,[zsbot zsbot+(bfw/2)]);
be=2*olokl/smax;
be=double(be);
a=be/bfw;
xx(d)=ii;
y(d)=a;

%arxi csr
 if L>=(bfw*(3^(0.5)))
    cc=1.12/(1+(1.75/(L/(bfw*(3^(0.5))))^1.6));
    dd=1;
    ee=min(cc,dd);
    befcsr=ee*bfw;

 else
    befcsr=0.2349815596*L;
 end
csr(d)=befcsr/bfw;
%telos csr

d=d+1;
end
```

```
plot(xx,y)
plot(xx,csr,'--')

%shade
a=[1 1/1.8478 1/2.5 1/3.4348 1/4.5   1/8.2174];
b=[0.3869 0.7087 0.8347 0.9087 0.9478   1];
aa=1:-10^(-3):(1/8.2174);
bb=spline(a,b,aa);
plot(aa,bb,'--')
%telos shade
```

Appendix B

Below, the results of each case are presented. For each case, there is a column for the dimensions of the transverse stiffeners for which the model was run, for the second moment of inertia for the transverse stiffeners (I), for the maximum stress and its position to the longitudinal stiffener and for the coefficient *k* that results from equation 4.15.

Case 1

Dimensions [mm × mm]	I [mm^4]	σ_{max} [MPa]	position	k
$200 \times 10 + 50 \times 10$	1.1×10^7	65.64	0	13.21
$270 \times 13 + 85 \times 13$	3.8×10^7	70.24	0	12.34
$330 \times 15 + 110 \times 15$	8.2×10^7	70.1	0	12.37
$375 \times 16 + 130 \times 16$	12.9×10^7	69.72	0	12.43
$425 \times 18 + 150 \times 18$	21.3×10^7	69.23	0	12.52

Case 2

Dimensions [mm × mm]	I [mm^4]	σ_{max} [MPa]	position	k
$340 \times 15 + 110 \times 15$	8.8×10^7	12.97	0	14.91
$360 \times 16 + 120 \times 16$	11.3×10^7	13.75	0	14.06
$380 \times 17 + 130 \times 17$	14.3×10^7	14.32	0	13.49
$400 \times 17 + 140 \times 17$	16.7×10^7	14.59	0	13.25
$425 \times 18 + 150 \times 18$	21.3×10^7	14.97	0	12.92

Case 3

Dimensions [mm × mm]	I [mm^4]	σ_{max} [MPa]	position	k
$200 \times 10 + 50 \times 10$	1.1×10^7	49.56	0	15.62
$270 \times 13 + 85 \times 13$	3.8×10^7	55.44	0	13.97
$330 \times 15 + 110 \times 15$	8.2×10^7	56.29	0	13.76
$375 \times 16 + 130 \times 16$	12.9×10^7	56.41	0	13.73
$425 \times 18 + 150 \times 18$	21.3×10^7	56.41	0	13.73

Case 4

Dimensions [mm × mm]	I [mm^4]	σ_{max} [MPa]	position	k
$340 \times 15 + 110 \times 15$	8.8×10^7	10.31	a/2	16.93
$360 \times 16 + 120 \times 16$	11.3×10^7	10.86	0	16.06
$380 \times 17 + 130 \times 17$	14.3×10^7	11.39	0	15.31
$400 \times 17 + 140 \times 17$	16.7×10^7	11.65	0	14.98
$425 \times 18 + 150 \times 18$	21.3×10^7	12.03	0	14.5

Case 5

Dimensions [mm × mm]	I [mm^4]	σ_{max} [MPa]	position	k
$200 \times 10 + 50 \times 10$	1.1×10^7	658	0	11.86
$270 \times 13 + 85 \times 13$	3.8×10^7	662.23	0	11.78
$330 \times 15 + 110 \times 15$	8.2×10^7	662.19	0	11.78
$375 \times 16 + 130 \times 16$	12.9×10^7	661.81	0	11.79
$425 \times 18 + 150 \times 18$	21.3×10^7	661.29	0	11.8

Case 6

Dimensions [mm × mm]	I [mm^4]	σ_{max} [MPa]	position	k
$340 \times 15 + 110 \times 15$	8.8×10^7	197.3	0	8.82
$360 \times 16 + 120 \times 16$	11.3×10^7	196.42	0	8.86
$380 \times 17 + 130 \times 17$	14.3×10^7	195.62	0	8.89
$400 \times 17 + 140 \times 17$	16.7×10^7	195.05	0	8.92
$425 \times 18 + 150 \times 18$	21.3×10^7	194.29	0	8.95

Case 7

Dimensions [mm × mm]	I [mm^4]	σ_{max} [MPa]	position	k
$200 \times 10 + 50 \times 10$	1.1×10^7	324.46	0	21.48
$270 \times 13 + 85 \times 13$	3.8×10^7	366.26	0	19.03
$330 \times 15 + 110 \times 15$	8.2×10^7	380.07	0	18.34
$375 \times 16 + 130 \times 16$	12.9×10^7	385.74	0	18.07
$425 \times 18 + 150 \times 18$	21.3×10^7	390.67	0	17.84

Case 8

Dimensions [mm × mm]	I [mm^4]	σ_{max} [MPa]	position	k
$340 \times 15 + 110 \times 15$	8.8×10^7	120.07	0	13.08
$360 \times 16 + 120 \times 16$	11.3×10^7	121.09	0	12.97
$380 \times 17 + 130 \times 17$	14.3×10^7	121.92	0	12.88
$400 \times 17 + 140 \times 17$	16.7×10^7	122.32	0	12.84
$425 \times 18 + 150 \times 18$	21.3×10^7	122.96	0	12.77

Case 9

Dimensions [mm × mm]	I [mm^4]	σ_{max} [MPa]	position	k
$200 \times 10 + 50 \times 10$	1.1×10^7	103.64	a/2	12.29
$270 \times 13 + 85 \times 13$	3.8×10^7	91.53	0	13.93
$330 \times 15 + 110 \times 15$	8.2×10^7	97.23	0	13.11
$375 \times 16 + 130 \times 16$	12.9×10^7	98.18	0	12.98
$425 \times 18 + 150 \times 18$	21.3×10^7	98.19	0	12.98

Case 10

Dimensions [mm × mm]	I [mm^4]	σ_{max} [MPa]	position	k
$340 \times 15 + 110 \times 15$	8.8×10^7	30.7	a/2	9.11
$360 \times 16 + 120 \times 16$	11.3×10^7	27.05	a/2	10.34
$380 \times 17 + 130 \times 17$	14.3×10^7	24.2	a/2	11.55
$400 \times 17 + 140 \times 17$	16.7×10^7	22.63	a/2	12.35
$425 \times 18 + 150 \times 18$	21.3×10^7	22.13	a/2	12.63

Case 11

Dimensions [mm × mm]	I [mm^4]	σ_{max} [MPa]	position	k
$200 \times 10 + 50 \times 10$	1.1×10^7	76.39	a/2	14.92
$270 \times 13 + 85 \times 13$	3.8×10^7	70.36	0	16.2
$330 \times 15 + 110 \times 15$	8.2×10^7	76.09	0	14.98
$375 \times 16 + 130 \times 16$	12.9×10^7	77.32	0	14.74
$425 \times 18 + 150 \times 18$	21.3×10^7	77.81	0	14.65

Case 12

Dimensions [mm × mm]	I [mm^4]	σ_{max} [MPa]	position	k
$340 \times 15 + 110 \times 15$	8.8×10^7	25.79	a/2	9.93
$360 \times 16 + 120 \times 16$	11.3×10^7	22.79	a/2	11.24
$380 \times 17 + 130 \times 17$	14.3×10^7	20.47	a/2	12.51
$400 \times 17 + 140 \times 17$	16.7×10^7	19.2	a/2	13.34
$425 \times 18 + 150 \times 18$	21.3×10^7	17.48	a/2	14.65

Case 13

Dimensions [mm × mm]	I [mm^4]	σ_{max} [MPa]	position	k
$200 \times 10 + 50 \times 10$	1.1×10^7	983.32	0	11.67
$270 \times 13 + 85 \times 13$	3.8×10^7	978.64	0	11.72
$330 \times 15 + 110 \times 15$	8.2×10^7	974.52	0	11.77
$375 \times 16 + 130 \times 16$	12.9×10^7	972.18	0	11.79
$425 \times 18 + 150 \times 18$	21.3×10^7	969.89	0	11.83

Case 14

Dimensions [mm × mm]	I [mm^4]	σ_{max} [MPa]	position	k
$340 \times 15 + 110 \times 15$	8.8×10^7	221.58	0	11.37
$360 \times 16 + 120 \times 16$	11.3×10^7	220.53	0	11.41
$380 \times 17 + 130 \times 17$	14.3×10^7	219.55	0	11.46
$400 \times 17 + 140 \times 17$	16.7×10^7	218.86	0	11.49
$425 \times 18 + 150 \times 18$	21.3×10^7	217.19	0	11.59

Case 15

Dimensions [mm × mm]	I [mm^4]	σ_{max} [MPa]	position	k
$200 \times 10 + 50 \times 10$	1.1×10^7	635.93	0	16.13
$270 \times 13 + 85 \times 13$	3.8×10^7	719.59	0	14.26
$330 \times 15 + 110 \times 15$	8.2×10^7	744.07	0	13.79
$375 \times 16 + 130 \times 16$	12.9×10^7	753.3	0	13.62
$425 \times 18 + 150 \times 18$	21.3×10^7	760.57	0	13.49

Case 16

Dimensions [mm × mm]	I [mm^4]	σ_{max} [MPa]	position	k
$340 \times 15 + 110 \times 15$	8.8×10^7	192	0	12.01
$360 \times 16 + 120 \times 16$	11.3×10^7	192.79	0	11.96
$380 \times 17 + 130 \times 17$	14.3×10^7	193.32	0	11.93
$400 \times 17 + 140 \times 17$	16.7×10^7	193.54	0	11.91
$425 \times 18 + 150 \times 18$	21.3×10^7	193.82	0	11.89

Case 17

Dimensions [mm × mm]	I [mm^4]	σ_{max} [MPa]	position	k
$280 \times 14 + 90 \times 14$	4.6×10^7	94.43	0	11.91
$320 \times 15 + 105 \times 15$	7.4×10^7	94.43	0	11.91
$360 \times 16 + 120 \times 16$	11.3×10^7	94.29	0	11.93
$390 \times 17 + 140 \times 17$	15.7×10^7	94.15	0	11.94
$425 \times 18 + 150 \times 18$	21.3×10^7	93.00	0	11.96

Case 18

Dimensions [mm × mm]	I [mm^4]	σ_{max} [MPa]	position	k
$280 \times 14 + 90 \times 14$	4.6×10^7	138.42	0	11.92
$320 \times 15 + 105 \times 15$	7.4×10^7	138.88	0	11.88
$360 \times 16 + 120 \times 16$	11.3×10^7	138.62	0	11.89
$390 \times 17 + 140 \times 17$	15.7×10^7	138.22	0	11.93
$425 \times 18 + 150 \times 18$	21.3×10^7	137.76	0	11.97

Case 19

Dimensions [mm × mm]	I [mm^4]	σ_{max} [MPa]	position	k
$280 \times 14 + 90 \times 14$	4.6×10^7	24.72	a/2	14.03
$320 \times 15 + 105 \times 15$	7.4×10^7	21.38	0	16.22
$360 \times 16 + 120 \times 16$	11.3×10^7	23.54	0	14.73
$390 \times 17 + 140 \times 17$	15.7×10^7	24.73	0	14.03
$425 \times 18 + 150 \times 18$	21.3×10^7	25.45	0	13.63

Case 20

Dimensions [mm × mm]	I [mm^4]	σ_{max} [MPa]	position	k
$280 \times 14 + 90 \times 14$	4.6×10^7	263.62	0	11.84
$320 \times 15 + 105 \times 15$	7.4×10^7	264.47	0	11.8
$360 \times 16 + 120 \times 16$	11.3×10^7	264.73	0	11.79
$390 \times 17 + 140 \times 17$	15.7×10^7	264.79	0	11.78
$425 \times 18 + 150 \times 18$	21.3×10^7	264.74	0	11.79

Case 21

Dimensions [mm × mm]	I [mm^4]	σ_{max} [MPa]	position	k
$280 \times 14 + 90 \times 14$	4.6×10^7	128.14	0	11.44
$320 \times 15 + 105 \times 15$	7.4×10^7	127.23	0	11.52
$360 \times 16 + 120 \times 16$	11.3×10^7	126.29	0	11.6
$390 \times 17 + 140 \times 17$	15.7×10^7	125.56	0	11.67
$425 \times 18 + 150 \times 18$	21.3×10^7	124.89	0	11.73

Case 22

Dimensions [mm × mm]	I [mm^4]	σ_{max} [MPa]	position	k
$280 \times 14 + 90 \times 14$	4.6×10^7	107.01	0	12.46
$320 \times 15 + 105 \times 15$	7.4×10^7	108.13	0	12.33
$360 \times 16 + 120 \times 16$	11.3×10^7	108.63	0	12.27
$390 \times 17 + 140 \times 17$	15.7×10^7	108.83	0	12.25
$425 \times 18 + 150 \times 18$	21.3×10^7	108.89	0	12.24

Case 23

Dimensions [mm × mm]	I [mm^4]	σ_{max} [MPa]	position	k
$200 \times 10 + 50 \times 10$	1.1×10^7	322.73	0	12.54
$270 \times 13 + 85 \times 13$	3.8×10^7	330.59	0	12.24
$330 \times 15 + 110 \times 15$	8.2×10^7	331.4	0	12.21
$375 \times 16 + 130 \times 16$	12.9×10^7	331.37	0	12.21
$425 \times 18 + 150 \times 18$	21.3×10^7	331.17	0	12.22

Case 24

Dimensions [mm × mm]	I [mm^4]	σ_{max} [MPa]	position	k
$340 \times 15 + 110 \times 15$	8.8×10^7	76.18	0	11.74
$360 \times 16 + 120 \times 16$	11.3×10^7	76.22	0	11.73
$380 \times 17 + 130 \times 17$	14.3×10^7	76.18	0	11.74
$400 \times 17 + 140 \times 17$	16.7×10^7	76.08	0	11.76
$425 \times 18 + 150 \times 18$	21.3×10^7	75.94	0	11.78

Case 25

Dimensions [mm × mm]	I [mm^4]	σ_{max} [MPa]	position	k
$280 \times 14 + 90 \times 14$	4.6×10^7	117.12	0	11.84
$320 \times 15 + 105 \times 15$	7.4×10^7	117.07	0	11.85
$360 \times 16 + 120 \times 16$	11.3×10^7	116.75	0	11.88
$390 \times 17 + 140 \times 17$	15.7×10^7	116.43	0	11.91
$425 \times 18 + 150 \times 18$	21.3×10^7	116.09	0	11.95